Synthèse cinématique d'un octopode parallèle sans surcontrainte avec conditions de singularité simples

Mémoire

Jonathan Lacombe

Maîtrise en génie mécanique - avec mémoire
Maître ès sciences (M. Sc.)

Québec, Canada

Synthèse cinématique d'un octopode parallèle sans surcontrainte avec conditions de singularité simples

Mémoire

Jonathan Lacombe

Sous la direction de:

Clément Gosselin, directeur de recherche

Résumé

Ce mémoire présente l'étude du lieu des singularités de type II pour un mécanisme parallèle cinématiquement redondant à (6+2) degrés de liberté dont l'architecture est préalablement donnée. Cette étude se concentre sur les conditions mathématiques telles que le déterminant de la matrice jacobienne s'annule pour toutes configurations dues à la mobilité interne du mécanisme permise par la redondance cinématique. Pour ce faire, la construction d'une matrice partageant les mêmes conditions de singularité que la matrice jacobienne du mécanisme est présentée. La réécriture du déterminant de cette matrice par une sommation de quatre sous-déterminants pondérée par les paramètres de mobilité interne du mécanisme mène à un système d'équations non linéaires à résoudre pour obtenir le lieu des singularités. Une méthode d'élimination de variables, le résultant des polynômes, est ensuite appliquée de manière récursive à ce système d'équations afin d'en extraire les conditions pouvant le résoudre. Les lieux de singularité sont ensuite analysés suivant deux cas de figure. Le premier se penche sur les configurations spécifiques du mécanisme où l'angle de torsion de la plateforme est nul, et le second se concentre sur le cas général, où cet angle de torsion n'est pas nécessairement nul. Dans le premier cas d'analyse, il est montré que les lieux de singularité se situent à l'extérieur de l'espace atteignable du mécanisme cinématiquement redondant. Dans le second cas d'analyse, il est montré que l'espace en orientation demeure quelque peu affecté par la présence de singularités, bien que leur localisation par des équations mathématiques analytiques simples soit possible. Finalement, une comparaison graphique des espaces atteignables en orientation entre le mécanisme cinématiquement redondant et le mécanisme non redondant standard est effectuée afin de visualiser l'impact de l'ajout de la redondance cinématique sur l'agrandissement de l'espace en orientation.

Abstract

This thesis presents the study of the type II singularity locus of a kinematically redundant (6+2) degree-of-freedom parallel mechanism whose architecture is prescribed. This study focuses on the mathematical conditions for which the determinant of the Jacobian matrix vanishes for all configurations of the internal mobility in the mechanism due to its kinematic redundancy. To do so, a matrix that captures the same conditions of singularity as the Jacobian matrix is presented. The expansion of the determinant of the aforementioned matrix into a weighted sum of four sub-determinants whose weighting factors correspond to the internal mobility parameters leads to a nonlinear system of equations whose solution yields the locus of singularity. A method of elimination theory, the resultant of polynomials, is applied afterwards on the system of equations in a recursive manner to extract the mathematical conditions corresponding to the solution. The loci of singularity are then analyzed following two cases. The first case focuses on the specific configurations of the mechanism where the torsion angle of the platform is zero, whereas the second case takes into account the general configurations, i.e. the configurations in which the torsion angle is not necessarily zero. In the former case of analysis, it is shown that the loci of singularity lie outside of the reachable orientational workspace of the kinematically redundant mechanism. In the latter case of analysis, it is presented that the orientational workspace is still somewhat restrained by singularities, yet their localization by simple analytical mathematical equations is possible. Finally, a graphical comparison of the orientational reachable workspace of the kinematically redundant mechanism and that of the standard non-redundant mechanism is performed to visualize the impact of the kinematic redundancy on the enhancement of the orientational workspace.

Table des matières

Liste des tableaux

Liste des figures

À ma famille,
À mes amis,
À mon amoureuse

Remerciements

Deux années de maîtrise ne s'accomplissent pas toutes seules et sont certainement le fruit de l'influence de plusieurs personnes d'importance. Si le soutien technique et théorique viennent des uns, le soutien moral et émotionnel viennent des autres. Ici, je tiens à souligner l'apport grandement apprécié de ces personnes.

Tout d'abord, à la première personne qui m'a ouvert les bras et qui m'a fait découvrir et aimer la robotique. Clément, je vous suis intensément reconnaissant pour le temps, la patience et la dévotion que vous m'avez accordés durant cette période. Je n'aurais certainement pas pu parvenir à ce point dans le projet sans vos idées et votre supervision.

Ensuite, à mes parents envers qui je ne pourrai jamais être assez redevable, et qui par leurs sacrifices se sont toujours assurés que je puisse bénéficier des meilleures conditions et du meilleur environnement pour parvenir à mes aspirations. Tous mes accomplissements vous sont entièrement dédiés.

À ma soeur, pour qui les mathématiques n'ont jamais été la tasse de thé, mais qui m'a démontré, coup après coup, que toute difficulté est surmontable lorsqu'on sait bien s'entourer et que notre persévérance face à notre découragement est, le plus souvent, infaillible.

Je tiens à remercier mon collègue de maîtrise et très bon ami, Mario Philip, qui me rappelle de toujours voir le bon côté des choses, de demeurer en tout temps positif face au défi et à l'imprévu, et pour sa contribution incessante à l'ambiance amicale et détendue au Laboratoire durant mon passage.

Finalement, je ne peux passer sous silence mon amoureuse, qui a fait le choix de s'éloigner de sa famille et de ses amis, et qui a écarté de belles opportunités de carrière dans la région de notre ville natale pour rester à mes côtés durant la continuation de mes études graduées.

Avant-propos

Ce mémoire est présenté sous la forme d'un mémoire par insertion d'articles. Les deux premiers chapitres correspondent chacun à un article qui a été publié à un journal scientifique. Le troisième chapitre est de type traditionnel.

Le Chapitre 1 correspond au premier article intitulé *Singularity Analysis of a Kinematically Redundant (6+2)-DOF Parallel Mechanism for Zero-Torsion Configurations*. Celui-ci a été soumis le 15 septembre 2021, accepté le 3 décembre 2021 et publié le 12 janvier 2022 dans le journal *Mechanism and Machine Theory*, de l'éditeur *Elsevier*. L'insertion de ce premier article comporte des modifications par rapport à la version publiée. Une première se situe dans la mise en page des annexes. Le titre de l'annexe a aussi été modifié afin de faciliter sa référence au texte. La Figure 1.4 a été déplacée pour des raisons de clarté. Le texte de l'insertion de ce premier article comporte des modifications mineures de reformulations de mots suggérées par le jury d'évaluation. Ma contribution pour ce premier article est celui de premier auteur. J'ai participé à l'écriture de l'article dans son entièreté, la production des figures et l'analyse des résultats. Professeur Clément Gosselin est coauteur pour ce premier article. Il a activement supervisé les travaux de recherche et participé à la révision détaillée de chaque partie de l'article.

Le Chapitre 2 comporte le second article, intitulé *Singularity Analysis of a Kinematically Redundant (6+2)-DOF Parallel Mechanism for General Configurations*, qui a été soumis le 16 janvier 2022 au journal *Mechanism and Machine Theory*, de l'éditeur *Elsevier*. Cet article a été accepté pour publication le 30 juin 2022 et publié le 19 juillet 2022. L'insertion de ce second article ne comporte qu'une seule modification au niveau des équations par rapport à la version publiée et se trouve à l'équation (2.30) afin que celle-ci puisse bien entrer à l'intérieur des marges de texte. Le texte de l'insertion de ce second article comporte des modifications mineures de reformulations de mots suggérées par le jury d'évaluation. Ma contribution pour ce second article est celui de premier auteur. J'ai participé à l'écriture de l'article dans son entièreté, la production des figures et l'analyse des résultats. Professeur Clément Gosselin est coauteur pour ce second article. Il a activement supervisé les travaux de recherche et participé à la révision détaillée de chaque partie de l'article.

Introduction

Les robots à architecture parallèle, où plusieurs chaînes cinématiques disposées en parallèle relient une plateforme à une base, ont su démontrer leurs capacités prometteuses pour des critères clés d'applications robotiques. Parmi d'autres, on leur associe des performances dynamiques notables, des potentiels de déplacement de charges élevées ainsi qu'une précision sur le positionnement très intéressante. Ces fonctionnalités de l'architecture parallèle ont mené cette famille de robots à se faire une place dans une quantité d'applications. En effet, on peut retrouver des mécanismes parallèles dans des dispositifs d'isolation de microvibrations dans l'espace [1], mais surtout sur des chaînes d'empaquetage dans l'industrie alimentaire et pharmaceutique [2; 3]. Dans le domaine médical, on développe des robots parallèles pour des dispositifs d'assistance pour les manoeuvres chirurgicales, par exemple, durant la craniotomie [4], la télé-échographie [5] ou encore l'endoscopie [6]. Dû à leur faible inertie en mouvement, les robots parallèles sont aussi de bons candidats pour l'interaction humain-robot à faible impédance [7; 8; 9; 10]. Finalement, on observe les robots parallèles dans des tâches de préhension et positionnement (*pick-and-place*) à haute vitesse [11; 12], ou encore dans l'usinage [13; 14].

Le contrepoids principal à une utilisation plus vaste des architectures parallèles dans les applications robotiques est la présence de configurations singulières à l'intérieur de leur espace de travail atteignable [15]. De telles configurations singulières sont problématiques, car elles peuvent, entre autres, engendrer une perte locale de contrôle du mécanisme, des bris d'équipement ou porter atteinte à la sécurité d'un opérateur à proximité. Ainsi, il est primordial d'éviter ces configurations singulières dans la planification de trajectoire du robot, ce qui mène inévitablement à une réduction de son espace de travail utile. Afin de résoudre le problème des singularités dans les robots parallèles, plusieurs ont choisi d'insérer une redondance cinématique dans les architectures parallèles standards [16; 17; 18; 19; 20]. Ainsi, le mécanisme jouit de degrés de liberté supplémentaires, via un ajout d'articulations actionnées dans les chaînes cinématiques déjà existantes, ce qui rend possible une mobilité interne dans le mécanisme. Cette mobilité interne permet de reconfigurer certaines chaînes cinématiques dans le mécanisme pour une pose de la plateforme donnée, et cette fonctionnalité peut être judicieusement mise en oeuvre pour éviter des configurations singulières [21; 22; 23].

Plus récemment, des architectures ont été proposées pour lesquelles le nombre de degrés de liberté supplémentaires qui sont ajoutés au mécanisme par la redondance cinématique garantit d'éviter toutes les singularités dans l'espace de travail atteignable du robot [24; 25]. Autrement dit, pour toute position et orientation de l'effecteur, il existe au moins une configuration des articulations actionnées telle que le mécanisme n'est pas en configuration singulière. Des architectures de robots plans avec les mêmes capacités d'évitement de toutes les singularités ont été proposées [26; 27]. Dans [26], le robot cinématiquement redondant possède trois degrés de libertés supplémentaires (six degrés de liberté au total dans le plan) pour s'assurer l'évitement de toute singularité. D'un autre côté, [27] propose une architecture ne requérant qu'un seul degré de liberté redondant supplémentaire pour les mêmes performances d'évitement de singularité. Il est donc pertinent de se demander si un nombre maximum de degrés de liberté redondants ajoutés au mécanisme est toujours nécessaire pour garantir l'évitement de toutes configurations singulières.

Ce mémoire se concentre donc sur l'analyse du lieu des singularités pour une architecture cinématique très semblable à celle proposée par [25], mais ayant deux degrés de liberté redondants au lieu de trois (huit degrés de libertés au total au lieu de neuf). L'objectif est donc de déterminer en quoi est-ce que retirer un degré de liberté redondant à une architecture cinématiquement redondante exempte de configurations singulières affecte l'espace de travail utile du robot résultant. On peut donc s'attendre à découvrir des configurations singulières dans lesquelles la redondance cinématique ne sera d'aucune utilité à leur évitement. La question est plutôt d'évaluer si, malgré la présence de ces potentielles singularités, le mécanisme parallèle offre tout de même des débattements en orientation qui soient significativement élargis par rapport à un mécanisme non redondant standard.

Chapitre 1

Singularity Analysis of a Kinematically Redundant (6+2)-DOF Parallel Mechanism for Zero-Torsion Configurations

1.1 Résumé

Il est connu que l'espace en orientation des mécanismes parallèles est restreint par les configurations singulières de type II. Récemment, un mécanisme parallèle cinématiquement redondant à (6+3) degrés de liberté (DDLs) a été proposé. Il a été montré que, pour l'architecture spécifique proposée, un minimum de trois DDLs redondants est nécessaire pour garantir l'existence d'une configuration non singulière pour toute pose de la plateforme. Ce travail présente une architecture différente comportant plutôt deux DDLs redondants, et a pour objectif de déterminer le lieu des singularités pour des configurations à torsion nulle. Les résultats indiquent que les singularités mathématiquement possibles se situent à l'extérieur de l'espace atteignable, suggérant que pour des trajectoires à torsion nulle, deux DDLs redondants sont suffisants pour agrandir considérablement l'espace de travail de l'architecture proposée. Un exemple de trajectoire est présenté afin de démontrer les capacités du mécanisme d'atteindre de telles orientations sans rencontrer de singularités inévitables.

1.2 Abstract

The orientational workspace of parallel mechanisms is known to be restricted due to singular configurations of type II. Recently, a (6+3)-degree-of-freedom (DOF) kinematically redundant parallel mechanism was proposed based on the well-known Gough-Stewart platform. It was shown that, for the specific architecture proposed, a minimum of three redundant

DOFs is necessary to guarantee the existence of a non-singular configuration for any pose of the platform. This work presents a different architecture with two redundant DOFs instead of three, and has for primary objective to derive the singularity locus for zero-torsion configurations. The results indicate that the mathematically possible singularities are outside of the reachable workspace, suggesting that for zero-torsion trajectories, two kinematically redundant DOFs are sufficient to greatly enhance the orientational workspace of the proposed architecture. An example path with large tilting angle is presented in a multimedia extension of the article in order to demonstrate the capability of the mechanism to reach such orientations without encountering inevitable singularities.

1.3 Introduction

Parallel mechanisms are known to have advantageous payload to mass ratio, low inertia and dynamic properties compared to conventional serial mechanisms. However, such benefits are obtained at the expense of poor orientational workspace, due to the presence of type II singularities inside the reachable workspace of the mechanism [15]. This type of singularity corresponds to configurations in which some forces and moments at the platform cannot be supported by the mechanism even if all actuators are locked, resulting in a local loss of control over the mechanism.

Different approaches have been explored to increase the rotational workspace of parallel mechanisms, namely actuation redundancy and kinematic redundancy (see [28] for a review). In redundantly actuated parallel mechanisms, the number of DOFs is smaller than the number of actuators. Hence, internal antagonistic forces can be produced at the platform, making the control of such mechanisms more challenging [29; 30; 31; 32; 33]. Yet, effective approaches were proposed to simultaneously measure internal and external forces for the control of redundantly actuated parallel mechanisms [34], to compare the singularity loci of non-redundant and redundant mechanisms [35; 36] and to enlarge the workspace by singularity-free mode changes [37].

On the other hand, kinematically redundant parallel mechanisms possess as many DOFs as actuators. Thus, the platform has fewer DOFs than the whole mechanism, resulting in possible internal motion of the mechanism for singularity avoidance for a given pose of the platform and without generating internal antagonistic forces. This feature has been exploited, for example, to allow infinite rotation of the platform of kinematically redundant planar parallel mechanisms [27; 38; 39] and even to operate a gripper while avoiding singular configurations [40; 41].

In [42; 25], a novel kinematically redundant architecture with (6+3)-DOF akin to the well-known Gough-Stewart (GS) platform was presented. It was shown that the orientational workspace is much larger than that of the conventional GS platform and that any singular configuration can theoretically be avoided using three redundant DOFs. In [43], it was pointed out that conventional Jacobian-based methods sometimes fail to identify singularities or wrongly identify some in the presence of kinematic redundancy. In [44; 45], an alternative geometric approach for singularity avoidance in kinematically redundant planar parallel mechanisms was proposed. The approach is based on instantaneous centres of rotation (ICR), providing a more intuitive sense of closeness to a singularity. However, the use of ICR is better suited to locate singularities for specific and instantaneous poses of the mechanism in its workspace rather than to describe a locus of singular configurations in all the workspace. Moreover, the extension of the proposed method to kinematically redundant spatial manipulators may be very difficult.

In this paper, a kinematically redundant (6+2)-DOF parallel manipulator, whose specifically chosen geometry is similar to that of the MSSM Gough-Stewart platform, is introduced. The novel architecture is meant to be a compromise between the singularity-free (6+3)-DOF robot proposed in [25] and the relative geometric simplicity of the standard Gough-Stewart platform, which limits possible mechanical interferences. The singularity locus of the proposed architecture is derived for zero-torsion orientations (tilted rotations only). The derivation is conducted using the linear expansion of the determinant of the Jacobian matrix [46] to assess type II singularities while establishing the assumptions that guarantee the robustness of the method. The objective is to observe how removing one DOF from the singularity-free (6+3)-DOF GS platform presented in [42; 25] affects the performances in tilted orientations for a particular architecture designed to simplify the singularity conditions. It is to be mentioned that this work has not for objective to propose any new method for singularity analysis as a general framework, but to focus more precisely on the study of the singularity locus of a given kinematically redundant (6+2)-DOF parallel mechanism.

1.4 Kinematic modelling

In this section, the kinematic modelling of a general kinematically redundant platform based on the principle of redundant leg proposed in [42; 25] is recalled. Consider an architecture with k redundant degrees of freedom, i.e., k redundant legs and $6-k$ non-redundant legs. Each non-redundant leg is of type H$\underline{\text{P}}$S, where H stands for a Hooke-joint, $\underline{\text{P}}$ stands for an actuated prismatic joint and S stands for a spherical joint. The two sub-legs of a redundant leg are of type S$\underline{\text{P}}$R, where R stands for a revolute joint. A fixed frame $O(x, y, z)$ is defined at the base and a mobile frame $P(x', y', z')$ is defined on the platform. The attachment points at the base for non-redundant legs are noted A_j with $j = (k+1), \ldots, 6$, whereas attachment points of redundant legs are noted $A_{i,1}$ and $A_{i,2}$ with $i = 1, \ldots, k$. The attachment points at the platform for the redundant legs are noted B_i, $i = 1, \ldots, k$, while for non-redundant legs, they are noted B_j, $j = (k+1), \ldots, 6$. The two sub-legs of redundant leg i are connected at point S_i, which is a revolute joint, constraining points B_i, S_i, $A_{i,1}$, $A_{i,2}$ to remain in the same plane. Next, vector $\mathbf{p}$ is the position vector of the origin of the mobile reference frame attached to the platform expressed in the fixed reference frame, and vector $\mathbf{e}_i$ is a unit vector along the axis passing through the attachment points $A_{i,1}$, $A_{i,2}$. Matrix $\mathbf{Q}$ is the rotation matrix from the base frame to the moving frame. Finally, all vectors are expressed in the fixed reference frame, except for $\mathbf{b}'_i$ and $\mathbf{b}'_j$, which connect the origin of the moving frame to points B_i, B_j, and are expressed in the moving frame. The constraint equation corresponding to the

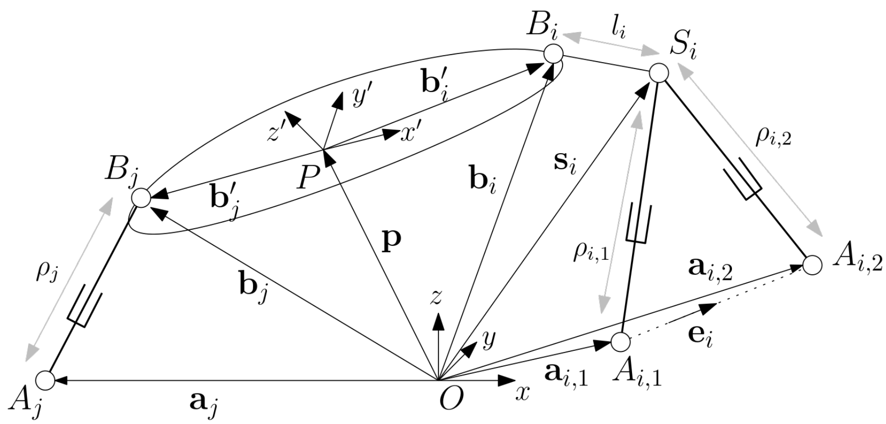

FIGURE 1.1 – Geometric modelling of a kinematically redundant spatial robot based on the architecture proposed in [25].

length of a non-redundant leg is given by

$$\rho_j^2 = (\mathbf{b}_j - \mathbf{a}_j)^T(\mathbf{b}_j - \mathbf{a}_j), \quad j = (k+1), \ldots, 6, \tag{1.1}$$

with

$$\mathbf{b}_j = \mathbf{p} + \mathbf{Q}\mathbf{b}'_j, \tag{1.2}$$

where $\mathbf{a}_j$ is the position vector of point A_j expressed in the fixed frame. The constraint equation corresponding to the length of the redundant link $\overline{B_iS_i}$ is written as

$$l_i^2 = (\mathbf{s}_i - \mathbf{b}_i)^T(\mathbf{s}_i - \mathbf{b}_i), \quad i = 1, \ldots, k \tag{1.3}$$

Next, the constraint equation for the length of the sub-legs of a redundant leg is given by

$$\rho_{i,h}^2 = (\mathbf{s}_i - \mathbf{a}_{i,h})^T(\mathbf{s}_i - \mathbf{a}_{i,h}), \quad i = 1, \ldots, k, \quad h = 1, 2 \tag{1.4}$$

where $\mathbf{a}_{i,h}$ is the position vector of point $A_{i,h}$ in the fixed frame. Finally, the constraint equation representing the coplanarity of points B_i, S_i, $A_{i,1}$, $A_{i,2}$ is written as

$$[(\mathbf{b}_i - \mathbf{a}_{i,1}) \times \mathbf{e}_i]^T(\mathbf{s}_i - \mathbf{a}_{i,1}) = 0, \quad i = 1, \ldots, k \tag{1.5}$$

After taking the derivative with respect to time of constraint equations (1.1),(1.3),(1.4), and (1.5), the expressions can be rearranged to obtain the system of equations

$$\mathbf{J}\mathbf{t} = \mathbf{K}\dot{\boldsymbol{\rho}} \tag{1.6}$$

where $\mathbf{t} = [\dot{\mathbf{p}}^T \boldsymbol{\omega}^T]^T$ is the six-dimensional Cartesian velocity vector of the platform, including the angular velocity vector of the platform, noted $\boldsymbol{\omega}$, and $\dot{\boldsymbol{\rho}}$ is the joint velocity vector of dimension $(6+k) \times 1$, noted :

$$\dot{\boldsymbol{\rho}} = [\dot{\rho}_{1,1}, \dot{\rho}_{1,2}, \ldots, \dot{\rho}_{k,1}, \dot{\rho}_{k,2}, \dot{\rho}_{k+1}, \ldots, \dot{\rho}_6]^T. \tag{1.7}$$

Matrices $\mathbf{J}$ and $\mathbf{K}$ are the Jacobian matrices, which are written as

$$\mathbf{J} = \begin{bmatrix} (\mathbf{s}_1 - \mathbf{b}_1)^T & [\mathbf{Q}\mathbf{b}'_1 \times (\mathbf{s}_1 - \mathbf{b}_1)]^T \\ \vdots & \vdots \\ (\mathbf{s}_k - \mathbf{b}_k)^T & [\mathbf{Q}\mathbf{b}'_k \times (\mathbf{s}_k - \mathbf{b}_k)]^T \\ (\mathbf{b}_{k+1} - \mathbf{a}_{k+1})^T & [\mathbf{Q}\mathbf{b}'_{k+1} \times (\mathbf{b}_{k+1} - \mathbf{a}_{k+1})]^T \\ \vdots & \vdots \\ (\mathbf{b}_6 - \mathbf{a}_6)^T & [\mathbf{Q}\mathbf{b}'_6 \times (\mathbf{b}_6 - \mathbf{a}_6)]^T \end{bmatrix}_{6\times 6} \tag{1.8}$$

and

$$\mathbf{K} = \begin{bmatrix} \mathbf{K}_1 & \mathbf{0}_{k\times(6-k)} \\ \mathbf{0}_{(6-k)\times 2k} & \mathbf{K}_2 \end{bmatrix}_{6\times(6+k)} \tag{1.9}$$

where

$$\mathbf{K}_2 = \begin{bmatrix} \rho_{k+1} & \cdots & 0 \\ \vdots & \ddots & \vdots \\ 0 & \cdots & \rho_6 \end{bmatrix}_{(6-k)\times(6-k)} \tag{1.10}$$

$$\mathbf{K}_1 = \begin{bmatrix} \mathbf{r}_1^T\mathbf{m}_1 & \mathbf{r}_1^T\mathbf{n}_1 & 0 & \cdots & 0 \\ \vdots & & \ddots & & \vdots \\ 0 & \cdots & 0 & \mathbf{r}_k^T\mathbf{m}_k & \mathbf{r}_k^T\mathbf{n}_k \end{bmatrix}_{k\times 2k} \tag{1.11}$$

with

$$\mathbf{r}_i = (\mathbf{s}_i - \mathbf{b}_i), \tag{1.12}$$

$$\mathbf{m}_i = \frac{\rho_{i,1}}{\mu_i}[(\mathbf{s}_i - \mathbf{a}_{i,2}) \times [(\mathbf{b}_i - \mathbf{a}_{i,1}) \times \mathbf{e}_i]], \tag{1.13}$$

$$\mathbf{n}_i = \frac{\rho_{i,2}}{\mu_i}[[(\mathbf{b}_i - \mathbf{a}_{i,1}) \times \mathbf{e}_i] \times (\mathbf{s}_i - \mathbf{a}_{i,1})], \tag{1.14}$$

$$\mu_i = [(\mathbf{s}_i - \mathbf{a}_{i,1}) \times (\mathbf{s}_i - \mathbf{a}_{i,2})]^T[(\mathbf{b}_i - \mathbf{a}_{i,1}) \times \mathbf{e}_i]. \tag{1.15}$$

The reader is referred to [25] for the detailed derivation of the velocity equations leading to the Jacobian matrices.

1.5 Proposed architecture and simplified model for the singularity analysis

A (6+2)-DOF kinematically redundant parallel robot is proposed in this work. The architecture of the robot is illustrated schematically in Figure 1.2a, while a physical model is shown in Figure 1.3 for better visualisation. The robot includes four non-redundant legs and two redundant legs. The geometric arrangement of the robot is akin to that of the Gough-Stewart platform with the attachment points of the non-redundant and redundant legs on the platform and the base located on the vertices of a square. The robot is shown in its reference configuration in Figure 1.2a (top view), where the fixed and moving reference frames coincide, except for an offset along the z axis. The singularity analysis of this robot can be performed using the formulation of the Jacobian matrix derived in Section 1.4. However, in order to simplify the singularity analysis, an alternative approach is used, in which a matrix that captures the singular behaviour is formulated. Here, singularities refer to poses (position and orientation) of the platform that are singular for any configuration of internal motion allowed by the kinematic redundancy. These configurations may also be referred to as inevitable singularities since they cannot be avoided using the kinematic redundancy. It should be emphasized that the matrix defined here and used for the singularity analysis is an alternative form of the Jacobian matrix $\mathbf{J}$ defined above, in which some of the lines might be scaled. Since applying a scaling factor to some of the lines of a matrix does not affect the singularity conditions, the alternative form of the Jacobian matrix nevertheless captures the singular behaviour of the robot and is used as a tool to simplify the determination of singularities. Indeed, referring to Figure 1.2a and given the architecture of the redundant legs, it is clear that the force applied on the platform by the redundant links is constrained to lie in a direction that is a linear combination of the directions of the two sub-legs. In other words, the redundancy of the leg can be used to select the direction in which the redundant leg applies a force to the platform, as long as this direction is in the plane formed by the sub-legs. Therefore, for the purpose of singularity analysis, an alternative form of matrix $\mathbf{J}$ is then constructed in which the force applied to the platform by a redundant leg is written as a linear combination of the two non-redundant legs replacing the given redundant leg in the mechanism of Fig. 1.2b. Indeed, because of the constraint introduced by the revolute joint at point S_i, the plane of motion of the redundant link can be described by the plane formed by the corresponding non-redundant legs in the mechanism of Fig. 1.2b. This formulation is now detailed.

Consider the architecture presented in Figure 1.2b. A fixed reference frame $R(O, x, y, z)$ and a mobile reference frame $R'(P, x', y', z')$ are defined. Vector $\mathbf{p}$ connecting the origin of the fixed frame O to the origin of the moving frame P describes the position of the platform in the fixed reference frame. The distance from the attachment points $B_i, i = 1, 2$ and $B_j, j = 3, \ldots, 6$ at the platform to point P is set to one unit for scaling purposes. The distance from the attachment points at the base, i.e., points $A_j,\ j = 3, \ldots, 6$, for the non redundant legs, and $A_{i,h},\ i = 1, 2,\ h = 1, 2$, for the sub-legs of a redundant leg, to point O is equal to $\sqrt{2}\beta$, where β is a scaling factor used to define the ratio between the base and the platform. Vector $\mathbf{a}_j$ is the constant position vector of point A_j expressed in the reference frame, whereas $\mathbf{b}'_j$ is the constant position vector of point B_j in the mobile frame. The same is said for vector $\mathbf{a}_{i,h}$ as

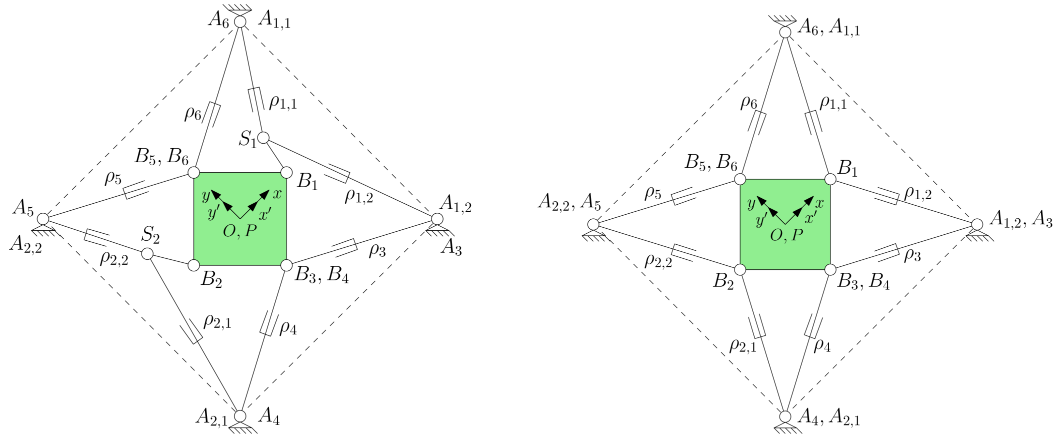

(a) (b)

FIGURE 1.2 – Top view of the proposed architecture with the nomenclature used in Section 1.4 (1.2a) and top view of a redundantly actuated architecture that is used as a geometric construction for singularity analysis purposes (1.2b).

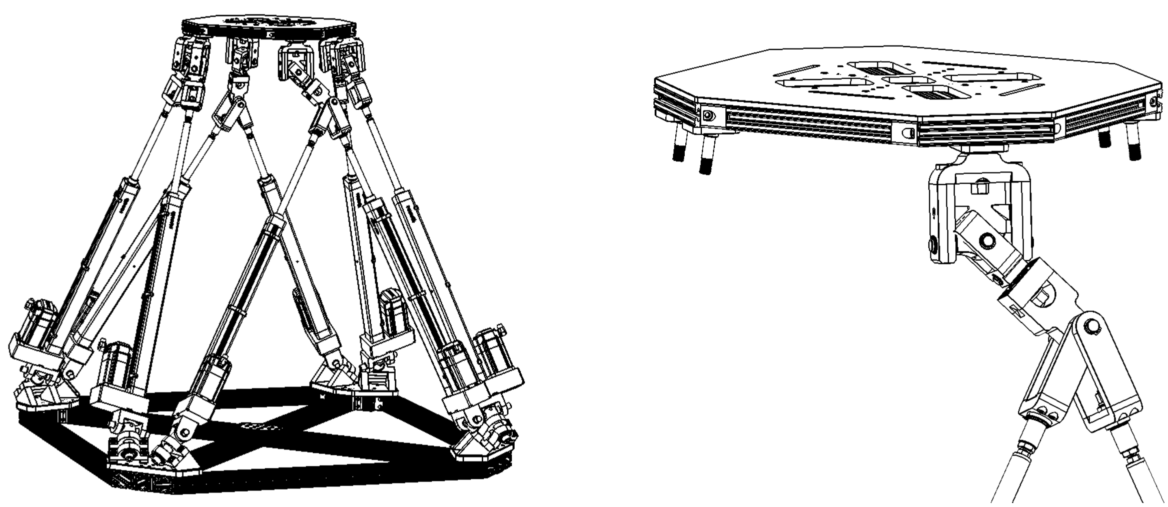

(a) CAD model of the proposed architecture. (b) Detailed view of a redundant link.

FIGURE 1.3 – Physical model of the presented architecture.

the constant position vector of point $A_{i,h}$ and for vector $\mathbf{b}'_i$ as the constant position vector of point B_i, expressed in the fixed and mobile reference frames respectively. These vectors are given by :

$$\mathbf{a}_6 = \mathbf{a}_{11} = [\beta, \beta, 0]^T, \quad \mathbf{a}_{12} = \mathbf{a}_3 = [\beta, \text{-}\beta, 0]^T, \quad \mathbf{a}_4 = \mathbf{a}_{21} = [\text{-}\beta, \text{-}\beta, 0]^T, \quad \mathbf{a}_{22} = \mathbf{a}_5 = [\text{-}\beta, \beta, 0]^T \tag{1.16}$$

$$\mathbf{b}'_1 = [1, 0, 0]^T, \quad \mathbf{b}'_2 = [\text{-}1, 0, 0]^T, \quad \mathbf{b}'_3 = \mathbf{b}'_4 = [0, \text{-}1, 0]^T, \quad \mathbf{b}'_5 = \mathbf{b}'_6 = [0, 1, 0]^T. \tag{1.17}$$

We also have in the fixed reference frame :

$$\mathbf{b}_i = \mathbf{p} + \mathbf{Q}\mathbf{b'}_i, \qquad i = 1, 2, \tag{1.18}$$

$$\mathbf{b}_j = \mathbf{p} + \mathbf{Q}\mathbf{b'}_j, \qquad j = 3, \ldots, 6, \tag{1.19}$$

where $\mathbf{b}_i$ and $\mathbf{b}_j$ are the position vectors of points B_i and B_j expressed in the fixed reference frame, and $\mathbf{Q}$ is the rotation matrix between the fixed and mobile reference frames. The convention of rotation used here is the one proposed in [47], namely the Tilt and Torsion representation. The choice of this convention for rotations is preferred over the classical ZYZ convention for robotic applications, because it facilitates the visualization of tilted orientations without any intrinsic torsion. The rotation matrix $\mathbf{Q}$ is written as

$$\mathbf{Q} = \begin{bmatrix} c(\phi)\,c(\theta)\,c(\psi) + s(\phi)\,s(\psi) & c(\phi)\,c(\theta)\,s(\psi) - s(\phi)\,c(\psi) & c(\phi)\,s(\theta) \\ s(\phi)\,c(\theta)\,c(\psi) - c(\phi)\,s(\psi) & s(\phi)\,c(\theta)\,s(\psi) + c(\phi)\,c(\psi) & s(\phi)\,s(\theta) \\ -s(\theta)\,c(\psi) & -s(\theta)\,s(\psi) & c(\theta) \end{bmatrix}, \tag{1.20}$$

where $c(\cdot)$ and $s(\cdot)$ stand for $\cos(\cdot)$ and $\sin(\cdot)$, and $\psi = \phi - \sigma$. Angles θ, σ, ϕ are respectively the tilt angle, the torsion angle, and the orientation of the axis around which the tilt rotation is performed.

As mentioned above, in the architecture proposed in this paper, four legs are non-redundant, and four others belong to two redundant legs. A redundant leg consists of two sub-legs joined together by a revolute joint with a common link attached to the platform by a spherical joint (Fig. 1.4).

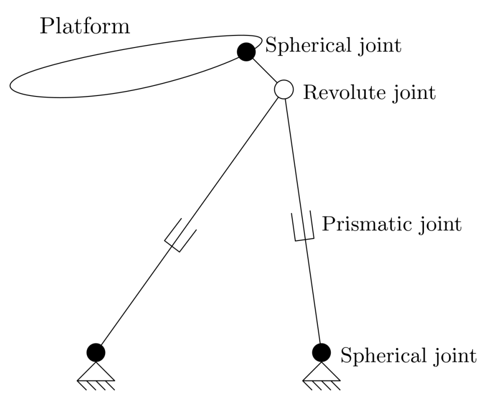

FIGURE 1.4 – Layout of a redundant leg.

The two sub-legs and the redundant link lie in the same plane. Thus, the forces applied by the redundant leg are transmitted to the platform via the common link. Because the lines of the Jacobian matrix are based on the Plücker coordinates of the forces applied to the platform, two of the six lines, associated with the redundant legs, can be represented as a linear combination of the Plücker coordinates of the sub-legs. The proposed architecture has the attachment points of the two redundant links at the platform on opposite sides of point P. According to the architecture presented (see Fig. 1.2a), we choose legs $\rho_3, \rho_4, \rho_5, \rho_6$ as non-redundant, and $\rho_{11}, \rho_{12}, \rho_{21}, \rho_{22}$ as the sub-legs of the two redundant legs. The construction of a matrix $\mathbf{J}'$ capturing the same conditions of singularity as the Jacobian matrix $\mathbf{J}$ from equation (1.8), i.e. their determinant vanishes for the same configurations of the platform, is then conducted. The four lines of matrix $\mathbf{J}'$ corresponding to the initial non-redundant legs are derived exactly as for the original Jacobian matrix $\mathbf{J}$ (see equations (1.1) and (1.2)). The two lines of the matrix corresponding to the direction of the redundant links are now expressed as a linear combination of the two lines connecting point B_i to the base attachment points of the sub-legs $A_{i,1}$ and $A_{i,2}$, as illustrated in the construction of Fig. 1.2b. It is pointed out that the expression of these lines of the matrix are equivalent, except for possibly a scaling factor. Indeed, the kinematically redundant legs constrain the redundant link to lie in the given plane but kinematic redundancy can be used to select any direction in that plane. One can then define matrix $\mathbf{J}'$ as

$$\mathbf{J}' = \begin{bmatrix} \mathbf{u}_1^T & (\mathbf{Q}\mathbf{b}'_1 \times \mathbf{u}_1)^T \\ \mathbf{u}_2^T & (\mathbf{Q}\mathbf{b}'_2 \times \mathbf{u}_2)^T \\ (\mathbf{b}_3 - \mathbf{a}_3)^T & (\mathbf{Q}\mathbf{b}'_3 \times (\mathbf{b}_3 - \mathbf{a}_3))^T \\ (\mathbf{b}_4 - \mathbf{a}_4)^T & (\mathbf{Q}\mathbf{b}'_4 \times (\mathbf{b}_4 - \mathbf{a}_4))^T \\ (\mathbf{b}_5 - \mathbf{a}_5)^T & (\mathbf{Q}\mathbf{b}'_5 \times (\mathbf{b}_5 - \mathbf{a}_5))^T \\ (\mathbf{b}_6 - \mathbf{a}_6)^T & (\mathbf{Q}\mathbf{b}'_6 \times (\mathbf{b}_6 - \mathbf{a}_6))^T \end{bmatrix}, \tag{1.21}$$

with

$$\mathbf{u}_1 = \cos\epsilon_1(\mathbf{b}_1 - \mathbf{a}_{11}) + \sin\epsilon_1(\mathbf{b}_1 - \mathbf{a}_{12}), \tag{1.22}$$

$$\mathbf{u}_2 = \cos\epsilon_2(\mathbf{b}_2 - \mathbf{a}_{21}) + \sin\epsilon_2(\mathbf{b}_2 - \mathbf{a}_{22}), \tag{1.23}$$

where ϵ_1, ϵ_2 are the kinematic redundancy parameters representing the possible reorientation of the common link of each redundant leg. Vectors $\mathbf{u}_1, \mathbf{u}_2$ represent the orientation of the force vectors from the linear combination of the forces direction exerted by the two sub-legs applied at the attachment points at the platform. These two vectors are constructed in order to capture the behaviour in force transmission of the redundant links. It is now clearly apparent that rows 1 and 2 of matrix $\mathbf{J}'$ are linear combinations of the directions corresponding to the plane defined by the sub-legs and therefore they capture the possible directions of the forces applied to the platform by the redundant legs. In order to visualize this feature in terms of Plücker vectors, one can rearrange matrix $\mathbf{J}'$ as

$$\mathbf{J}' = \begin{bmatrix} \cos\epsilon_1 \mathbf{v}_{11} + \sin\epsilon_1 \mathbf{v}_{12} \\ \cos\epsilon_2 \mathbf{v}_{21} + \sin\epsilon_2 \mathbf{v}_{22} \\ \mathbf{v}_3 \\ \mathbf{v}_4 \\ \mathbf{v}_5 \\ \mathbf{v}_6 \end{bmatrix}, \tag{1.24}$$

with

$$\begin{aligned} \mathbf{v}_{i,h} &= \left[(\mathbf{b}_i - \mathbf{a}_{i,h})^T \quad (\mathbf{Q}\mathbf{b}'_i \times (\mathbf{b}_i - \mathbf{a}_{i,h}))^T \right], i = 1,2 \quad h = 1,2, \\ \mathbf{v}_j &= \left[(\mathbf{b}_j - \mathbf{a}_j)^T \quad (\mathbf{Q}\mathbf{b}'_j \times (\mathbf{b}_j - \mathbf{a}_j))^T \right], \quad j = 3, \ldots, 6, \end{aligned} \tag{1.25}$$

where the linear combination of vectors $\mathbf{v}_{11}, \mathbf{v}_{12}$ and $\mathbf{v}_{21}, \mathbf{v}_{22}$, defining the vectors associated with the common links of the redundant legs appears more clearly. Vectors $\mathbf{v}_{i,h}$ and $\mathbf{v}_j$ are the Plücker vectors of the lines corresponding to the sub-legs of the redundant legs illustrated as non-redundant legs in the construction of Fig. 1.2b. It is recalled that equation (1.24) is equivalent to the Jacobian matrix $\mathbf{J}$ except for the fact that the magnitude of the vectors of lines 1 and 2 may be scaled. Nevertheless, the directions of the vectors characterized by the lines of matrix $\mathbf{J}'$, which are the same directions of the forces applied to the platform by the legs, are thus the same as those of the real Jacobian matrix. This results in matrices $\mathbf{J}'$ and $\mathbf{J}$ having the same singularity conditions, and simplifying the derivation of these conditions. In the next section, equation (1.24) is used to determine the singularity conditions for orientations with zero-torsion.

1.6 Singularity Analysis

As mentioned above, the Jacobian matrix $\mathbf{J}$ and matrix $\mathbf{J}'$ share the same conditions for singularity. An inevitable singular configuration is one for which, from equation (1.24), the determinant of $\mathbf{J}'$ vanishes for any value of the kinematic redundancy parameters, ϵ_1 and ϵ_2. In order to facilitate the determination of the singularities, the approach presented in [46] is adapted to the kinematically redundant robot. Applying the linear decomposition of the determinant [48] to equation (1.24), we can rearrange $\det(\mathbf{J}')$ as

$$\begin{aligned} \det(\mathbf{J}') = c(\epsilon_1)c(\epsilon_2) \left| \mathbf{v}_{11} \quad \mathbf{v}_{21} \quad \mathbf{v}_3 \quad \mathbf{v}_4 \quad \mathbf{v}_5 \quad \mathbf{v}_6 \right| + c(\epsilon_1)s(\epsilon_2) \left| \mathbf{v}_{11} \quad \mathbf{v}_{22} \quad \mathbf{v}_3 \quad \mathbf{v}_4 \quad \mathbf{v}_5 \quad \mathbf{v}_6 \right| \\ + s(\epsilon_1)c(\epsilon_2) \left| \mathbf{v}_{12} \quad \mathbf{v}_{21} \quad \mathbf{v}_3 \quad \mathbf{v}_4 \quad \mathbf{v}_5 \quad \mathbf{v}_6 \right| + s(\epsilon_1)s(\epsilon_2) \left| \mathbf{v}_{12} \quad \mathbf{v}_{22} \quad \mathbf{v}_3 \quad \mathbf{v}_4 \quad \mathbf{v}_5 \quad \mathbf{v}_6 \right|, \end{aligned} \tag{1.26}$$

$$\det(\mathbf{J}') = c(\epsilon_1)c(\epsilon_2)D_1 + c(\epsilon_1)s(\epsilon_2)D_2 + s(\epsilon_1)c(\epsilon_2)D_3 + s(\epsilon_1)s(\epsilon_2)D_4, \tag{1.27}$$

where $D_1, \ldots, D_4$ form together the linear decomposition of the determinant of $\mathbf{J}'$. Hence, it is clear that an inevitable singular configuration occurs when $D_i = 0, \;\; i = 1, \ldots, 4$, i.e., all four determinants defined in equation (1.26) are equal to zero simultaneously, because in such a situation the internal motion of the mechanism represented by parameters ϵ_1, ϵ_2 will be of no help to stay away from the singular configuration. The locus of inevitable singularities then consists of the intersection of four singularity loci, namely the loci defined by $D_1 = 0, \ldots, D_4 = 0$. For the standard Gough-Stewart platform, Fichter [49] described a singular configuration that can occur for any position of the platform, namely when the platform undergoes a rotation of $\pm 90^\circ$ around an axis orthogonal to the plane of the base, when the platform is parallel to the base. Therefore, we introduce two sub-types of inevitable singular configurations for our analysis, namely, the singular configurations that are independent from the position of the platform (they depend solely on orientation), and those that depend on orientation and position.

1.6.1 Singular configurations independent from the position

Applying the linear decomposition of the determinant on the Jacobian matrix of the general Gough-Stewart platform, Mayer St-Onge and Gosselin [46] obtained a general expression for its expansion. This linear decomposition may be applied to all four sub-determinants to obtain expressions written as

$$\begin{aligned} D_i = {} & F_{i,1}x^3 + F_{i,2}x^2y + F_{i,3}x^2z + F_{i,4}x^2 + F_{i,5}xy^2 + F_{i,6}xyz + F_{i,7}xy \\ & + F_{i,8}xz^2 + F_{i,9}xz + F_{i,10}x + F_{i,11}y^3 + F_{i,12}y^2z + F_{i,13}y^2 + F_{i,14}yz^2 \\ & + F_{i,15}yz + F_{i,16}y + F_{i,17}z^3 + F_{i,18}z^2 + F_{i,19}z + F_{i,20}, \qquad i = 1, \ldots, 4, \end{aligned} \tag{1.28}$$

where $F_{i,1}, \ldots, F_{i,20}$ with $i = 1, \ldots, 4$, are coefficients depending only on the orientation coordinates and the architecture parameters, and variables x, y, z are the Cartesian coordinates of the origin of the mobile frame. It may be seen that if $F_{i,1}, \ldots, F_{i,20}$ with $i = 1, \ldots, 4$, are all equal to zero simultaneously, then the mechanism is in a singular configuration independent from position coordinates and unavoidable with kinematic redundancy.

To simplify the upcoming derivation, the substitution of the tangent of the half-angle is used. Hence, this substitution is applied to the tilt and azimuth angles (θ, ϕ) of [47] which are now replaced by t_1, t_2, where

$$t_1 = \tan\frac{\theta}{2}, \qquad t_2 = \tan\frac{\phi}{2}. \tag{1.29}$$

The approach is rather straightforward and consists in finding the conditions for t_1, t_2 that make all 80 coefficients of the application of equation (1.28) to the four determinants $D_1, \ldots, D_4$ vanish. The strategy employed is to target the coefficient $F_{i,j}$, $j = 1, \ldots, 20$, among the 80 possible and non-zero coefficients with the simplest expression in t_1, t_2, so that its roots for these two angles are easily obtained. These roots are then the only conditions in t_1, t_2 that cancel this specific coefficient and so might cancel all the 80 coefficients simultaneously. Thus, the roots obtained in one variable (t_1 or t_2) are then substituted one at a time into the remaining coefficients to verify what additional conditions on the other variable (t_2 or t_1) make all of the non-zero remaining coefficients vanish. For example, one of the non-zero coefficients with the easiest form to work with is given by

$$F_{2,6} = \frac{256\beta^3 t_1^2 t_2 (t_2^2 - 1)}{(t_1^2 + 1)^2 (t_2^2 + 1)^2}. \tag{1.30}$$

Thus, independently from the expressions of the other coefficients, this specific coefficient vanishes for

$$t_1 = 0, \tag{1.31}$$

$$t_2 = 0, \tag{1.32}$$

$$t_2 = \pm 1, \tag{1.33}$$

$$t_1 \to \pm\infty, \tag{1.34}$$

$$t_2 \to \pm\infty. \tag{1.35}$$

Hence, to make all 80 coefficients equal to zero simultaneously, at least one condition among equations (1.31) to (1.35) must be met. Following this remark, each of the conditions from equations (1.31) to (1.35) are substituted one at a time into the remaining non-zero coefficients to evaluate if an additional condition on the second variable, t_1 or t_2 depending on the variable of the first condition, may cancel all coefficients. Applying this framework leads to equation (1.34) being the only condition among the five previously mentioned that may cancel all 80 coefficients with a second condition on variable t_2. These pairs of conditions are given by

$$\begin{aligned} &(t_1 \to \pm\infty, t_2 = 1 + \sqrt{2}), \qquad &(t_1 \to \pm\infty, t_2 = 1 - \sqrt{2}) \\ &(t_1 \to \pm\infty, t_2 = -1 + \sqrt{2}), \qquad &(t_1 \to \pm\infty, t_2 = -1 - \sqrt{2}) \end{aligned} \tag{1.36}$$

which correspond to a tilt angle of 180° around four specific axis orientations with respect to the y axis in the fixed reference frame, namely ±45° and ±135°. Indeed, when $t_1 \to \pm\infty$ is substituted into the remaining non-zero coefficients among the initial 80, all but two vanish. The last two non-zero coefficients are given by

$$F_{2,17} = \frac{32\beta^3 (t_2^4 - 6t_2^2 + 1)}{(t_2^2 + 1)^2}, \tag{1.37}$$

$$F_{3,17} = -\frac{32\beta^3 (t_2^4 - 6t_2^2 + 1)}{(t_2^2 + 1)^2}, \tag{1.38}$$

where it is easier to see that the second condition in variable t_2 to cancel all coefficients simultaneously is to have $t_2 = 1 \pm \sqrt{2}$ or $t_2 = -1 \pm \sqrt{2}$. All other first conditions of equations (1.31), (1.32), (1.33) and (1.35) lead to no other singularity locus.

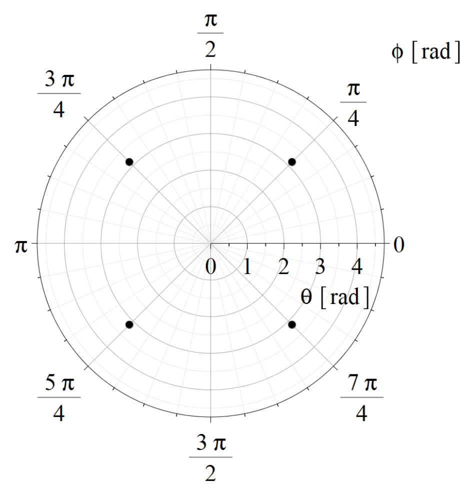

FIGURE 1.5 – Inevitable singularities (black dots) in tilted orientation independent from platform position.

Figure 1.5 emphasizes the fact that in tilted trajectories, singular configurations that are independent from the platform position are not really restrictive in practice. Indeed, the platform is theoretically able to be tilted by 180° in all directions before encountering a potential singularity. Such orientations of the platform could not be reached in practice due to mechanical interference. The singularities presented in Figure 1.5 may also be confirmed using a geometric approach, that is to say with Grassmann geometry, firstly introduced by Merlet [50] for parallel robots whose Jacobian matrices are based on Plücker vectors. Indeed, the above singular configurations correspond to condition 3b of the Grassmann analysis, in which four lines belong to the union of two pencils of lines that are not coplanar and that share a common line. In the proposed architecture, the condition occurs when the platform is in an orientation such that the line passing through points B_5, B_6 and B_3, B_4 is parallel to segments $\overline{A_3A_4}$ and $\overline{A_5A_6}$. Then, segment $\overline{B_{3,4}B_{5,6}}$ is the intersection of the two flat pencils of lines spanned by non-redundant legs $3, 4$ and $5, 6$. Any internal motion of the redundant mechanism cannot avoid this singularity.

1.6.2 Position dependent singular configurations

The determination of the position dependent inevitable singularities is based on the use of the resultant of polynomials. Consider the general univariate polynomials

$$P_1(x) = a_n x^n + \ldots + a_1 x + a_0, \tag{1.39}$$

$$P_2(x) = b_m x^m + \ldots + b_1 x + b_0, \tag{1.40}$$

with $n, m \neq 0$. The resultant of $P_1(x)$ and $P_2(x)$ for variable x is given by

$$\text{Resultant}(P_1, P_2, x) = a_n^m b_m^n \prod_{i,j} (\alpha_i - \beta_j), \tag{1.41}$$

where α_i is a root of polynomial $P_1(x)$, and β_j is a root of polynomial $P_2(x)$. The resultant vanishes if and only if $P_1(x)$ and $P_2(x)$ have at least one root in common. For example, the resultant of $P_1^*(x, y)$ and $P_2^*(x, y)$, with respect to variable x yields a polynomial in y, whose roots are the conditions on variable y for $P_1^*(x, y), P_2^*(x, y)$ to have at least one common root in x.

Expanding the coefficients $F_{i,1}, \ldots, F_{i,20}$, $i = 1, \ldots, 4$ for each of the determinants $D_1, \ldots, D_4$, we observe that all of these determinants are of degree 1 for variable x, degree 2 for variable y, and degree 2 (D_1, D_4) or 3 (D_2, D_3) for variable z. When all the $D_1, \ldots, D_4$ vanish, their four roots in x are equal. If x_i is the root in x of determinant D_i, then a necessary condition, but not yet sufficient, would be to have simultaneously $x_1 = x_4$ and $x_2 = x_3$. These pairs were chosen because D_1 and D_4 represent two arrangements of the legs of the architecture that show a certain symmetry, as well as the pair D_2, D_3. To obtain the above two necessary conditions, we apply the resultant with respect to variable x on the pairs D_1, D_4 and D_2, D_3, which is calculated from the determinant of their Sylvester matrix :

$$f(y, z, t_1, t_2) = \text{Resultant}(D_1, D_4, x) = \begin{vmatrix} d_{1,1} & d_{4,1} \\ d_{1,0} & d_{4,0} \end{vmatrix}, \tag{1.42}$$

$$g(y, z, t_1, t_2) = \text{Resultant}(D_2, D_3, x) = \begin{vmatrix} d_{2,1} & d_{3,1} \\ d_{2,0} & d_{3,0} \end{vmatrix}, \tag{1.43}$$

with

$$d_{i,1} = F_{i,5}y^2 + F_{i,6}yz + F_{i,7}y + F_{i,8}z^2 + F_{i,9}z + F_{i,10}, \qquad i = 1, \ldots, 4, \tag{1.44}$$

$$\begin{aligned} d_{i,0} = {} & F_{i,11}y^3 + F_{i,12}y^2z + F_{i,13}y^2 + F_{i,14}yz^2 + F_{i,15}yz \\ & + F_{i,16}y + F_{i,17}z^3 + F_{i,18}z^2 + F_{i,19}z + F_{i,20}, \qquad i = 1, \ldots, 4. \end{aligned} \tag{1.45}$$

However, to have at the same time $x_1 = x_4$ and $x_2 = x_3$, f and g must share a common root. Because f, g are of degree 2 in y and of degree 4 in z, we apply, in a similar manner, another resultant to f and g with respect to variable y, namely

$$h(z, t_1, t_2) = \text{Resultant}(f, g, y) = \begin{vmatrix} f_2 & 0 & g_2 & 0 \\ f_1 & f_2 & g_1 & g_2 \\ f_0 & f_1 & g_0 & g_1 \\ 0 & f_0 & 0 & g_0 \end{vmatrix}, \tag{1.46}$$

where f_i and $g_i, i = 0, 1, 2$, are the coefficients of the powers i of variable y in expressions $f(y, z, t_1, t_2)$ and $g(y, z, t_1, t_2)$. Figure 1.6 shows the complete diagram of the resultant's application over the determinants expressions. From equation (1.46), we see that the roots of

$h(z, t_1, t_2)$ give the conditions for which $f(y, z, t_1, t_2)$ and $g(y, z, t_1, t_2)$ share a common root in variable y, such that substituted in $D_1, \ldots, D_4$ gives simultaneously $x_1 = x_4$ and $x_2 = x_3$. One must then verify the last condition so that $x_1 = x_2 = x_3 = x_4$ to obtain all the requirements for an inevitable singularity. The detailed expressions of equations (1.42),(1.43) and (1.46) are given in Appendix A.

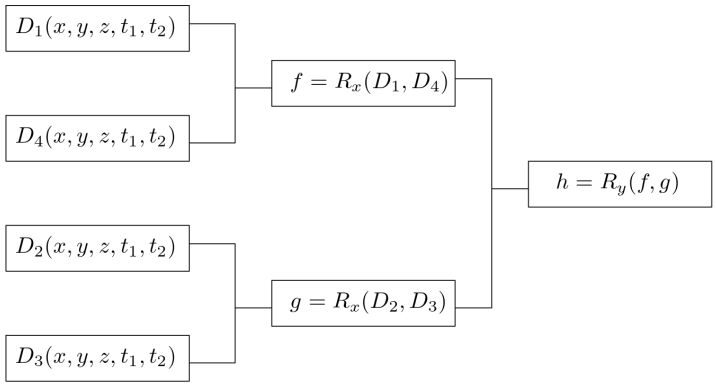

FIGURE 1.6 – Cascaded application of the resultant on the polynomials.

From equation (1.46), one can obtain that the roots of $h(z, t_1, t_2)$ for $\beta > 1$ are

$$z_1 = \frac{4t_1t_2}{(t_1^2+1)(t_2^2+1)}, \tag{1.47}$$

$$z_2 = -\frac{4t_1t_2}{(t_1^2+1)(t_2^2+1)}, \tag{1.48}$$

$$z_3 = \frac{2t_1\left((\beta-1)t_2^4 + (-6\beta-2)t_2^2 + \beta - 1\right)}{\sqrt{3t_2^4 - 2t_2^2 + 3}(t_2^2+1)(t_1^2+1)}, \tag{1.49}$$

$$z_4 = -\frac{2t_1\left((\beta-1)t_2^4 + (-6\beta-2)t_2^2 + \beta - 1\right)}{\sqrt{3t_2^4 - 2t_2^2 + 3}(t_2^2+1)(t_1^2+1)}, \tag{1.50}$$

$$t_1 = 0, \tag{1.51}$$

$$t_2 = -1, 0, 1. \tag{1.52}$$

It is pointed out that none of the denominators of the roots in z can vanish for values of t_1, t_2 in $\mathbb{R}$. Substituting z_1 in equations (1.42) and (1.43) leads to a unique root in y in f and g which is

$$y_1 = \frac{(t_1^2+1)(\beta-1)t_2^4 + ((2\beta+6)t_1^2 + 2\beta - 2)t_2^2 + (t_1^2+1)(\beta-1)}{(t_2^2+1)^2(t_1^2+1)}. \tag{1.53}$$

Substituting z_1 and y_1 in $D_1, \ldots, D_4$ makes all four expressions equal to zero, independently from the value of x. Proceeding the same way with z_2 leads to the negative of equation (1.53). This locus of inevitable singularities is presented in Figure 1.7 for $\beta = 2$.

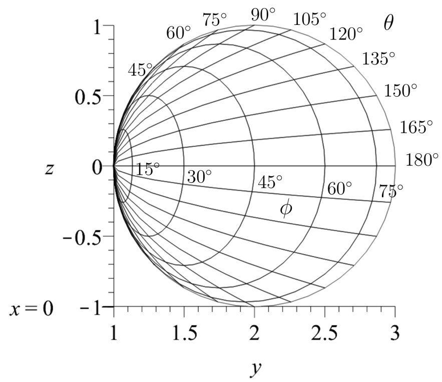

FIGURE 1.7 – Singularity Locus described by equations (1.47) and (1.53).

Figure 1.7 is a representation of the singularity locus described by equations (1.47) and (1.53), independent from the position along the x axis, which are parameterized by the tangent of the half-angles of tilted orientation. The shape of this singularity locus in the Cartesian space is a pair of solid cylinders whose longitudinal axis is in the plane $z = 0$ and parallel to the x axis of the fixed referential frame. The cylinders are symmetrical with respect to the xz plane. A section of this locus is presented in Fig 1.7 for $x = 0$. Inside the disk-shaped section of the locus in the Cartesian space appears graduation marks for the orientation variables (ϕ, θ). To each pair of spatial coordinates (y, z) of the locus corresponds a pair of angular coordinates in tilt (ϕ, θ) that leads to a singular configuration. However, one may verify that this type of singularity places the platform in a configuration such that the attachment point of two adjacent non-redundant legs at the platform is on the line passing through their attachment points at the base. In other words, the two adjacent non-redundant legs are colinear in the base plane. This configuration may be easily avoided by design, for instance, by having the minimum length of all legs longer than β units.

Next, replacing z_3 from equation (1.49) into equations (1.42) and (1.43), and solving for y yields four roots, two for each resultant, namely y_1, y_2 for $f(y, z, t_1, t_2)$ and y_3, y_4 for $g(y, z, t_1, t_2)$. It is easily noted that y_1 and y_3 are the two equal roots of f, g under $z = z_3$ given by

$$y_{1,3} = \frac{8t_2\left(((-\frac{1}{4}+\beta)t_2^4 + (-2\beta - \frac{1}{2})t_2^2 + \beta - \frac{1}{4})t_1^2 + \frac{(\beta+\frac{1}{2})(t_2^2+1)^2}{2}\right)}{\sqrt{3t_2^4 - 2t_2^2 + 3}(t_2^2+1)^2(t_1^2+1)}. \tag{1.54}$$

Back substituting again $y = y_1 = y_3$ and $z = z_3$ into the four determinants leads to $x_1 = x_4$ and $x_2 = x_3$, but not yet $x_1 = x_2 = x_3 = x_4$. The additional condition to get $x_1 = x_2 = x_3 = x_4$ is not achievable in $\mathbb{R}$ for t_1, t_2. Thus, the determinants $D_1, \ldots, D_4$ do not all vanish for a common root in x. However, one may see that the back substitution of $y = y_1 = y_3$ and $z = z_3$ brings common roots in t_2 for the pairs D_1, D_4 and for D_2, D_3, but distinct from one pair to the other. This means that while D_1 and D_4 may be cancelled for their common root in x, D_2 and D_3 may simultaneously be cancelled for their common root in t_2, and vice versa. Yet, any of the roots of t_2 of D_1, D_4 or D_2, D_3 substituted into the expression of z_3 leads to a global maximum of one unit for coordinate z. This means that for these singular configurations to occur, the platform is always at an elevation lower than one unit, which is a region of poor interest. The surface given by the expression of z under this singularity is shown in Figure 1.8. Furthermore, it can be observed that this singularity brings two legs coplanar to the base plane for any value of the scaling factor $\beta \neq 1$.

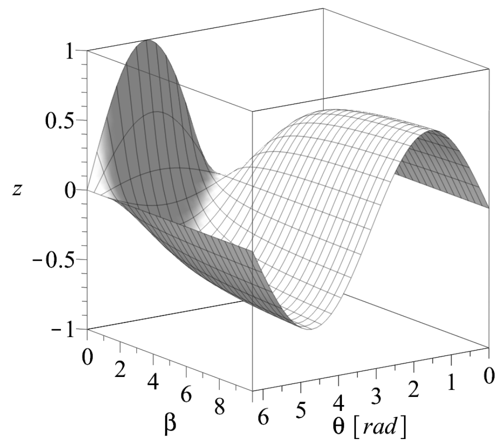

FIGURE 1.8 – Surface plot of z_3 from equation (1.49) under the corresponding conditions of singularity.

The last condition to investigate with $z = z_3$ is the case when $y_2 = y_4$. The equation is verified for the additional condition $t_2 = \pm 1 \pm \sqrt{2}$, but the rest of the development leads to a specific instance of the derivation with $z = z_{1,2}$, and will not be expanded here. Also, the derivation for $z = z_4$ yields results similar to those obtained for $z = z_3$.

The following roots of equation (1.46), namely equations (1.51) and (1.52), are associated with specific tilt orientations. The root $t_1 = 0$, a tilt angle of zero degree, refers to the platform being parallel to the base, and in this case, the singularity occurs only if $z = 0$, which has no practical purpose. The root $t_2 = 0$, the angle describing the axis with respect to the y axis in the fixed reference frame around which the platform is tilted, leads to one singularity locus of significance :

$$z = \frac{2t_1(\beta - 1)}{t_1^2 + 1}, \qquad x = -\frac{t_1^2 + 2\beta - 1}{t_1^2 + 1}, \qquad y = 0, \tag{1.55}$$

$$z = -\frac{2t_1(\beta - 1)}{t_1^2 + 1}, \qquad x = \frac{t_1^2 + 2\beta - 1}{t_1^2 + 1}, \qquad y = 0. \tag{1.56}$$

This locus is represented in Figure 1.9. The singular configurations of the platform are parameterized by the tilt angle θ when $y = \phi = 0$. Though this locus may appear dangerous because the value of z is not constrained to be lower than one unit, this singularity implies two pairs of legs being superimposed, a configuration that is mechanically unreachable. Indeed, one could substitute respectively (1.55) and (1.56) into (1.25) and observe that

$$\mathbf{v}_4 = \frac{\beta - 1}{\beta}\mathbf{v}_{21}, \qquad \mathbf{v}_5 = \frac{\beta - 1}{\beta}\mathbf{v}_{22}, \tag{1.57}$$

$$\mathbf{v}_6 = \frac{\beta - 1}{\beta}\mathbf{v}_{11}, \qquad \mathbf{v}_3 = \frac{\beta - 1}{\beta}\mathbf{v}_{12}. \tag{1.58}$$

It is now clear that this singular configuration requires two non-redundant legs to be colinear with the two sub-legs of a redundant leg. More specifically, two non-redundant legs intersect at the attachment point at the platform of a redundant link while being coplanar with the plane of the redundant leg. Thus, whatever the orientation of the redundant link, three Plücker vectors will form a planar pencil of lines. Using Grassmann analysis described by Merlet [50], the singular condition 2 is fulfilled in these circumstances. The locus is depicted in Fig. 1.9, where the mechanism is shown in a side view at a home position — and not in the just presented singular configuration — to expose the scaling of the singularity locus with respect to the mechanism. To lie in the singular configuration, point P of the platform must remain on the circular curves of Fig. 1.9, in the plane $y = 0$, with the corresponding tilt angle θ. Equations (1.55) and (1.56) prescribe the x and z coordinates of this singularity locus as functions of the tilt angle and scaling parameter β.

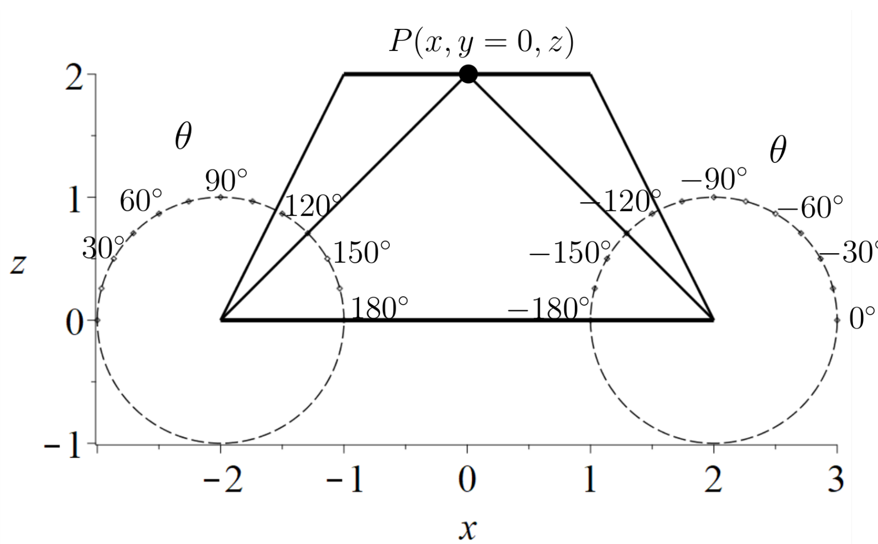

FIGURE 1.9 – Singularity locus represented by equations (1.55) and (1.56) (left and right circle respectively) for $\beta = 2$ in the xz plane.

While the singular locus represented in Figure 1.9 may not be reachable in practice due to mechanical interference, it can still be approached, resulting in potentially undesirable large efforts in the joints, thus making the analytical expressions of the locus relevant.

The last two roots of equation (1.46), namely $t_2 = \pm 1$, lead to another singularity locus of the form

$$y = \pm \frac{(\beta + 1)\, {t_1}^2 + \beta - 1}{{t_1}^2 + 1}, \tag{1.59}$$

$$z = \pm \frac{2t_1}{t_1^2 + 1}, \tag{1.60}$$

which places again the z coordinate of the platform at a maximum value of one unit for all t_1.

1.7 Discussion on the Singularity Locus

In Section 1.6, the methods to analyze the singularity conditions of the (6+2)-DOF kinematically redundant manipulator were introduced and the results were presented. Concerning the singular configurations that are independent from the platform's position (equation (1.36)), it was shown that a tilt angle of 180° is necessary to reach such singular pose. However, because of the architecture of the manipulator, mechanical interferences prevent such rotations at the platform. We consider this inevitable singularity to be out of the reachable workspace. The singularity locus associated with equations (1.47) and (1.48) implies two non-redundant legs of the mechanism being coplanar with the base plane, which is rejected. While the singular configurations corresponding to equations (1.49) and (1.50) may be located inside the reachable workspace, the elevation of the platform always remains below one unit, for all values of the tilt angles and scaling factor β. Moreover, it can be observed that, again, this singular configuration brings two non-redundant legs in the plane of the base, which is rejected. As long as the distance between the reference point on the platform and the base plane is larger than one unit ($z > 1$), which is very low considering the scaling of the mechanism, it can be guaranteed that the robot is far from possible singular configurations. In cases where it would be desired to operate the robot below this limit, it is still possible to find analytical expressions characterizing the singularity locus. Next, singular configurations corresponding to equation (1.51) are of no interest because they require the platform to be coplanar with the base. Finally, the singularity locus described by the condition of equations (1.55) and (1.56) is pratically unreachable because of mechanical interferences, but it may be approached, resulting in large forces in the legs. Mathematical expressions describing this locus are then necessary to stay away from the locus during the path planning stage. Thereby, with all the singular configurations that are mathematically correct for the particular architecture proposed in this paper, we may suggest that for a workspace with zero torsion, the conditions for singularities lie either outside of the reachable workspace due to mechanical interference, or at an elevation of the platform that is considered of poor interest for most applications. Thus, we note that for the particular architecture presented, having only two redundant degrees of freedom greatly enhances the performance of the GS platform for tilted trajectories.

In a general perspective, the chosen approach to derive the conditions for singularity had the benefit of dissociating the singular configurations dependent from position coordinates from those that are not, although the results of the latter may be obtained with the analysis of the former. Secondly, the use of the linear decomposition of the determinant of the alternative Jacobian matrix $\mathbf{J}'$ fragments the initial system of one equation into a system of four nonlinear equations to be simultaneously satisfied, which facilitates the further derivation. Lastly, the strategic application of the resultant of polynomials eliminates a Cartesian variable at each step and makes it possible in most cases to parameterize independently the x, y, z coordinates of a singular locus in the orientation variables t_1 and t_2, which is easier to interpret than an implicit equation.

1.8 Path planning

Usually, the path planning for kinematically redundant manipulators [51] is conducted using

$$\dot{\boldsymbol{\theta}} = \mathbf{J}^I \mathbf{t} + (\mathbf{I} - \mathbf{J}^I \mathbf{J})(-u \frac{\partial \eta}{\partial \boldsymbol{\theta}}), \tag{1.61}$$

with $\dot{\boldsymbol{\theta}}$, the joint velocity vector, $\mathbf{J}^I$, the generalized inverse of Jacobian matrix $\mathbf{J}$, $\mathbf{I}$, the identity matrix, u, a scaling constant and $-\frac{\partial \eta}{\partial \boldsymbol{\theta}}$, the gradient of an objective function $\eta(\boldsymbol{\theta})$. However, this approach does not guarantee that mechanical limitations and interference are avoided, even if the objective function $\eta(\boldsymbol{\theta})$ is a distance to such mechanical limits. Thus, a numerical method is preferred in this work for path planning, where a performance index, the singularity locus and the mechanical limitations are functions of the orientation of the redundant links. It is then possible to elaborate algorithms for path planning that include more faithfully such mechanical constraints.

1.8.1 Mechanical limitations

The redundancy resolution in the redundant parameters space has to take into account the maximum and minimum lengths of the sub-legs as well as the possible mechanical interference between the redundant leg, the spherical joint and the platform. Figure 1.10 illustrates the limits of an angle γ ($\gamma_{lim,lower}$) due to the maximum length of a sub-leg ($\rho_{i1,max}$) for a given position of point B_i, $i = 1, 2$ (a given pose of the platform).

Without loss of generality, consider the mechanical limits in actuator length of sub-leg $\rho_{i,1}$. Let $\mathbf{r}_{i1}$ be the vector from point B_i to A_{i1}, and r_{i1}, its norm. A mechanical limit restricts angle γ due to ρ_{i1} if $\rho_{i1,max} < r_{i1} + l$ or if $\rho_{i1,min} > r_{i1} - l$, where l is the length of the redundant

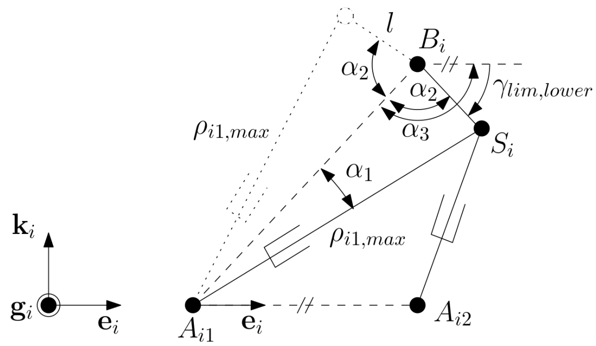

FIGURE 1.10 – Mechanical limit of a sub-leg.

link. In that case, with the law of cosines, one can write

$$\rho_{i1,max}^2 = r_{i1}^2 + l^2 - 2lr_{i1}\cos\alpha_2, \tag{1.62}$$

$$\cos\alpha_2 = \frac{r_{i1}^2 + l^2 - \rho_{i1,max}^2}{2lr_{i1}}. \tag{1.63}$$

The same calculation may be conducted for a limitation due to $\rho_{i1,min}$. Also, one can obtain

$$\cos\alpha_3 = \frac{\mathbf{e}_i \cdot \mathbf{r}_{i1}}{||\mathbf{e}_i||||\mathbf{r}_{i1}||}. \tag{1.64}$$

Thus, in order to respect the limitation in maximum length of a sub-leg (i.e., $\rho_{i1,max}$), the lower and upper values of γ are given by

$$\gamma_{lim} = \alpha_3 \pm \alpha_2. \tag{1.65}$$

Similar expressions can be obtained for the minimum length of a sub-leg ($\rho_{i1,min}$). Concerning the mechanical interference between a sub-leg and the spherical joint or the redundant link and the platform, the reader is referred to [42] due to space limitation. A reference frame ($\mathbf{e}_i, \mathbf{k}_i, \mathbf{g}_i$) with $\mathbf{g}_i$ being normal to the plane of the two sub-legs is defined to easily express vector $\mathbf{s}_i$ in the fixed reference frame from angle γ_i. This transformation is obtained with

$$\mathbf{g}_i = \frac{\mathbf{e}_i \times (\mathbf{b}_i - \mathbf{a}_{i1})}{||\mathbf{e}_i \times (\mathbf{b}_i - \mathbf{a}_{i1})||}, \tag{1.66}$$

$$\mathbf{k_i} = \frac{\mathbf{g}_i \times \mathbf{e}_i}{||\mathbf{g}_i \times \mathbf{e}_i||}, \tag{1.67}$$

$$\mathbf{s}_i = \mathbf{b}_i + l_i\cos\gamma_i\mathbf{e}_i - l_i\sin\gamma_i\mathbf{k}_i. \tag{1.68}$$

In the next sub-section, the results for the path planning are presented. Because the main objective is to assess the capabilities of singularity avoidance in the mechanism, only mechanical limitations due to mechanical interference and minimum/maximum lengths of the legs that constrain the possible orientations of the redundant links were implemented in the redundancy resolution. In order to consider mechanical limitations associated with joints minimum/maximum velocities, a framework is found in [42] and [51].

1.8.2 Performance index

The kinematic redundancy yields infinitely many solutions to the inverse kinematic problem. Hence, one may exploit this feature to stay away from singularities along a given Cartesian trajectory. It is known that approaching a singular configuration results in high force/torque in the actuators. Thus, the redundancy resolution consists here in following the minimum value of a force index in the actuators while abiding by the mechanical limitations. From the kinematic-static duality, one can write

$$\boldsymbol{\tau} = \mathbf{K}^T \mathbf{J}^{-T} \mathbf{w}, \tag{1.69}$$

which describes the relation between the efforts (forces and moments) applied on the platform, $\mathbf{w}$, and the forces/torques at the actuators, $\boldsymbol{\tau}$, for a general parallel manipulator. Kinematic redundancy permits changes in matrices $\mathbf{K}, \mathbf{J}$, thus distributing differently the efforts applied on the platform to the legs. Many approaches can be chosen for the redundancy resolution. One could find the coordinates $\boldsymbol{\gamma} = [\gamma_1, \ldots, \gamma_k]$ such that the Euclidean norm of $\boldsymbol{\tau}$ is minimal. Another approach could be to choose $\boldsymbol{\gamma}$ so that the maximum component of $\boldsymbol{\tau}$ is the farthest from a certain threshold (infinity norm). Yet another approach would be to minimize the maximum norm of a row of matrix $\mathbf{K}^T \mathbf{J}^{-T}$, in other words, the minimization of the force transmission index [42]. This last method was applied for the redundancy resolution of the path planning presented in this paper.

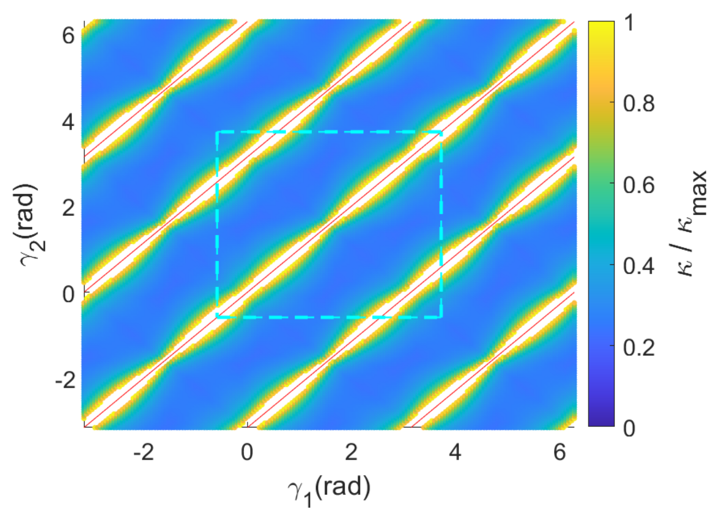

FIGURE 1.11 – Singularity locus in the redundant parameters space.

Figure 1.11 exposes the singularity locus (red curves) in the space of the redundant parameters (namely γ_1, γ_2) for the first step of a path with a tilt angle of 80°. The full animation of the path planning is available in the multimedia extension of the article. The dashed cyan box refers to the most restrictive limits on angles γ_1, γ_2 due to the different types of mechanical interference presented above. The coloring represents the ratio between the maximal force transmission index of matrix $\mathbf{K}^T\mathbf{J}^{-T}$, κ, over the maximum force index of an actuator, κ_{max}. This last index is the ratio between the maximum force produced by an actuator over the payload carried by the platform. For this application, actuators capable of providing 5200 N and a payload of 75 kg whose centre of mass is located 0.3 m above the plane passing through the spherical joints at the platform are used. The path consists in tilting the platform from 0° to 80° around an axis parallel to the reference frame x axis (see Fig. 1.2a), and then rotating this axis from 0° to 360° before tilting back the platform from 80° to 0°. Also, the planned path for the full tilt rotation was defined by a polynomial of degree five to guarantee the continuity up to the second degree between the three steps of the path. The path is conducted at a fixed Cartesian point, $[0, 0, 1.75]$m. The scaling factor β used is equal to 2.25 and the unit is set to 0.35 m. The path has continuous profile in angular position, velocity and acceleration for the tilt and azimuth angles. The animation of the path planning in the multimedia extension shows the redundant links orientation chosen (red star) in the space of redundant parameters over path progression in order to minimize the force transmission index while remaining inside the boundary imposed by mechanical interference (cyan dashed boxes). The algorithm used for this task is simply a gradient descent of the performance index along the closest neighbors in γ_1, γ_2 space while respecting the mechanical constraints defined in the same space. For the specific path chosen, the forces in the eight actuators to support the inertia of the payload during the path are shown in Figure 1.12.

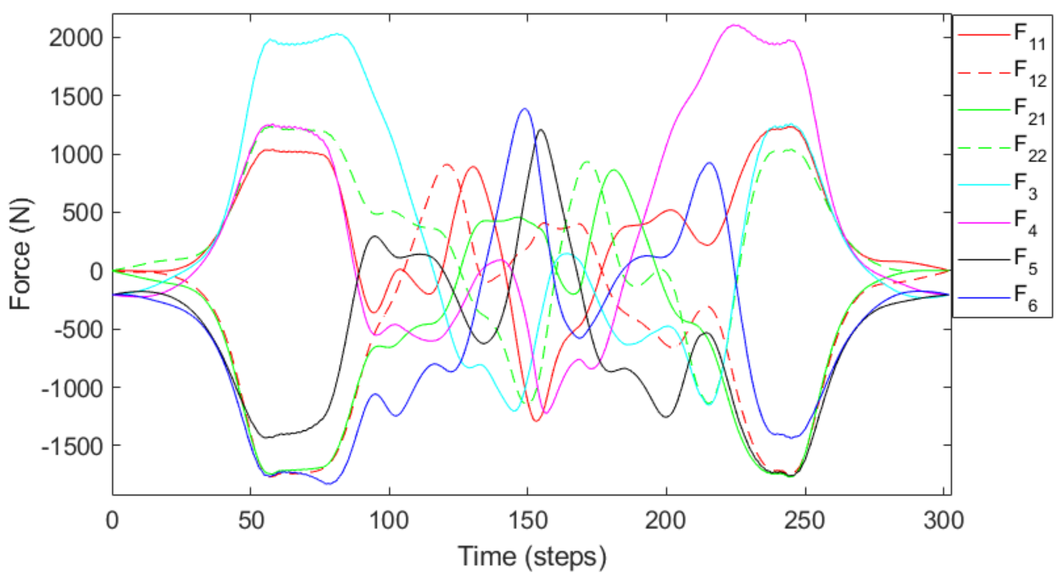

FIGURE 1.12 – Forces in the actuators along the 80° tilt path.

From Fig. 1.12, the profile of the actuator forces emphasizes the fact that the platform does not approach singular configurations along the path with a tilt angle of 80° of the platform in every direction. Indeed, the forces in the actuators never exceed three times the weight of the platform payload. It is also interesting to observe a certain symmetry in the force profile of the actuators, mainly due to the symmetry of the architecture added to the symmetry of the path. Finally, the smoothness of the path planning is confirmed by the profiles of the forces in the actuators.

1.9 Conclusion

The primary objective of this paper was to study the impact of having two redundant DOFs —instead of three, as proposed in [25]— in a slightly different architecture, on the orientational workspace for zero torsion of a GS-like platform. The kinematic equations were recalled, as well as the derivation of the Jacobian matrices **J** and **K**. A simplified model of the architecture with the same condition of singularities was proposed in order to facilitate its analysis. Then, the singular locus was partitioned into two sub-types of singular configurations. The analysis showed that, for zero-torsion trajectories, the proposed architecture has only four specific orientations of inevitable singularities independent from position. However, these orientations require the platform to be tilted by 180°, which is not limiting in a practical sense, because mechanical interference will occur prior to these singular configurations. The other mathematically possible singular configurations were shown to be either of no interest because of the position of the platform in the workspace, or mechanically unreachable. Indeed, the only singular locus that may be approachable requires a tilt angle of the platform of more than 90° above the area bounded by attachment points at the base of the legs (referring to Fig. 1.9). Hence, the singularity analysis of the proposed mechanism suggests that the orientational workspace is still greatly enhanced for zero-torsion trajectories compared to a standard Gough-Stewart platform, for which the maximum reachable tilt angle is close to 45° [25], even with only two kinematically redundant DOFs. Finally, path planning was conducted for a 80° tilt angle of the platform while respecting the mechanical limitations and force limitations of the actuators for a large payload to visualize the avoidance of singular configurations. For application purposes, tasks that are accomplished with axisymmetric tools at the end-effector, for example, welding of machining, do not require torsion rotations. Thus, these applications would find much interest for the proposed mechanism due to its performances of singularity avoidance in tilted orientations. Moreover, the torsion rotation could even be implemented directly at the end-effector for certain application objectives such as motion simulation, at the cost of affecting the parallel nature of the mechanism. Future work will concentrate on the development of a prototype as well as on the derivation of the singular locus of the mechanism with non-zero torsion to fully observe the impact of having two redundant DOFs instead of three.

1.10 Multimedia extension

A video named "80degrees_TiltedTrajectory.mp4" is given with the electronic version of the article. This short video is an animation of a simulated path planning for zero torsion of the end-effector, with a tilt orientation of 80 degrees. In the animation, the red star represents the choice of redundant angles γ_1 and γ_2 according to a gradient descent of a performance index, while respecting the mechanical limits of the mechanism (dashed cyan boxes) and the singularities (red curves) along the path.

1.11 Acknowledgment

The authors would like to thank the Natural Sciences and Engineering Research Council of Canada (NSERC), the Fonds de Recherche du Québec Nature et Technologie (FRQNT, grant number : 302763) and the Chaire de Recherche du Canada en Robotique et Mécatronique for their financial support during the presented work. The authors also wish to thank M. Mathias Bourgault for his help with the preparation of the CAD model of Figure 1.3.

1.12 Declaration of Interests

The authors declare no conflict of interests with third parties or organizations of any kind.

Chapitre 2

Singularity Analysis of a Kinematically Redundant (6+2)-DOF Parallel Mechanism for General Configurations

2.1 Résumé

Les mécanismes parallèles souffrent de singularités de type II qui réduisent leur espace utile de travail en orientation. Ajouter la redondance cinématique dans ces mécanismes agrandit leur espace de travail en leur fournissant des capacités d'évitement de singularités. Cependant, un nombre croissant de degrés de liberté (DDLs) cinématiquement redondants requiert des actionneurs supplémentaires et peut rendre la résolution de la redondance plus complexe. De plus, des exemples existent dans la littérature dans lesquels un nombre minimal de DDLs redondants sont utilisés afin de produire un espace de travail libre de singularités pour un mécanisme plan. Dans ce travail, l'architecture d'un mécanisme parallèle cinématiquement redondant à (6+2)-DDLs est étudiée et son lieu de singularité est déterminé. Les résultats montrent que, même si certaines singularités demeurent toujours à l'intérieur de l'espace atteignable du mécanisme, celles-ci peuvent être localisées précisément à l'aide d'expressions mathématiques simples pour des besoins de planification de trajectoire.

2.2 Abstract

Parallel mechanisms suffer from type II singularities which reduce their useful orientational workspace. Adding kinematic redundancy in parallel mechanisms enhances their orientational workspace by providing singularity avoidance capabilities. However, an increasing number of kinematically redundant degrees of freedom (DOFs) requires additional actua-

tors and makes the redundancy resolution more complex. Moreover, examples in the literature exist where a minimal number of kinematically redundant DOFs was used to produce a singularity-free orientational workspace for planar mechanisms. In this work, the architecture of a kinematically redundant (6+2)-DOF parallel mechanism akin to the well-known Gough-Stewart platform is studied, and its singularity locus is derived. The results show that, while some singularities still remain in the useful workspace of the mechanism, they can be accurately localized with simple closed-form analytical expressions for trajectory planning purposes. Furthermore, the redundancy resolution may find itself easy to handle, since the avoidable singularities and mechanical interference can be mapped into the 2-D space of the redundant parameters. Finally, the proposed architecture is considered as a compromise between obtaining a singularity-free workspace and handling easily the redundancy resolution for the trajectory planning.

2.3 Introduction

Parallel mechanisms have attracted much attention in the past decades due to their dynamic performances and their load carrying capacity advantages over their serial counterparts [50]. The main restriction to such interesting features is the presence of singularities inside their workspace. These singular configurations come in three types [15], where the first two are defined here. Type I singularities imply that nonzero joint velocity vectors produce a null Cartesian velocity vector, and happen typically at the boundary of the workspace. Type II singularities occur when, for a null joint velocity vector, the Cartesian velocity vector is nonzero. In type II singular configurations, the end-effector may not resist some forces and moments, and the control of the mechanism is lost. Two approaches are generally used to avoid singular configurations at the design stage, namely, actuation redundancy and kinematic redundancy [28]. While both approaches successfully reduce the singular configurations in parallel mechanisms [52; 53], they also have their own limitations.

On one hand, actuation redundancy induces antagonistic forces in the mechanism because there are more actuators than the number of degrees of freedom (DOFs), resulting in a more challenging control, but it allows the modulation of the stiffness in the mechanism. In [34] for example, a device to measure the internal forces in the redundantly actuated planar parallel mechanism had to be designed to facilitate its control. In [31], the problem of minimal independent coordinates mode switching in the command of redundantly actuated parallel mechanisms was addressed with a solution that includes a formulation of the dynamic model of the mechanism by its n redundant coordinates.

On the other hand, kinematic redundancy brings internal motion in the mechanism due to its number of DOFs being higher than that required at the end-effector, resulting in easier control. However, in this case, the redundancy resolution becomes more difficult with an increasing number of kinematically redundant DOFs. Despite this last issue, great progress has been recently presented with kinematically redundant parallel mechanisms, due to their capability to enhance their singularity-free workspace [54; 27; 41]. In [27; 38; 39], a kinematically redundant parallel mechanism with full rotability is presented. In [41], [24], [25] and [42] for example, kinematically redundant parallel mechanisms with (6+3)-DOF were presented, each with a workspace exempt of singular configurations. It is even discussed in [24] and [40] to operate a gripper with a kinematically redundant degree of freedom.

While in [26; 55] the authors proposed a kinematically redundant (3+3)-DOF planar parallel mechanism proven to avoid all type II singularities, the authors of [27] presented a kinematically redundant (3+1)-DOF planar parallel mechanism with the same capability of singularity avoidance, plus a very simple redundancy resolution. In this work, it is thus of interest to investigate the effect of the withdrawal of one kinematically redundant DOF out of three on the presence of singularity of type II for a parallel mechanism whose architecture is similar to the one presented in [25].

The analysis of singular configurations is of paramount importance while designing a parallel mechanism. In [44; 45], a geometric method based on instantaneous centre of rotation was proposed. In [56], the singular value decomposition was used for the physical interpretation and analytical formulation of the singularities. In [57; 58; 35], screw theory was employed to approach the singularity analysis, while in [59], the Linear Implicitization Algorithm (LIA) and the Study kinematic mapping were preferred. In [60], a kinematically redundant (3+3)-DOF parallel robot was divided into two sub-mechanisms in order to facilitate the singularity analysis. In [61], the constant orientation singularity surfaces were investigated when transformed into a characteristic plane corresponding to the plane of the platform.

In a recent work [62], a method based on the linear decomposition of the determinant of the Jacobian matrix combined with the application of the resultant of polynomials to form nonlinear systems of equations was proposed for the singularity analysis of a given kinematically redundant (6+2)-DOF parallel mechanism. More specifically, in the singularity analysis presented in [62], the linear decomposition of the determinant of the Jacobian matrix $\mathbf{J}$ was firstly applied in order to factor out the variables describing the internal motion in the mechanism (kinematic redundancy), i.e., the feature allowing the avoidance of singularity. An equivalent form of the Jacobian matrix determinant was then found, where the determinant is expressed as a summation of four sub-determinants, each of which multiplied by a coefficient written as a function of the variables corresponding to the kinematic redundancy. Thus, the condition to meet an unavoidable singularity was to verify that all four sub-determinants equal zero simultaneously. This first system of four equations gave the conditions for unavoidable singularities. The four equations to satisfy, the expressions of four sub-determinants in six variables, were written as polynomials in one of the Cartesian variables with the lowest degree, where the coefficients of the particular Cartesian variable were functions of the remaining five variables. Secondly, the resultant of polynomials was applied on three pairs of sub-determinants in order to eliminate the first Cartesian variable, and by doing so, building a second system of equations to be solved. The application of the resultant of polynomials was then used a second time on the new set of equations, again considered as polynomials of the Cartesian variable with the lowest degree. Finally, the conditions to satisfy this second set of equations could be found, which were also used to verify that the initial system of four equations could be solved. Then, the expression of a locus of unavoidable singularities was discovered. However, the analysis was limited to configurations with zero torsion only in order to investigate the singularity locus of tilted orientations.

In this paper, a generalization of the method presented in [62] is conducted that takes into account all orientations in the singularity analysis of the specified architecture. Hence, the main objective of this paper is to investigate the singularity locus of type II of a given kinematically redundant (6+2)-DOF parallel mechanism rather than to propose a new framework for the singularity analysis of general parallel mechanisms. This paper is structured as follows : Section 2.4 introduces the kinematic modelling of the general architecture of a kinematically redundant $(6+k)$-DOF parallel mechanism and the particular architecture studied in this work. Section 2.5 presents the singularity analysis of the proposed architecture. Finally, Section 2.6 discusses the limitations of the orientational workspace of the proposed mechanism due to unavoidable singularities.

2.4 Kinematic Modelling

2.4.1 General architecture

This section briefly recalls the kinematic modelling of a general kinematically redundant (6+k)-DOF parallel mechanism as firstly described in [25]. The reader is referred to the derivation presented in [25] for more details. Consider an architecture with k redundant legs — i.e., k redundant DOFs — and $6-k$ non-redundant legs. The non-redundant legs are of type H$\underline{\text{P}}$S while the two sublegs of a redundant leg are of type S$\underline{\text{P}}$R, where H refers to a Hooke joint, $\underline{\text{P}}$ refers to an actuated prismatic joint, S to a spherical joint and R refers to a revolute joint. A simplified CAD model of the proposed mechanism is exposed in Fig. 2.1 to visualize the architecture of interest. A redundant leg is defined by points $A_{i,1}$, $A_{i,2}$, S_i and B_i in Figure 2.2, which introduces the nomenclature used for the upcoming derivation for a general case of kinematically redundant parallel mechanism.

For the redundant leg i, with $i = 1, \ldots, k$, the sublegs have their attachment points at the base in $A_{i,1}$ and $A_{i,2}$ by spherical joints, and are linked in S_i by a revolute joint. While it may not seem obvious in Fig. 2.1 that the attachment points at the base in $A_{i,1}$ and $A_{i,2}$ are spherical joints (they are in fact universal joints), a revolute joint along the axis of each subleg, not shown in Fig. 2.1, is necessary to obtain the desired equivalent spherical joint in

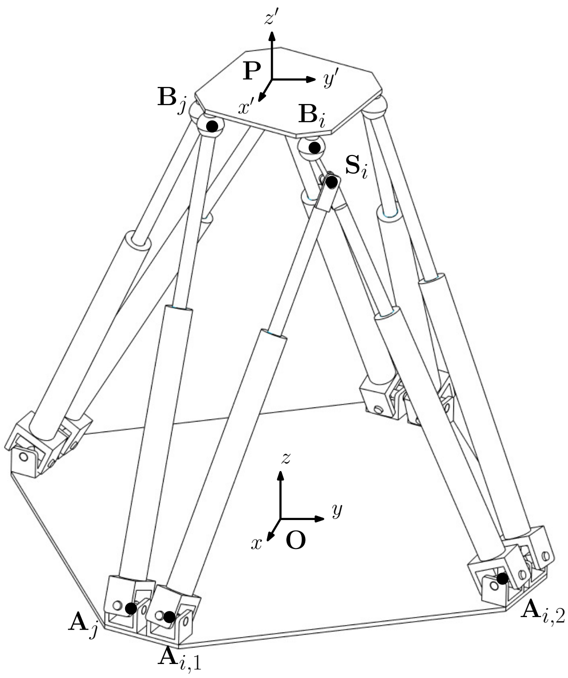

FIGURE 2.1 – Simplified CAD model of the specific architecture.

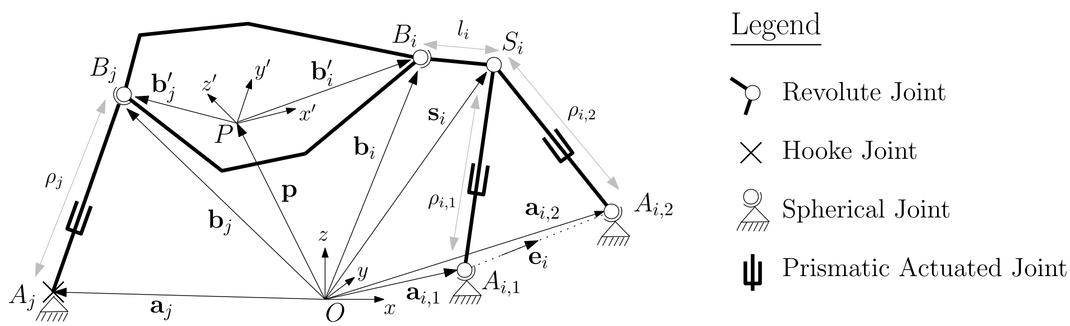

FIGURE 2.2 – Geometric representation of a kinematically redundant parallel mechanism as firstly proposed in [25].

$A_{i,1}$ and $A_{i,2}$. The redundant link $\overline{B_i S_i}$ associated with the redundant leg i is attached by a spherical joint at the platform in B_i. The joint coordinates associated with redundant leg i are the lengths of the two sublegs, noted $\rho_{i,1}$ and $\rho_{i,2}$. Moreover, because the two sublegs and the redundant link of a redundant leg are linked together by a revolute joint, $A_{i,1}, A_{i,2}, S_i$ and B_i are constrained to belong to the same plane, i.e., both sublegs and the redundant link are coplanar. The non-redundant leg j, with $j = k+1, \ldots, 6$, is attached at the base in A_j by a Hooke joint and at the platform in B_j by a spherical joint. The joint coordinate associated with non-redundant leg j is the extension of the leg, noted ρ_j. A fixed reference frame $O(x, y, z)$ is attached at the base while a moving reference frame $P(x', y', z')$ is attached at the moving platform. Vector $\mathbf{p}$ is the position vector of point P expressed in the fixed reference frame. A rotation matrix $\mathbf{Q}$ describes the rotation of the reference frame $P(x', y', z')$ with respect to the fixed reference frame. Vectors $\mathbf{b}'_i$ and $\mathbf{b}'_j$ are the position vectors of the attachment points on the platform for the redundant and non-redundant legs respectively, and are expressed in the moving reference frame. All other position vectors, namely $\mathbf{a}_{i1}$, $\mathbf{a}_{i2}$, $\mathbf{a}_j$, $\mathbf{s}_i$, $\mathbf{b}_i$, $\mathbf{b}_j$ and $\mathbf{e}_i$ are expressed in the fixed reference frame. Referring to Figure 2.2, the constraint equations are given by

$$\rho_j^2 = (\mathbf{b}_j - \mathbf{a}_j)^T(\mathbf{b}_j - \mathbf{a}_j), \quad j = (k+1), \ldots, 6, \tag{2.1}$$

with

$$\mathbf{b}_j = \mathbf{p} + \mathbf{Q}\mathbf{b}'_j, \tag{2.2}$$

for a non-redundant leg, and

$$l_i^2 = (\mathbf{s}_i - \mathbf{b}_i)^T(\mathbf{s}_i - \mathbf{b}_i), \quad i = 1, \ldots, k, \tag{2.3}$$

with

$$\mathbf{b}_i = \mathbf{p} + \mathbf{Q}\mathbf{b}'_i, \tag{2.4}$$

for a redundant link. The constraint equation for a subleg of a redundant leg is expressed as

$$\rho_{i,h}^2 = (\mathbf{s}_i - \mathbf{a}_{i,h})^T(\mathbf{s}_i - \mathbf{a}_{i,h}), \quad i = 1, \ldots, k, \quad h = 1, 2. \tag{2.5}$$

The last constraint equation represents the coplanarity of points A_{i1}, A_{i2}, S_i, B_i and is written as

$$[(\mathbf{b}_i - \mathbf{a}_{i,1}) \times \mathbf{e}_i]^T(\mathbf{s}_i - \mathbf{a}_{i,1}) = 0, \quad i = 1, \ldots, k, \tag{2.6}$$

with $\mathbf{e}_i$, the unit vector oriented from point A_{i1} to point A_{i2}. Taking the time derivative of equations (2.1), (2.3), (2.5) and (2.6) with further simplifications and substitutions (see [25]) leads to the system of equations

$$\mathbf{J}\mathbf{t} = \mathbf{K}\dot{\boldsymbol{\rho}}, \tag{2.7}$$

with $\mathbf{J}$ and $\mathbf{K}$, the Jacobian matrices, $\mathbf{t}$, the six-dimensional Cartesian velocity vector and $\dot{\boldsymbol{\rho}}$, the joint velocity vector. Vectors $\mathbf{t}$ and $\dot{\boldsymbol{\rho}}$ are respectively given as

$$\mathbf{t} = [\dot{\mathbf{p}}^T \boldsymbol{\omega}^T]^T, \tag{2.8}$$

$$\dot{\boldsymbol{\rho}} = [\dot{\rho}_{1,1}, \dot{\rho}_{1,2}, \ldots, \dot{\rho}_{k,1}, \dot{\rho}_{k,2}, \dot{\rho}_{k+1}, \ldots, \dot{\rho}_6]^T, \tag{2.9}$$

with $\dot{\mathbf{p}}$ and $\boldsymbol{\omega}$, respectively the velocity of point P and the angular velocity of the platform. The Jacobian matrices are written as follows

$$\mathbf{J} = \begin{bmatrix} (\mathbf{s}_1 - \mathbf{b}_1)^T & [\mathbf{Q}\mathbf{b}'_1 \times (\mathbf{s}_1 - \mathbf{b}_1)]^T \\ \vdots & \vdots \\ (\mathbf{s}_k - \mathbf{b}_k)^T & [\mathbf{Q}\mathbf{b}'_k \times (\mathbf{s}_k - \mathbf{b}_k)]^T \\ (\mathbf{b}_{k+1} - \mathbf{a}_{k+1})^T & [\mathbf{Q}\mathbf{b}'_{k+1} \times (\mathbf{b}_{k+1} - \mathbf{a}_{k+1})]^T \\ \vdots & \vdots \\ (\mathbf{b}_6 - \mathbf{a}_6)^T & [\mathbf{Q}\mathbf{b}'_6 \times (\mathbf{b}_6 - \mathbf{a}_6)]^T \end{bmatrix}_{6\times 6} \tag{2.10}$$

and

$$\mathbf{K} = \begin{bmatrix} \mathbf{K}_1 & \mathbf{0}_{k\times(6-k)} \\ \mathbf{0}_{(6-k)\times 2k} & \mathbf{K}_2 \end{bmatrix}_{6\times(6+k)} \tag{2.11}$$

where

$$\mathbf{K}_2 = \begin{bmatrix} \rho_{k+1} & \dots & 0 \\ \vdots & \ddots & \vdots \\ 0 & \dots & \rho_6 \end{bmatrix}_{(6-k)\times(6-k)} \tag{2.12}$$

$$\mathbf{K}_1 = \begin{bmatrix} \mathbf{r}_1^T\mathbf{m}_1 & \mathbf{r}_1^T\mathbf{n}_1 & 0 & \dots & 0 \\ \vdots & & \ddots & & \vdots \\ 0 & \dots & 0 & \mathbf{r}_k^T\mathbf{m}_k & \mathbf{r}_k^T\mathbf{n}_k \end{bmatrix}_{k\times 2k} \tag{2.13}$$

with

$$\mathbf{r}_i = (\mathbf{s}_i - \mathbf{b}_i), \tag{2.14}$$

$$\mathbf{m}_i = \frac{\rho_{i,1}}{\mu_i}[(\mathbf{s}_i - \mathbf{a}_{i,2}) \times [(\mathbf{b}_i - \mathbf{a}_{i,1}) \times \mathbf{e}_i]], \tag{2.15}$$

$$\mathbf{n}_i = \frac{\rho_{i,2}}{\mu_i}[[(\mathbf{b}_i - \mathbf{a}_{i,1}) \times \mathbf{e}_i] \times (\mathbf{s}_i - \mathbf{a}_{i,1})], \tag{2.16}$$

$$\mu_i = [(\mathbf{s}_i - \mathbf{a}_{i,1}) \times (\mathbf{s}_i - \mathbf{a}_{i,2})]^T[(\mathbf{b}_i - \mathbf{a}_{i,1}) \times \mathbf{e}_i]. \tag{2.17}$$

2.4.2 Particular architecture

A specific architecture for a kinematically redundant (6+2)-DOF parallel mechanism was proposed in [62] and its singularity analysis for general configurations is addressed in this paper. The specific architecture studied is now recalled. In the proposed architecture, the attachment points at the base and the platform are located on the vertices of a square. The architecture of the proposed mechanism is represented in Figure 2.3 using the notation presented in Section 2.4.1, where the mechanism lies in its reference configuration, with an offset along the z axis. Because the force applied to the platform by a redundant link is in fact a linear combination of the forces deployed by the associated sublegs, a similar matrix sharing the same conditions for singularity as the Jacobian matrix from equation (2.10) may be constructed. Indeed, referring to Figure 2.4, vector $\mathbf{s}_i$ may be expressed as

$$\mathbf{s}_i = \mathbf{b}_i + l_i \cos\gamma_i \mathbf{e}_i - l_i \sin\gamma_i \mathbf{k}_i, \tag{2.18}$$

with

$$\mathbf{g}_i = \frac{\mathbf{e}_i \times (\mathbf{b}_i - \mathbf{a}_{i,2})}{||\mathbf{e}_i \times (\mathbf{b}_i - \mathbf{a}_{i,2})||}, \tag{2.19}$$

$$\mathbf{k}_i = \mathbf{g}_i \times \mathbf{e}_i, \tag{2.20}$$

where l_i is the length of the redundant link, and γ_i is the orientation of the redundant link with respect to the reference axis $\mathbf{e}_i$.

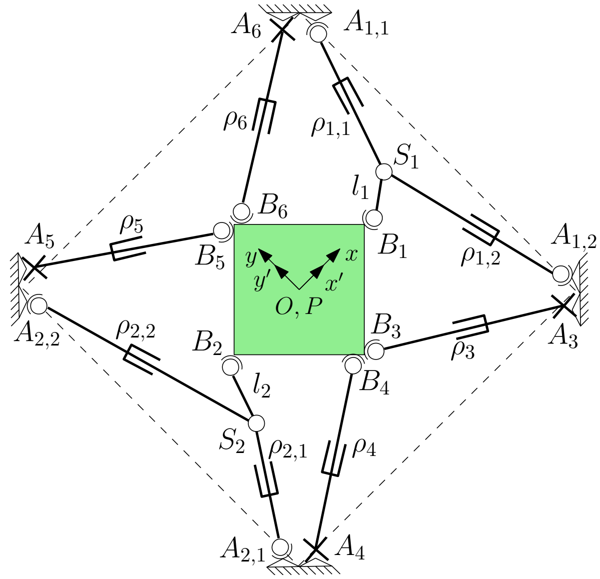

FIGURE 2.3 – Top view of the proposed architecture in its home configuration with an offset along the z-axis (Joints symbols are the same as in Fig. 2.2).

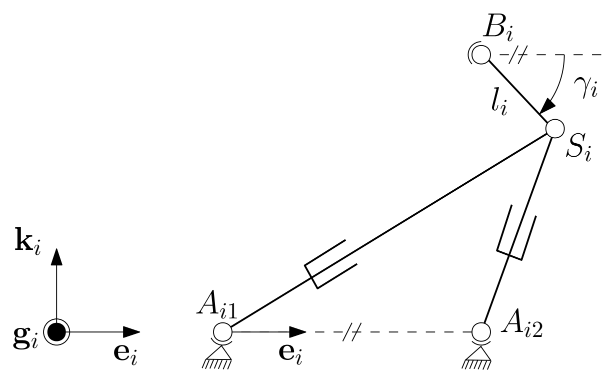

FIGURE 2.4 – Orientation of the redundant link in the plane of the redundant leg i.

Once equation (2.18) is substituted into equation (2.10), the Jacobian matrix $\mathbf{J}$ becomes

$$\mathbf{J} = \begin{bmatrix} (l_1 \cos\gamma_1 \mathbf{e}_1 - l_1 \sin\gamma_1 \mathbf{k}_1)^T & [\mathbf{Q}\mathbf{b}'_1 \times (l_1 \cos\gamma_1 \mathbf{e}_1 - l_1 \sin\gamma_1 \mathbf{k}_1)]^T \\ (l_2 \cos\gamma_2 \mathbf{e}_2 - l_2 \sin\gamma_2 \mathbf{k}_2)^T & [\mathbf{Q}\mathbf{b}'_2 \times (l_2 \cos\gamma_2 \mathbf{e}_2 - l_2 \sin\gamma_2 \mathbf{k}_2)]^T \\ (\mathbf{b}_3 - \mathbf{a}_3)^T & [\mathbf{Q}\mathbf{b}'_3 \times (\mathbf{b}_3 - \mathbf{a}_3)]^T \\ \vdots & \vdots \\ (\mathbf{b}_6 - \mathbf{a}_6)^T & [\mathbf{Q}\mathbf{b}'_6 \times (\mathbf{b}_6 - \mathbf{a}_6)]^T \end{bmatrix}_{6\times 6}. \tag{2.21}$$

It is clear from equation (2.21) that the first two rows of the Jacobian matrix $\mathbf{J}$ are linear combinations of the Plücker coordinates of lines of orthogonal vectors in the planes of the redundant legs (namely the lines parallel to $\mathbf{e}_i$ and $\mathbf{k}_i$, see Fig. 2.4). These linear combinations of vectors represent the Plücker coordinates of lines in the direction of the redundant links $\overline{B_i S_i}$. Moreover, any pair of linearly independent vectors lying in the plane of a redundant leg may generate all vectors in that plane. Thus, because the objective of the present work is to find singular poses of the mechanism which cannot be avoided with the kinematic redundancy, i.e., for any linear combination in the first two rows of Jacobian matrix $\mathbf{J}$, those first two rows may be replaced by any linear combination of two linearly independent vectors in the plane of each of the redundant legs. Then, it is of interest to find vectors in each plane of the redundant legs whose expressions are simple. The chosen vectors to replace $\mathbf{k}_1, \mathbf{e}_1, \mathbf{k}_2, \mathbf{e}_2$ are the vectors going from point $A_{i,h}$ to point B_i, with $i = 1, 2$ and $h = 1, 2$. These vectors cease to be linearly independent when point B_i lies on the segment passing through points $A_{i,1}$ and $A_{i,2}$, which is a configuration generally avoided in trajectory planning considering the near coplanarity of the sublegs of a redundant leg to the plane of the base. Thereby, a matrix $\tilde{\mathbf{J}}$ capturing the same unavoidable singular configurations as Jacobian matrix $\mathbf{J}$ is given by

$$\tilde{\mathbf{J}} = \begin{bmatrix} \mathbf{u}_1^T & [\mathbf{Q}\mathbf{b}'_1 \times \mathbf{u}_1]^T \\ \mathbf{u}_2^T & [\mathbf{Q}\mathbf{b}'_2 \times \mathbf{u}_2]^T \\ (\mathbf{b}_3 - \mathbf{a}_3)^T & [\mathbf{Q}\mathbf{b}'_3 \times (\mathbf{b}_3 - \mathbf{a}_3)]^T \\ (\mathbf{b}_4 - \mathbf{a}_4)^T & [\mathbf{Q}\mathbf{b}'_4 \times (\mathbf{b}_4 - \mathbf{a}_4)]^T \\ (\mathbf{b}_5 - \mathbf{a}_5)^T & [\mathbf{Q}\mathbf{b}'_5 \times (\mathbf{b}_5 - \mathbf{a}_5)]^T \\ (\mathbf{b}_6 - \mathbf{a}_6)^T & [\mathbf{Q}\mathbf{b}'_6 \times (\mathbf{b}_6 - \mathbf{a}_6)]^T \end{bmatrix}, \tag{2.22}$$

with

$$\mathbf{u}_1 = \cos\epsilon_1(\mathbf{b}_1 - \mathbf{a}_{1,1}) + \sin\epsilon_1(\mathbf{b}_1 - \mathbf{a}_{1,2}), \tag{2.23}$$

$$\mathbf{u}_2 = \cos\epsilon_2(\mathbf{b}_2 - \mathbf{a}_{2,1}) + \sin\epsilon_2(\mathbf{b}_2 - \mathbf{a}_{2,2}), \tag{2.24}$$

where ϵ_1, ϵ_2 are kinematic parameters describing the linear combination of the two pairs of linearly independent vectors in each plane of the redundant legs that gives the direction of the forces applied to the platform. In other words, ϵ_1 and ϵ_2 are generic variables used as coefficients in the linear combinations of vectors that give the orientation of the redundant link $\overline{B_i S_i}$. Their interpretation is purely mathematical, i.e., they represent the set of all linear combinations of two given vectors in the plane of their respective redundant leg in order to express the orientation of the vector along the corresponding redundant link. An unavoidable singular configuration happens if the determinant of matrix $\tilde{\mathbf{J}}$ is zero for any value of parameters ϵ_1, ϵ_2.

Following the nomenclature for the geometric entities in Section 2.4.1 and referring to Figure 2.3, the geometric parameters are now detailed and given as

$$\begin{aligned} \mathbf{a}_{1,1} &= \mathbf{a}_6 = [\beta, \beta, 0]^T, & \mathbf{b}'_1 &= [1, 0, 0]^T, \\ \mathbf{a}_{1,2} &= \mathbf{a}_3 = [\beta, -\beta, 0]^T, & \mathbf{b}'_2 &= [-1, 0, 0]^T, \\ \mathbf{a}_{2,1} &= \mathbf{a}_4 = [-\beta, -\beta, 0]^T, & \mathbf{b}'_3 &= \mathbf{b}'_4 = [0, -1, 0]^T, \\ \mathbf{a}_{2,2} &= \mathbf{a}_5 = [-\beta, \beta, 0]^T, & \mathbf{b}'_5 &= \mathbf{b}'_6 = [0, 1, 0]^T, \end{aligned} \tag{2.25}$$

where one unit is defined as the distance between the attachment points on the platform and its centroid. Parameter β is a scaling factor and must be positive, and the length of the vertices at the base is 2β. The convention used to represent the rotations is the one proposed in [47], namely the Tilt and Torsion representation. With this representation, it is easier to decouple the tilt of the platform from the intrinsic torsion induced with the representation of Euler angles. The rotation matrix, $\mathbf{Q}$, is given as

$$\mathbf{Q} = \begin{bmatrix} c(\phi)\,c(\theta)\,c(\psi) + s(\phi)\,s(\psi) & c(\phi)\,c(\theta)\,s(\psi) - s(\phi)\,c(\psi) & c(\phi)\,s(\theta) \\ s(\phi)\,c(\theta)\,c(\psi) - c(\phi)\,s(\psi) & s(\phi)\,c(\theta)\,s(\psi) + c(\phi)\,c(\psi) & s(\phi)\,s(\theta) \\ -s(\theta)\,c(\psi) & -s(\theta)\,s(\psi) & c(\theta) \end{bmatrix}, \quad (2.26)$$

where $c(\cdot)$ and $s(\cdot)$ are respectively the cosine and sine of the argument $(\cdot)$, and $\psi = \phi - \sigma$. Also, the rotation angles σ, θ, ϕ are respectively the torsion angle, the tilt angle, and the angle of the axis, with respect to the y axis in the fixed reference frame, around which the tilt of the platform is performed.

With the Plücker coordinates of lines,

$$\mathbf{v}_{i,h} = \left[[\mathbf{b}_i - \mathbf{a}_{i,h}]^T \quad [\mathbf{Q}\mathbf{b}'_i \times (\mathbf{b}_i - \mathbf{a}_{i,h})]^T \right], \quad i = 1,2 \quad h = 1,2, \quad (2.27)$$

$$\mathbf{v}_j = \left[[\mathbf{b}_j - \mathbf{a}_j]^T \quad [\mathbf{Q}\mathbf{b}'_j \times (\mathbf{b}_j - \mathbf{a}_j)]^T \right], \quad j = 3, \ldots, 6, \quad (2.28)$$

equation (2.22) is rewritten as

$$\tilde{\mathbf{J}} = \begin{bmatrix} c(\epsilon_1)\mathbf{v}_{1,1} + s(\epsilon_1)\mathbf{v}_{1,2} \\ c(\epsilon_2)\mathbf{v}_{2,1} + s(\epsilon_2)\mathbf{v}_{2,2} \\ \mathbf{v}_3 \\ \mathbf{v}_4 \\ \mathbf{v}_5 \\ \mathbf{v}_6 \end{bmatrix} \quad (2.29)$$

to simplify further derivations. In the next section, the conditions for singularity will be derived from equation (2.29).

2.5 Singularity Analysis

In this work, singular configurations are defined as poses (position and orientation) of the platform in which the mechanism is in a singularity for any configuration of the redundant legs. In other words, in such a Cartesian pose, the kinematic redundancy of the mechanism cannot be used to avoid the singularity. In this section, the general singularity locus of the proposed mechanism is derived in two steps. Firstly, the singular configurations that depend only on orientation coordinates are addressed to visualize their impact on the orientational workspace. Secondly, a more general framework is presented to assess the singularities that also depend on position coordinates.

2.5.1 Position independent configurations

In order to completely separate the position coordinates from the orientation coordinates in the expression of the determinant of matrix $\tilde{\mathbf{J}}$, a double application of the linear decomposition of the determinant [46] is conducted. With the property $\det(\mathbf{M}^{\mathbf{T}}) = \det(\mathbf{M})$, where $\mathbf{M}$ is a square matrix, and from the linear dependency of the determinant on its columns, from equation (2.29) one has

$$\det(\tilde{\mathbf{J}}) = c(\epsilon_1)c(\epsilon_2)\left|\mathbf{v}_{1,1}^T \quad \mathbf{v}_{2,1}^T \quad \mathbf{v}_3^T \quad \mathbf{v}_4^T \quad \mathbf{v}_5^T \quad \mathbf{v}_6^T\right| + c(\epsilon_1)s(\epsilon_2)\left|\mathbf{v}_{1,1}^T \quad \mathbf{v}_{2,2}^T \quad \mathbf{v}_3^T \quad \mathbf{v}_4^T \quad \mathbf{v}_5^T \quad \mathbf{v}_6^T\right|$$
$$+ s(\epsilon_1)c(\epsilon_2)\left|\mathbf{v}_{1,2}^T \quad \mathbf{v}_{2,1}^T \quad \mathbf{v}_3^T \quad \mathbf{v}_4^T \quad \mathbf{v}_5^T \quad \mathbf{v}_6^T\right| + s(\epsilon_1)s(\epsilon_2)\left|\mathbf{v}_{1,2}^T \quad \mathbf{v}_{2,2}^T \quad \mathbf{v}_3^T \quad \mathbf{v}_4^T \quad \mathbf{v}_5^T \quad \mathbf{v}_6^T\right|, \tag{2.30}$$

which separates the expression of the original determinant in a weighted sum of four simpler sub-determinants, namely

$$D_1 = \left|\mathbf{v}_{1,1}^T \quad \mathbf{v}_{2,1}^T \quad \mathbf{v}_3^T \quad \mathbf{v}_4^T \quad \mathbf{v}_5^T \quad \mathbf{v}_6^T\right|, \tag{2.31}$$

$$D_2 = \left|\mathbf{v}_{1,1}^T \quad \mathbf{v}_{2,2}^T \quad \mathbf{v}_3^T \quad \mathbf{v}_4^T \quad \mathbf{v}_5^T \quad \mathbf{v}_6^T\right|, \tag{2.32}$$

$$D_3 = \left|\mathbf{v}_{1,2}^T \quad \mathbf{v}_{2,1}^T \quad \mathbf{v}_3^T \quad \mathbf{v}_4^T \quad \mathbf{v}_5^T \quad \mathbf{v}_6^T\right|, \tag{2.33}$$

$$D_4 = \left|\mathbf{v}_{1,2}^T \quad \mathbf{v}_{2,2}^T \quad \mathbf{v}_3^T \quad \mathbf{v}_4^T \quad \mathbf{v}_5^T \quad \mathbf{v}_6^T\right|, \tag{2.34}$$

where $|\cdot|$ stands for the determinant of its matrix argument. This first linear decomposition of the determinant brings out the condition to meet in order to reach a singular configuration unavoidable with kinematic redundancy, which is

$$D_1 = D_2 = D_3 = D_4 = 0. \tag{2.35}$$

Based on the structure of the determinant of the Jacobian matrix, whose rows are the Plücker coordinates of the lines associated with the direction of the legs in the mechanism, a second linear decomposition on each of the sub-determinants with the strategy employed in [46] leads to expressions of the form

$$\begin{aligned} D_i = {} & F_{i,1}x^3 + F_{i,2}x^2y + F_{i,3}x^2z + F_{i,4}x^2 + F_{i,5}xy^2 + F_{i,6}xyz + F_{i,7}xy \\ & + F_{i,8}xz^2 + F_{i,9}xz + F_{i,10}x + F_{i,11}y^3 + F_{i,12}y^2z + F_{i,13}y^2 + F_{i,14}yz^2 \\ & + F_{i,15}yz + F_{i,16}y + F_{i,17}z^3 + F_{i,18}z^2 + F_{i,19}z + F_{i,20}, \qquad i = 1, \ldots, 4. \end{aligned} \tag{2.36}$$

In equation (2.36), coefficients $F_{i,j}$ with $j = 1, \ldots, 20$ are strictly dependent on orientation coordinates and geometric parameters. Hence, the second application of the linear decomposition on each of the four sub-determinants leads to a total of 80 coefficients $F_{i,j}$ dependent on orientation coordinates. To satisfy equation (2.35) independently from position coordinates, all of the 80 coefficients must be equal to zero simultaneously. Thus, the strategy proposed here is to target one of the 80 coefficients whose expression is of the simplest form, and to list the conditions on the orientation variables for which this coefficient vanishes. Each of the conditions found may be substituted one at a time into all other nonzero coefficients to obtain the additional conditions on the two remaining orientation variables that make the remaining coefficients vanish. Again, to find the additional conditions that make the other coefficients vanish, one of the nonzero remaining coefficients whose expression is the simplest is targeted for the rest of the derivation. The detailed derivation is now presented. For simplicity, the substitution of the tangent of half-angles is used, in order to bring together the sine and cosine of an orientation angle under one variable. Hence, the orientation angles θ, ϕ, σ may now be referred to by their corresponding orientation parameter, t_1, t_2, t_3 for the rest of the derivation, which are given by

$$t_1 = \tan\frac{\theta}{2}, \quad t_2 = \tan\frac{\phi}{2}, \quad t_3 = \tan\frac{\sigma}{2}. \tag{2.37}$$

After analyzing the nonzero coefficients among the 80 from the double linear decomposition of the determinant, one of the simplest expressions is given by

$$F_{2,6} = 256\,\frac{(t_2-1)\,(t_2+1)\,(t_2t_3+1)\,(-t_3+t_2)\,\beta^3{t_1}^2}{\left({t_3}^2+1\right)\left({t_1}^2+1\right)^2\left({t_2}^2+1\right)^2}. \tag{2.38}$$

It can be observed from equation (2.38) that, independently from the expression of all the other coefficients, the conditions to make this particular coefficient vanish are

$$t_1 = 0, \tag{2.39}$$

$$t_1 \to \pm\infty, \tag{2.40}$$

$$t_2 = \pm 1, \tag{2.41}$$

$$t_2 = t_3, \tag{2.42}$$

$$t_2 = -\frac{1}{t_3}. \tag{2.43}$$

If the condition $t_1 = 0$ is substituted into the coefficient from equation (2.38) and the other $F_{i,j}$ nonzero coefficients, all but two vanish. The last two coefficients have together the only additional condition $t_3 = \pm 1$ to make them equal to zero. Thus, a singular configuration independent from position coordinates is found if $(t_1, t_2, t_3) = (0, t_2, \pm 1)$ and corresponds to a rotation of $\pm 90°$ around an axis perpendicular to the plane of the base while the platform is parallel to the base. This singularity is well known with parallel mechanisms akin to the Gough-Stewart architecture [49] and is referred to as Fichter's singularity. Next, applying the same procedure from the start with the initial condition $t_1 \to \pm\infty$, which corresponds to a tilt angle of $\pm 180°$ of the platform, substituted into the other $F_{i,j}$ nonzero coefficients, all but two vanish. The last two nonzero coefficients are given by

$$F_{2,17} = \frac{-32\beta^3\big((t_2^2-2t_2-1)t_3+t_2^2+2t_2-1\big)\big((t_2^2+2t_2-1)t_3-t_2^2+2t_3+1\big)}{(t_2^2+1)^2(t_3^2+1)}, \tag{2.44}$$

$$F_{3,17} = \frac{32\beta^3\big((t_2^2-2t_2-1)t_3+t_2^2+2t_2-1\big)\big((t_2^2+2t_2-1)t_3-t_2^2+2t_3+1\big)}{(t_2^2+1)^2(t_3^2+1)}, \tag{2.45}$$

and they yield the same two additional conditions to cancel them simultaneously, namely,

$$t_3 = -\frac{{t_2}^2 + 2\,t_2 - 1}{{t_2}^2 - 2\,t_2 - 1}, \tag{2.46}$$

$$t_3 = \frac{{t_2}^2 - 2\,t_2 - 1}{{t_2}^2 + 2\,t_2 - 1}. \tag{2.47}$$

These conditions on variable t_3 and $t_1 \to \pm\infty$ constitute another singular configuration, and consist in a generalisation of the preceding singularity for which the platform is parallel to the base, but for $\theta = \pm 180°$ instead of $\theta = 0°$. The next condition from equation (2.38) is $t_2 = 1$. After substituting this condition into the other coefficients, twenty-six of them remain nonzero. The additional condition to make the expression of the remaining simplest coefficients vanish is $t_3 = \pm 1$. This condition is sufficient to make all the remaining twenty-six coefficients go to zero simultaneously, and thus constitutes a singular configuration. The same results for t_3 are obtained with the condition $t_2 = -1$. Hence, a singularity locus independent from position coordinates exists for $(t_1, t_2, t_3) = (t_1, 1, \pm 1)$ and $(t_1, t_2, t_3) = (t_1, -1, \pm 1)$. Moreover, the derivation with the first conditions $t_2 = t_3$ and $t_2 = -\frac{1}{t_3}$ leads to the same results as for the first condition $t_2 = \pm 1$ and are thus not displayed here. This singular configuration is associated with condition 3b) of Grassmann geometry, presented in [50], for which the intersection of two planar pencils of lines is possible between the four non-redundant legs of the mechanism. Such a configuration is obtained when the line passing through attachment points $B_{3,4}$ and $B_{5,6}$ (see Figure 2.3) is parallel to lines $\overline{A_3A_4}$ and $\overline{A_5A_6}$. In this configuration, whatever the orientation of the two redundant links, the intersection of the two planar pencils of lines generated by the lines in direction of the four non redundant legs 3, 4, 5 and 6 still exists, as represented in Figure 2.5 by the line D, which belongs to both planar pencils of lines. In Fig. 2.5, the two redundant legs were omitted for clarity purposes, because they do not participate directly in the singular configuration. Moreover, in the description of the singularity locus, the attachment points B_3 and B_4 are assumed to be coincident, as well as points B_5 and B_6. In the real mechanism, these points are not coincident (see Fig. 2.5), but are really close to each other with respect to the dimensions of the mechanism. Hence, the singular configuration may not be perfectly met in practice, but it could certainly be closely approached, resulting in enormous efforts in the actuators.

This last case concludes the analysis for position independent singularities analysis. The locus of singularities in the space of the orientation variables θ, ϕ, σ in cylindrical coordinates is shown in Figure 2.6, where all three different sets of equations previously derived are graphically represented. The locus is symmetrical with respect to the plane $\theta = 0°$, and only the upper part of the graph is shown (i.e., $\theta \in [0, 180°]$). In Figure 2.6, the circle at $\theta = 0$ corresponds to the Fichter's singularity, i.e., the platform is rotated of $\pm 90°$ around an axis perpendicular to the base while the platform is parallel to the base. The curves at $\theta = 180°$ are an equivalent of the Fichter's singularity, but when the platform is upside down. The structure of the curves may seem more complicated to visualize. This is due to the fact that

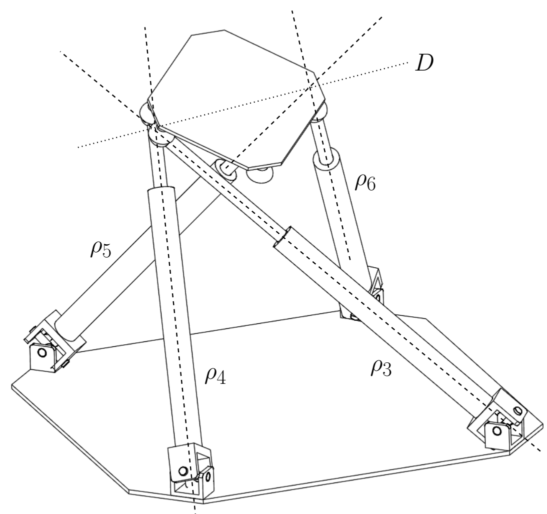

FIGURE 2.5 – Intersection of two planar pencils of lines for $\theta = -\frac{\pi}{6}, \phi = \frac{\pi}{2}, \sigma = -\frac{\pi}{2}, \beta = 2.25$.

when the platform is tilted of $\theta = \pm 180°$ around a given axis of orientation ϕ with respect to the y axis of the fixed reference frame in the plane of the base, a certain torsion angle σ will place the platform into Fichter's singularity. This angle σ is a function of the axis orientation angle ϕ around which the platform is tilted (see equations (2.46) and (2.47)). Finally, the two vertical lines in Figure 2.6 correspond to a configuration of the platform where the segment $\overline{B_{3,4}B_{5,6}}$ is parallel to the segments $\overline{A_3A_4}$ and $\overline{A_5A_6}$. Thus, whatever the tilt angle θ of the platform, an intersection between two planar pencils of lines generated by four non-redundant legs is formed and a singularity occurs (see Fig. 2.5).

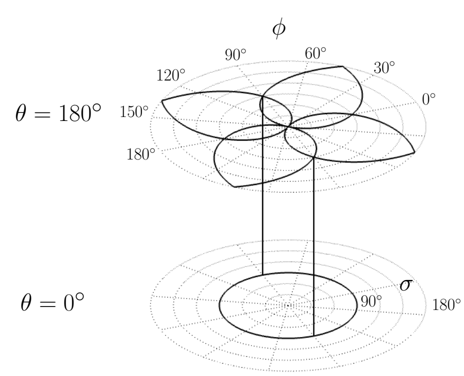

FIGURE 2.6 – Locus of singular configurations independent from position coordinates.

Nonetheless, the orientational workspace is restrained mainly when the torsion angle σ is equal to $\pm 90°$ for $-180° < \theta < 180°$. Moreover, the singularity locus depicted in Figure

2.6 is generally not really restrictive considering that for large tilt angles, mechanical interference will occur before singular configurations can be reached. Indeed, for this particular architecture, numerical simulations taking into account the maximum and minimum length of the legs, physical contact between a pair of legs and passive joints limits indicate that the maximum tilt angle at a reference configuration of the platform is almost 105°. However, even with minimal mechanical interference (i.e. larger reachable orientational workspace), it is almost certain that a tilt angle of $\pm 180°$ results in the legs colliding with the platform itself. Thereby, these results close the derivation of the singularity locus independent from position coordinates.

2.5.2 Position dependent configurations

From equation (2.35), a highly nonlinear system of four equations in six variables (x, y, z, t_1, t_2, t_3) is obtained that describes the general singularity locus. In previous work [62], this system of equations was manipulated using the resultant of polynomials on the expressions of the sub-determinants $D_i, i = 1, \ldots, 4$, but only for zero-torsion configurations. A similar approach is used here. By inspection of the expressions of the coefficients $F_{i,1}, F_{i,2}, F_{i,3}$ and $F_{i,4}$ with $i = 1, \ldots, 4$ (see equation (2.36)) for all four sub-determinants, it can be observed that they are all equal to zero for any value of the orientation variables, which is to say that all sub-determinants are of degree one in x (they have a unique expression for a root in x). If x_i is the root in x of sub-determinant D_i, then a necessary condition for an unavoidable singularity is to have $x_1 = x_2 = x_3 = x_4$. Using the resultant of polynomials, this condition can be translated to

$$\mathrm{Res}_x(D_1, D_2) = \mathrm{Res}_x(D_1, D_3) = \mathrm{Res}_x(D_1, D_4) = 0, \tag{2.48}$$

where $\mathrm{Res}_x(A, B)$ stands for the resultant of polynomials A and B with respect to variable x. The resultant of polynomials A and B with respect to variable x is given by the determinant of their Sylvester matrix, namely

$$\mathrm{Res}_x(A, B) = \begin{vmatrix} a_n & 0 & \ldots & 0 & b_m & 0 & \ldots & 0 \\ a_{n-1} & a_n & \ddots & \vdots & b_{m-1} & b_m & \ddots & \vdots \\ a_{n-2} & a_{n-1} & \ddots & \vdots & b_{m-2} & b_{m-1} & \ddots & \vdots \\ \vdots & a_{n-2} & \ddots & 0 & \vdots & b_{m-2} & \ddots & 0 \\ a_0 & \vdots & \ddots & a_n & b_0 & \vdots & \ddots & b_m \\ 0 & a_0 & \vdots & a_{n-1} & 0 & b_0 & \vdots & b_{m-1} \\ \vdots & 0 & \ddots & a_{n-2} & \vdots & 0 & \ddots & b_{m-2} \\ \vdots & \vdots & \ddots & \vdots & \vdots & \vdots & \ddots & \vdots \\ 0 & 0 & \ldots & a_0 & 0 & 0 & \ldots & b_0 \end{vmatrix}, \tag{2.49}$$

where a_f with $f = 0, \ldots, n$ is the coefficient of the power f of variable x in polynomial A of degree n, while b_g with $g = 0, \ldots, m$ is the coefficient of the power g of variable x in polynomial B of degree m. If expression (2.49) equals zero, then polynomials A and B share at least one common root in variable x. For example, the Sylvester matrices of pairs of polynomials in equation (2.48) are all 2×2 matrices, because all sub-determinants are of degree one in x. The use of the resultant of polynomials is also motivated by the fact that it captures the conditions for which a polynomial becomes independent from the initial variable taken by the resultant. This feature will be useful later in the derivation of some results.

Equation (2.48) represents a new system of three nonlinear equations in five variables (y, z, t_1, t_2, t_3). The three expressions of the resultants can also be considered as polynomials in variables y or z themselves. One would remark that the three resultants with respect to variable x obtained above are of degree two in y while they are of degree three or four in z. Therefore, with the definition

$$R_1 = \mathrm{Res}_x(D_1, D_2), \tag{2.50}$$

$$R_2 = \mathrm{Res}_x(D_1, D_3), \tag{2.51}$$

$$R_3 = \mathrm{Res}_x(D_1, D_4), \tag{2.52}$$

a strategic way to fulfill equation (2.48) would be to have R_1, R_2, R_3 sharing a same root in y. Another application of the resultant for variable y is conducted on R_1, R_2, R_3 leading to

$$R_4 = \mathrm{Res}_y(R_3, R_1), \tag{2.53}$$

$$R_5 = \mathrm{Res}_y(R_3, R_2), \tag{2.54}$$

and the last system of equations to be met is

$$R_4 = R_5 = 0. \tag{2.55}$$

A word of caution must be stated when considering equation (2.55). Indeed, because R_1, R_2, R_3 are of degree two in variable y (they each have two roots in y), satisfying equation (2.55) does not necessarily guarantee $y_1 = y_2 = y_3$, assuming y_j is one of the two roots of resultant R_j, $j = 1, 2, 3$. However, to meet equation (2.48), R_1, R_2, R_3 must share the same expression for their root in y, and a necessary but not yet sufficient condition is to satisfy equation (2.55). One must then verify that $y_1 = y_2 = y_3$ is possible after solving equation (2.55). The framework of the application of the resultant to eliminate variables x and y is represented schematically in Figure 2.7.

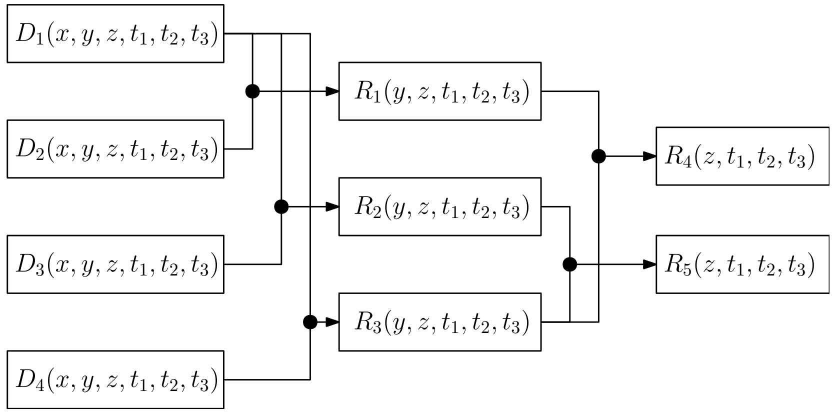

FIGURE 2.7 – Diagram of the resolution scheme.

After expanding the expressions of R_4 and R_5, it can be observed that their structure is similar. In fact, both expressions have four distinct roots in variable z (two of which are common to R_4 and R_5), and they share multiple common roots in variables t_1, t_2, t_3. The expression of R_4 and R_5 are given by

$$R_4(z, t_1, t_2, t_3) = p_1(t_1, t_2, t_3)p_2(t_2, t_3)p_3(t_2, t_3)\prod_{i=1}^{4}(z - z_i), \tag{2.56}$$

$$R_5(z, t_1, t_2, t_3) = p_1(t_1, t_2, t_3)p_2(t_2, t_3)p_3(t_2, t_3)\prod_{j=5}^{8}(z - z_j), \tag{2.57}$$

with

$$p_1 = (t_2t_3 + 1)\left(t_3^2 - 1\right)\left(t_2^2 - 1\right)\left({t_2}^2 - 2\,t_2 - 1\right)(t_2 - t_3)\,t_1, \tag{2.58}$$

$$p_2 = \left({t_3}^2 - 2\,t_3 - 1\right){t_2}^2 + \left(2\,{t_3}^2 + 4\,t_3 - 2\right)t_2 - {t_3}^2 + 2\,t_3 + 1, \tag{2.59}$$

$$p_3 = c_1{t_2}^2 + c_2t_2 - c_1, \tag{2.60}$$

and

$$c_1 = \left((\beta + 1)\,{t_3}^2 - 2\,t_3\beta - \beta + 1\right), \tag{2.61}$$

$$c_2 = 2\,\beta\,\left({t_3}^2 + 2\,t_3 - 1\right). \tag{2.62}$$

The powers of the factors $p_1, p_2, p_3, (z - z_i)$ and $(z - z_j)$ have been omitted for clarity. Also, z_i and z_j are the roots in z of the resultants R_4 and R_5. The roots in z for R_4 are

$$z_{1,2} = \pm\frac{4t_1(t_2t_3 + 1)(t_2 - t_3)}{(t_1^2 + 1)(t_2^2 + 1)(t_3^2 + 1)}, \tag{2.63}$$

$$z_3 = \frac{2t_1(g_1t_2^4 + g_2t_2^3 + g_3t_2^2 - g_2t_2 + g_1)}{g_4(t_2^2 + 2t_2 - 1)}, \tag{2.64}$$

$$z_4 = -\frac{2t_1(g_1t_2^4 + g_2t_2^3 + g_3t_2^2 - g_2t_2 + g_1)}{g_4(t_2^2 - 2t_2 - 1)}, \tag{2.65}$$

where

$$g_1 = (\beta+1)t_3^4 - 6\beta t_3^2 + \beta - 1, \tag{2.66}$$
$$g_2 = 16\beta t_3^3 - 16\beta t_3, \tag{2.67}$$
$$g_3 = (2-6\beta)t_3^4 + 36\beta t_3^2 - 6\beta - 2, \tag{2.68}$$
$$g_4 = (t_3^2+1)^2(t_2^2+1)(t_1^2+1), \tag{2.69}$$

while the roots in z for R_5 are

$$z_{5,6} = \pm\frac{4t_1(t_2t_3+1)(t_2-t_3)}{(t_1^2+1)(t_2^2+1)(t_3^2+1)}, \tag{2.70}$$
$$z_7 = \frac{2t_1(g_1t_2^4+g_2t_2^3+g_3t_2^2-g_2t_2+g_1)}{g_4(t_2^2-2t_2-1)}, \tag{2.71}$$
$$z_8 = -\frac{2t_1(g_1t_2^4+g_2t_2^3+g_3t_2^2-g_2t_2+g_1)}{g_4(t_2^2+2t_2-1)}. \tag{2.72}$$

One easily sees that R_4 and R_5 share their common roots $z_{1,2}$ and $z_{5,6}$. Moreover, as it can be observed from equations (2.56) and (2.57), R_4 and R_5 share the same expressions for their roots in t_1, t_2, t_3, and these roots are given by

$$t_1 = 0, \tag{2.73}$$
$$t_3 = \pm 1, \tag{2.74}$$
$$t_2 = \pm 1, \tag{2.75}$$
$$t_2 = 1 \pm \sqrt{2}, \tag{2.76}$$
$$t_2 = t_3, \tag{2.77}$$
$$t_2 = -\frac{1}{t_3}, \tag{2.78}$$
$$t_2 = \frac{1-2t_3-t_3^2 \pm (\sqrt{2}+\sqrt{2}t_3^2)}{t_3^2-2t_3-1}, \tag{2.79}$$
$$t_2 = \frac{(1-2t_3-t_3^2)\beta \pm \sqrt{2}\sqrt{(t_3^2+1)\left(\left(\beta^2+\beta+\frac{1}{2}\right)t_3^2 - 2\beta t_3 + \beta^2 - \beta + \frac{1}{2}\right)}}{(t_3^2-2t_3-1)\beta + t_3^2 + 1}. \tag{2.80}$$

To determine the position dependent singular configurations, the proposed strategy is as follows : for each pair of common roots in z, t_1, t_2, t_3 of R_4 and R_5, backsubstitute them into R_1, R_2, R_3, and verify whether a common root in y exists between the three resultants. If so, a common expression for a root in x should be found with the four sub-determinants, meaning that a singular configuration occurs under the conditions derived. In sub-section 2.5.3, attention will be given to the roots in z that make R_4 and R_5 vanish, while the sub-section 2.5.4 will focus on the roots in t_1, t_2, t_3 that make R_4 and R_5 equal to zero.

2.5.3 Roots in z making R_4 and R_5 equal to zero

From equation (2.63) making both R_4 and R_5 equal to zero, the common root in y for R_1, R_2, R_3 is given by

$$y = \pm \frac{u_1 t_2^4 + u_2 t_2^3 + u_3 t_2^2 - u_2 t_2 + u_1}{u_4}, \tag{2.81}$$

where

$$u_1 = ((\beta+1)t_3^2 + \beta - 1)(t_1^2 + 1), \tag{2.82}$$

$$u_2 = 8t_1^2 t_3, \tag{2.83}$$

$$u_3 = ((2\beta - 6)t_3^2 + 2\beta + 6)t_1^2 + (2\beta + 2)t_3^2 + 2\beta - 2, \tag{2.84}$$

$$u_4 = (t_1^2 + 1)(t_2^2 + 1)^2(t_3^2 + 1). \tag{2.85}$$

With the conditions on z and y mentioned above backsubstituted into the four sub-determinants, all of them vanish, independently from x. Bringing the investigation further, these singular configurations imply that the attachment points of two adjacent non-redundant legs on the platform are lying on the line passing through their attachment point at the base. In other words, two adjacent non-redundant legs are colinear in the plane of the base. This singular configuration is rejected, because it requires that two legs of the mechanism be coplanar to the plane of the base.

One could also be interested in finding additional conditions on t_1, t_2, t_3 so that the other roots in z, namely z_3, z_4, z_7, z_8 from equations (2.64), (2.65), (2.71) and (2.72) are equivalent. Four pairs of equations can be written, which are $z_3 = z_7, z_3 = z_8, z_4 = z_7$ and $z_4 = z_8$. Only the conditions $z_3 = z_7$ and $z_4 = z_8$ are of interest. Indeed, it is readily observed that, in fact, $z_3 = -z_8$ and $z_4 = -z_7$, so these expressions can only be met for $z = 0$, which is of no interest for most application purposes. Because the condition to meet $z_3 = z_7$ is very similar to the condition to satisfy $z_4 = z_8$, as well as their respective results, only the derivation for the condition $z_3 = z_7$ is presented. In trying to satisfy $z_3 = z_7$, one easily sees from equations (2.64) and (2.71) that the only additional condition on orientational variables which verifies the previous equation without having $z_3 = z_7 = 0$ is therefore $t_2 = 0$. Under the additional condition $t_2 = 0$, $z_3 = z_7$ is verified and the expression of the root in z becomes

$$z_{3,7} = -\frac{2t_1\big((\beta+1)t_3^4 - 6\beta t_3^2 + \beta - 1\big)}{(t_1^2+1)(t_3^2+1)^2}, \tag{2.86}$$

and $z = z_{3,7}$ backsubstituted into R_1, R_2, R_3 gives the following common root in y

$$y = -\frac{2t_3(2\beta t_3^2 + t_3^2 - 2\beta + 1)}{(t_3^2+1)^2}. \tag{2.87}$$

Finally, substituting the conditions on z, y, t_2 in the four sub-determinants leads to the common root in x, given by

$$x = \frac{(-t_1^2 + 2\beta + 1)t_3^4 + (8\beta t_1^2 - 4\beta)t_3^2 + t_1^2 + 2\beta - 1}{(t_1^2+1)(t_3^2+1)^2}. \tag{2.88}$$

The closed-form equations (2.86), (2.87) and (2.88) describe a singularity locus, and the configuration of the platform is such that the two non-redundant legs adjacent to a redundant leg are together coplanar to the plane of the redundant leg, and intersect the attachment point of the redundant link on the platform. This configuration is depicted in Figure 2.8, where non-redundant legs ρ_3 and ρ_6 are coplanar to redundant leg 1, and intersect at the attachment point of the redundant link at the platform. Also, it should be noted that, in Figure 2.8, the legs of the mechanism that do not take part directly in the singular configuration were removed for clarity purposes.

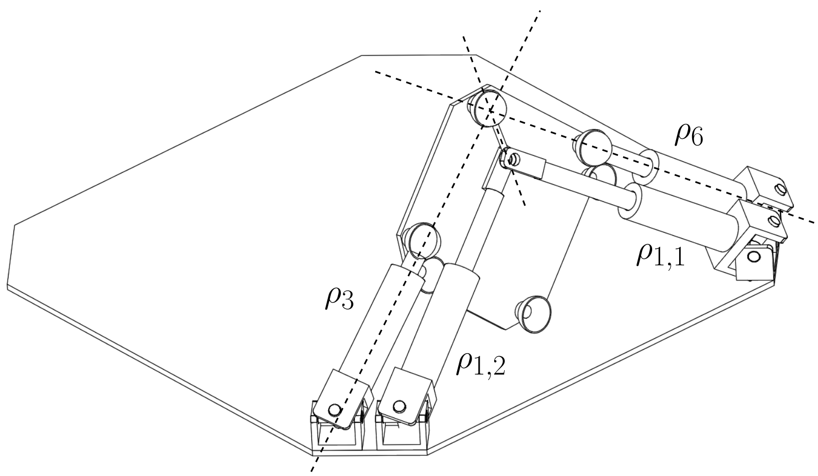

FIGURE 2.8 – Singular configuration of equations (2.86), (2.87) and (2.88) for $t_1 = -\frac{\pi}{2}, t_2 = 0, t_3 = 0$ and $\beta = 2.25$.

In terms of Grassmann geometry, this configuration is identified as condition 2, in which the lines associated with three Plücker vectors form a planar pencil of lines [50]. However, while this singularity locus exists, it requires very large tilt angles, plus two pairs of legs being almost superimposed, which is hardly mechanically reachable. Moreover, the platform lies in positions mostly unreachable by the mechanism, due to simultaneously large extension and retraction among the legs. Finally, in Figure 2.8, one may observe that the attachment points of the two sublegs at the base are not exactly coincident with the attachment points of legs ρ_3 and ρ_6. This arrangement results in the impossibility of non-redundant legs ρ_3 and ρ_6 to be exactly coplanar with the redundant leg 1. Thus, this singular configuration could be approached, but not precisely met in practice. Its description is nonetheless of great importance for trajectory planning. In fact, this singularity locus is a generalization of a result found in [62] for zero-torsion trajectories. This case closes the analysis for the roots in z that may make the resultants R_4 and R_5 equal to zero. In the next subsection, the derivation will focus on the roots in t_1, t_2, t_3 that simultaneously make the resultants R_4 and R_5 equal to zero.

2.5.4 Roots in t_1, t_2, t_3 making R_4 and R_5 equal to zero

In this section, the backsubstitution of the roots in t_1, t_2, t_3 into the resultants R_1, R_2, R_3 is presented in order to derive the conditions for singularity.

Backsubstitution of equation (2.73)

The first root in the orientation variables to be substituted into R_1, R_2, R_3 is $t_1 = 0$ (see equation (2.73)). This condition makes all three resultants vanish, as well as the two sub-determinants D_1, D_4. Only the expressions for D_2, D_3 remain nonzero, and the two additional necessary conditions to cancel them are $z = 0$, which is rejected, or $t_3 = \pm 1$, a result already found in Section 2.5.1.

Backsubstitution of equation (2.74)

From equation (2.74), the second roots that cancel simultaneously R_4, R_5 are $t_3 = \pm 1$. Because the results with $t_3 = 1$ and $t_3 = -1$ are similar, only those for $t_3 = -1$ are derived. After substituting $t_3 = -1$ into the first three resultants, a common root in y exists and is given by

$$y = \frac{2t_1(-\beta t_2^2 + z^2(t_1^2+1)t_2 + \beta)}{z(t_2^2+1)(t_1^2+1)}. \tag{2.89}$$

Once the above conditions are also substituted into the four sub-determinants, a common root in x is also found and its expression is

$$x = -\frac{t_1(((t_2^2-1)t_1^2 + t_2^2 - 1)z^2 + 4\beta t_2)}{z(t_1^2+1)(t_2^2+1)}. \tag{2.90}$$

Thus, the above equations describe a singularity locus that can be reached by the mechanism. Figure 2.9 shows the singularity locus in the x, y space described by equations (2.89) and (2.90). In this singular configuration, for any value of the z coordinate, the locus is akin to the ones pictured at Figure 2.9, where a pair of orientation variables t_1 and t_2, or orientation angles θ and ϕ, generates the corresponding x and y coordinates of the singular configuration. When comparing Figure 2.9a and Figure 2.9b, it can be observed that the locus changes significantly when the z coordinate is increasing, i.e., it is getting larger (see the graduations on the x and y axes). A representation of the platform for such a singular configuration is depicted in Figure 2.10. It can be seen in Figure 2.10 that this unavoidable singular configuration is met inside the reachable workspace of the mechanism without the occurrence of mechanical limitation or mechanical interference. Nonetheless, this singular locus is described by simple equations which can be easily implemented in a controller for path planning purposes.

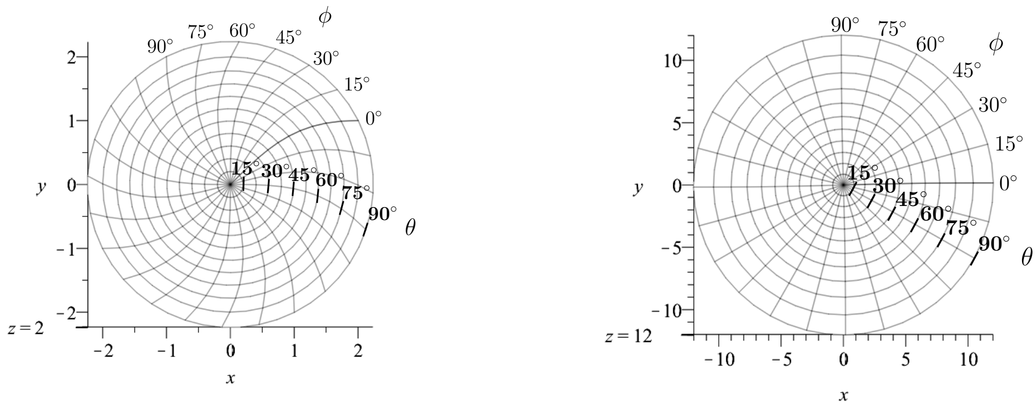

(a) (b)

FIGURE 2.9 – Singularity surface parameterized by orientation angles ϕ, θ in the x, y space for $\beta = 2, \sigma = -90°, \theta \in [0, 90°]$ and $z = 2$ units (2.9a) and $z = 12$ units (2.9b).

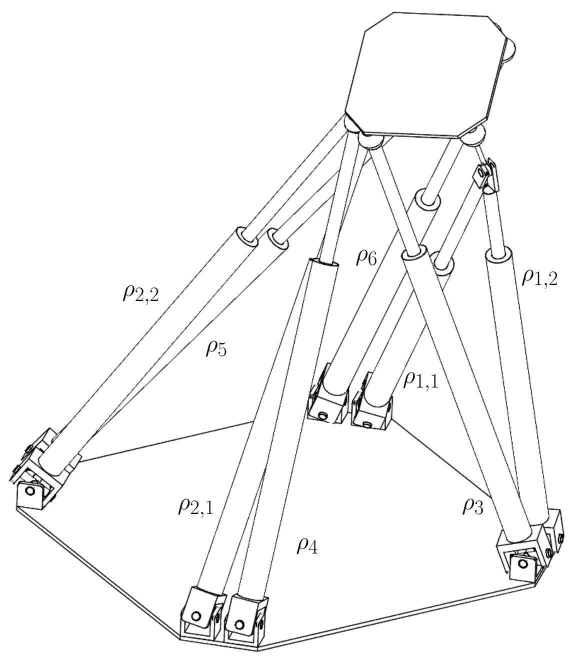

FIGURE 2.10 – Singular configuration of equations (2.89) and (2.90) for $\theta = -\frac{\pi}{6}, \phi = \frac{\pi}{6}, \sigma = -\frac{\pi}{2}, z = 600$mm and $\beta = 2.25$.

Backsubstitution of equation (2.75)

Afterwards, the roots $t_2 = \pm 1$ from equation (2.75) are addressed. Only the results for $t_2 = -1$ are derived. This condition cancels simultaneously R_1, R_2, R_3, and when substituted into the four sub-determinants, the expressions obtained do not depend on x, and they are simpler. The four sub-determinants can be cancelled by the additional condition $t_3 = \pm 1$, independently from position, and this case was addressed in Section 2.5.1. The other conditions for singularity from the simplified equations of sub-determinants are given by

$$y = \pm \frac{((\beta-1)t_3^2+\beta+1)t_1^2+(\beta+1)t_3^2+\beta-1}{(t_1^2+1)(t_3^2+1)}, \tag{2.91}$$

$$z = \pm \frac{2t_1(t_3^2-1)}{(t_1^2+1)(t_3^2+1)}. \tag{2.92}$$

However, it can be observed that this locus of singularity is a special case of equations (2.63) and (2.81) for $t_2 = -1$, which is a more general case, and moreover rejected because it implied legs to be coplanar with the plane of the base. Similar results are obtained with $t_2 = 1$.

Backsubstitution of equation (2.76)

The next roots common to R_4, R_5 are $t_2 = 1 \pm \sqrt{2}$ (see equation (2.76)). Only the derivation for $t_2 = 1+\sqrt{2}$ is presented. Once substituted into R_1, R_2, R_3, a common root in y may indeed be found, and its expression is

$$y = -\frac{\sqrt{2}z((\beta t_1^2+\beta+1)t_3^2+2t_1^2t_3+t_1^2\beta+\beta-1)}{2t_1(t_3^2-2t_3-1)}. \tag{2.93}$$

This condition also substituted into the four sub-determinants leads to their cancellation, independently from x, for

$$z = \pm \frac{\sqrt{2}t_1(t_3^2-2t_3-1)}{(t_1^2+1)(t_3^2+1)}. \tag{2.94}$$

These two conditions in y and z constitute a locus of singularity, but they are also a special case of equations (2.63) and (2.81) for $t_2 = 1+\sqrt{2}$, and are thus not interesting.

Backsubstitution of equations (2.77) and (2.78)

Next, the derivation of the two conditions $t_2 = t_3$ and $t_2 = -\frac{1}{t_3}$ from equations (2.77) and (2.78) leads to an impossibility of having $y_1 = y_2 = y_3$, assuming y_j is one of the two roots of resultant R_j, $j = 1, 2, 3$, if $z \neq 0$, which is rejected.

Backsubstitution of equation (2.79)

For equation (2.79) to be substituted into R_1, R_2, R_3, a simplification is firstly made with

$$t_2 = \frac{(-1+\sqrt{2})(t_3-1-\sqrt{2})}{t_3-1+\sqrt{2}}, \tag{2.95}$$

$$t_2 = \frac{(1+\sqrt{2})(t_3+\sqrt{2}-1)}{-t_3+1+\sqrt{2}}. \tag{2.96}$$

The derivation with equation (2.95) is introduced. Substituted into R_1, R_2, R_3, this condition gives a unique root in y for each resultant. These roots are given by

$$y_1 = -\frac{2\sqrt{2}z{t_1}^2 t_3 + \sqrt{2}z{t_3}^2 - 2\,\beta\, t_1 {t_3}^2 - \sqrt{2}z - 2\,\beta\, t_1}{2t_1\left({t_3}^2+1\right)}, \tag{2.97}$$

$$y_2 = -\frac{2\sqrt{2}z{t_1}^2 t_3 + \sqrt{2}z{t_3}^2 + 2\,\beta\, t_1 {t_3}^2 - \sqrt{2}z + 2\,\beta\, t_1}{2t_1\left({t_3}^2+1\right)}, \tag{2.98}$$

$$y_3 = -\frac{\left({t_1}^2{t_3}^2\beta + {t_1}^2\beta + {t_3}^2\beta + 2\,{t_1}^2 t_3 + {t_3}^2 + \beta - 1\right) z\sqrt{2}}{2t_1\left({t_3}^2+1\right)}. \tag{2.99}$$

The additional conditions on z to meet $y_1 = y_2$ and $y_1 = y_3$ are

$$z = -\frac{\sqrt{2}t_1}{t_1^2+1}, \tag{2.100}$$

$$z = \frac{\sqrt{2}t_1}{t_1^2+1}, \tag{2.101}$$

which means that y_1, y_2, y_3 cannot be equal if $z \neq 0$, which is obviously rejected. However, one can observe that $z = \pm\frac{\sqrt{2}t_1}{t_1^2+1}$ is also a root of R_1, R_2, R_3 once equation (2.95) is substituted into them. In other words, while $y_1 = y_2$ may be satisfied with the condition $z = -\frac{\sqrt{2}t_1}{t_1^2+1}$, for example, R_3 is still cancelled with this expression of z, independently from y. Thus, R_1, R_2, R_3 being cancelled by expressions in y and z, the four sub-determinants can be solved for their common root in x, and constitute a locus of singularity. Yet, the rest of the derivation is not presented, because this locus exists for a value of z under one unit for all t_1, which is considered of poor interest for application purposes. Because similar results are found with expression (2.96), the derivation is not presented.

Backsubstitution of equation (2.80)

The last case to be considered is that of equation (2.80), which is the last condition to make R_4, R_5 vanish simultaneously. Only the derivation for the positive form of equation (2.80) is presented. Backsubstituting the last root in t_2 into the resultants R_1, R_2 and R_3 leads to rather complex expressions. Nonetheless, they can be solved for their respective roots in y. Each resultant has two roots in y, one of which is common to the three resultants, and its expression is given by

$$y = \frac{3z(v_1+v_2)v_3}{4t_1(v_4v_5+v_6)}, \tag{2.102}$$

with

$$v_1 = -\frac{2}{3}\beta\,\left({t_3}^2 + 2\,t_3 - 1\right)\sqrt{2}\sqrt{\left(\left(\beta^2 + \beta + \frac{1}{2}\right){t_3}^2 - 2\,\beta\,t_3 + \beta^2 - \beta + \frac{1}{2}\right)\left({t_3}^2 + 1\right)}, \tag{2.103}$$

$$v_2 = \left({t_3}^4 + \frac{4}{3}{t_3}^3 + 2\,{t_3}^2 - \frac{4}{3}t_3 + 1\right)\beta^2 + \frac{2}{3}\left({t_3}^2 + 1\right)\left({t_3}^2 - 2\,t_3 - 1\right)\beta + \frac{1}{3}\left({t_3}^2 + 1\right)^2, \tag{2.104}$$

$$v_3 = \left({t_3}^2 + 1\right)\left({t_1}^2 + 1\right)\beta^2 + \left({t_3}^2 - 2\,t_3 - 1\right)\beta - \frac{1}{2}\left({t_3}^2 + 1\right)\left(t_1 - 1\right)\left(t_1 + 1\right), \tag{2.105}$$

$$v_4 = \left(-\frac{3}{4}{t_3}^4 - {t_3}^3 - \frac{3}{2}{t_3}^2 + t_3 - \frac{3}{4}\right)\beta^2 + \left(-\frac{1}{2}{t_3}^4 + {t_3}^3 + t_3 + \frac{1}{2}\right)\beta - \frac{1}{4}\left({t_3}^2 + 1\right)^2, \tag{2.106}$$

$$v_5 = \sqrt{2}\sqrt{\left(\left(\beta^2 + \beta + \frac{1}{2}\right){t_3}^2 - 2\,\beta\,t_3 + \beta^2 - \beta + \frac{1}{2}\right)\left({t_3}^2 + 1\right)}, \tag{2.107}$$

$$v_6 = \left({t_3}^2 + 1\right)\left(\left({t_3}^2 + 1\right)\beta^2 + \left({t_3}^2 - 2\,t_3 - 1\right)\beta + \frac{1}{2}{t_3}^2 + \frac{1}{2}\right)\left({t_3}^2 + 2\,t_3 - 1\right)\beta. \tag{2.108}$$

This root in y substituted into the four sub-determinants would be normally sufficient to find a unique common root in x among them. However, in this particular case, one observes that D_1 vanishes and that D_4 becomes independent from variable x, and has the easiest form to work with, which is expressed by a function of z multiplied by a polynomial in t_3 of degree 16. Because of the high degree of the polynomial in t_3 of D_4, it is not possible to find analytical expressions for its roots. Thus, a numerical method is required to completely investigate the cases where D_4 could be equal to zero due to one of its roots in t_3. The other possibility to make D_4 vanish is that the z coordinate of the platform is equal to the root in z of D_4, which is given by

$$z = \pm\frac{\sqrt{2}t_1\left(\left(\beta + 1\right){t_3}^2 + \beta - 1\right)}{\sqrt{\left(\left(\beta^2 + \beta + \frac{1}{2}\right){t_3}^2 - 2\,\beta\,t_3 + \beta^2 - \beta + \frac{1}{2}\right)\left({t_3}^2 + 1\right)\left({t_1}^2 + 1\right)}}. \tag{2.109}$$

While equation (2.109) along with equations (2.80) and (2.102) make D_4 equal to zero, and substituted into the last two sub-determinants D_2 and D_3 also make them vanish, it can be observed, from Figure 2.11, that the z coordinate of the platform in this singular configuration is always below one unit, for all values of torsion angle σ and tilt angle θ. Hence, this condition for singularity is considered non restrictive, because it may not even be reachable in practice, that is to say, this singularity locus lies outside of the mechanism's reachable workspace. This case concludes the derivation with the common root in y from equation (2.102).

One could be interested in finding additional conditions for which the second roots in y of resultants R_1, R_2 and R_3 are equal. Consider y_1, y_2, y_3, the second roots in y of resultants

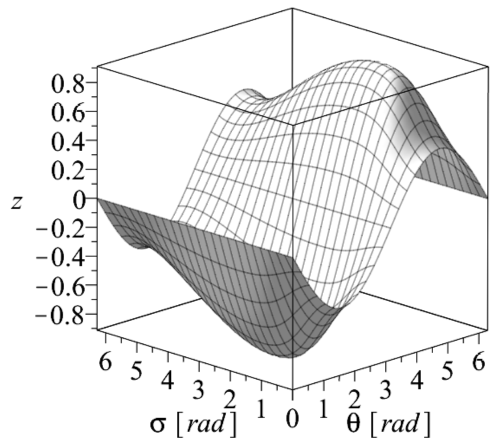

FIGURE 2.11 – Height of the platform (z coordinate, in units) for $\beta = 2$ with singularity conditions given by equations (2.80), (2.102) and (2.109).

R_1, R_2, R_3 following the backsubstitution of equation (2.80). The condition to observe, for example, $y_1 = y_2$ is met for one in

$$z = \pm \frac{\sqrt{2} t_1 \left((\beta + 1) \, {t_3}^2 + \beta - 1 \right)}{\sqrt{\left(\left(\beta^2 + \beta + \frac{1}{2} \right) {t_3}^2 - 2 \, \beta \, t_3 + \beta^2 - \beta + \frac{1}{2} \right) \left({t_3}^2 + 1 \right)} \left({t_1}^2 + 1 \right)}, \tag{2.110}$$

$$t_3 = \pm 1, \tag{2.111}$$

$$t_3 = \pm \frac{\sqrt{4 \, \beta^2 - 1}}{2 \, \beta + 1}. \tag{2.112}$$

It is readily observed that the expression of variable z to verify $y_1 = y_2$, as a necessary but not yet sufficient condition to obtain $y_1 = y_2 = y_3$, is the same as equation (2.109) and thus will not be taken any further. The condition $t_3 = \pm 1$ verifies $y_1 = y_2 = y_3$, but it constitutes in fact a particular case of the singularity condition from equation (2.89) with the value of t_2 given by equation (2.80). Thus, the expression $t_3 = \pm 1$ as a condition to verify $y_1 = y_2$ is not relevant. Finally, equation (2.112) may verify $y_1 = y_2 = y_3$ with the additional condition on variable z given by

$$z = \pm \frac{\left(2 \, \beta^2 - 1 \right) t_1}{\sqrt{2 \, \beta^2 - \sqrt{4 \, \beta^2 - 1}} \left({t_1}^2 + 1 \right) \beta}, \tag{2.113}$$

which is no other than equation (2.109) with the particular value of t_3 given by equation (2.112). Thus, these conditions do not lead to any further locus of singularity restraining the orientational workspace of the mechanism, and these last cases conclude the analysis for the singularities dependent from position coordinates.

2.6 Discussion

Sections 2.5.1 and 2.5.2 presented a method to derive the conditions for singularity in the kinematically redundant (6+2)-DOF parallel mechanism proposed in this work. It is to be mentioned that, in Sections 2.5.3 and 2.5.4, many results were chosen not to be disclosed, because they lead to either special cases of a more general result already derived, or to a z coordinate of the platform in singular configuration located under one unit, which is deemed non restrictive for the useful workspace. For the singular configurations that are independent from position coordinates, it is shown that the orientational workspace is mainly restrained when the torsion angle σ equals $\pm 90°$ (see Fig. 2.6), a condition also observed in many other architectures akin to the Gough-Stewart platform. Aside from this condition, the other position independent singularities require a tilt angle of the platform of $\pm 180°$, which is hardly reachable without encountering mechanical interference. Nonetheless, analytical expressions for singularities of this case were found.

Concerning the position dependent singularities, the derivation led to analytical expressions of two main loci of singular configurations of interest, namely those expressed by equations (2.86), (2.87), (2.88) (see Fig. 2.8), and equations (2.89), (2.90) (see Fig. 2.10). Indeed, these loci do not require legs to be coplanar to the plane of the base, nor a z coordinate of the platform under one unit. While the first locus seems mechanically unreachable, it may be approached resulting in large forces in the actuators, and thus its description by simple analytical equations is very important for trajectory planning. The second locus of interest is easier to run into, because it does not lead to mechanical interference prior to reaching the singular configuration.

With the application of the method for the derivation of the singularity locus for the proposed architecture, many singular configurations where found to be under one unit for the z coordinate. While these singularities exist and may be described by analytical expressions, they often result in configurations in which some legs in the mechanism are coplanar to the plane of the base, which is highly undesirable. Moreover, in such configurations, the structure is extremely flattened, resulting in the legs requiring large forces to support the payload, an unwanted situation in practical applications. Finally, while the use of the resultant of polynomials to solve the initial nonlinear system of equations of four sub-determinants led to many analytical expressions for singularity loci, very few cases require an alternative numerical method. In these cases, the general expressions become too complex and are difficult to work with, but they constitute a small fraction of the results derived.

From a general perspective, the analysis of the results shows that the workspace of the mechanism is mainly restricted by singularities occurring for a torsion of the platform of $\pm 90°$. Nevertheless, the singularity loci are accurately described by simple analytical expressions which is an interesting contribution for the singularity analysis of the given kinematically redundant mechanism. Finally, from the primary objective of this paper, the impact on the singularity loci of having two kinematically redundant DOFs instead of three, as proposed in [25], consists in few singular configurations still remaining in the workspace mainly caused by the torsion of the platform, though they are easily localized by simple closed-form analytical expressions for the vast majority. Moreover, the resolution of the kinematic redundancy for path planning may be simplified, because the mechanical interference associated to the orientation of the redundant links and the singularities can be mapped onto the 2-D space of the redundant angles along the path, instead of a space of higher dimension with a higher number of kinematically redundant DOFs.

2.7 Conclusion

This work presented the architecture of a kinematically redundant (6+2)-DOF parallel mechanism akin to the Gough-Stewart platform. The main objective consisted in analyzing how including two kinematically redundant DOFs instead of three — like in other recently proposed architectures — affects the capabilities of the mechanism to avoid singular configurations, as a motivation to develop an architecture that facilitates the redundancy resolution. The approach chosen for the derivation of the singularity locus of the specific architecture began with the construction of an alternative matrix $\tilde{\mathbf{J}}$ capturing the same conditions for singularity as Jacobian matrix $\mathbf{J}$. A combination of the linear decomposition of the determinant of matrix $\tilde{\mathbf{J}}$ followed by a cascaded application of the resultant of polynomials led to the elimination of position variables in order to raise the conditions for unavoidable singular configurations. These conditions were, for the vast majority, expressed by simple closed-form analytical equations, which is an interesting observation. From the relevant singularity loci derived and presented in this work, it is observed that the principal remaining singular configurations of the mechanism arise with a $\pm 90^\circ$ torsion angle of the platform. Thus, while the orientational workspace for tilted rotations for this particular architecture did not seem directly affected by singularities with two kinematically redundant DOFs, as proposed by [62], it is still restrained by type II singularities when torsion rotations are taken into account. Nevertheless, this work brought the contribution of describing the singularity loci with simple expressions, most of them parameterized by orientation variables, which is considered important for an architecture with such a high number of degrees of freedom. However, while the use of the linear decomposition of the determinant and the cascaded application of the resultant of polynomials to solve the system of equations of singularity may be applied to any kinematically redundant mechanism whose Jacobian matrix $\mathbf{J}$ has linear combinations of vectors in its rows or columns, the simplicity and symmetry of the architecture of the mechanism may have a significant impact on the complexity of the procedure involved in extracting simple analytical expressions for the locus of singularity. Finally, while the proposed architecture has not yet a fully singularity-free workspace, the mechanism may be considered as a compromise between a maximized enlargement of the orientational workspace and a lighter redundancy resolution due to a smaller number of kinematically redundant DOFs.

2.8 Acknowledgment

The authors would like to thank the Natural Sciences and Engineering Research Council of Canada (NSERC), the Fonds de Recherche du Québec Nature et Technologie (FRQNT, grant number : 302763) and the Chaire de Recherche du Canada en Robotique et Mécatronique for their financial support during the presented work.

2.9 Declaration of Interests

The authors declare no conflict of interests of any kind.

Chapitre 3

Comparaison de l'espace atteignable en orientation avec un mécanisme standard non redondant

3.1 Introduction

Les deux précédents chapitres se sont concentrés sur la résolution du système d'équations menant au lieu des singularités inévitables du mécanisme cinématiquement redondant à huit degrés de liberté. La démarche purement mathématique n'a abordé que la détermination des différents lieux de singularités pour le mécanisme d'intérêt, sans pour autant en exposer visuellement les impacts sur l'espace atteignable en orientation. De plus, une comparaison entre l'espace atteignable pour un mécanisme standard à six degrés de liberté et le mécanisme cinématiquement redondant n'a pas été présentée. Ce court chapitre traitera donc d'une analyse numérique comparative entre l'espace de travail atteignable pour le mécanisme standard et le mécanisme redondant.

3.2 Limites à l'espace de travail d'un mécanisme parallèle

Bien que les configurations singulières soient plutôt restrictives pour l'espace atteignable d'un mécanisme parallèle, les interférences mécaniques contribuent évidemment aussi à la réduction de son étendue. Pour les architectures parallèles inspirées de la plateforme de Gough-Stewart, ces interférences sont souvent situées aux configurations de la plateforme telles que les élongations minimales et maximales des actionneurs prismatiques sont dépassées, le débattement maximal des articulations passives est franchi, ou encore lorsque deux actionneurs prismatiques entrent en contact l'un avec l'autre. D'un autre côté, pour minimiser l'effet de certaines limitations mécaniques sur l'espace atteignable en orientation, nous allons évaluer celui-ci à une élévation de la plateforme telle que les actionneurs prismatiques sont à leur élongation moyenne, afin de maximiser le débattement possible à l'effecteur. Cette configuration de la plateforme sera appelée la configuration neutre. À partir de cette configuration à position constante, un balayage sur les trois angles caractérisant l'orientation de l'effecteur par rapport à la base est mené. À chaque incrément d'orientation, une vérification est faite pour s'assurer qu'aucune interférence mécanique n'est rencontrée, ou qu'aucune singularité n'est traversée. En ce qui concerne la rencontre d'une singularité pour le mécanisme cinématiquement redondant, cela correspond au passage d'une orientation à une autre au cours duquel le signe des quatre sous-déterminants change simultanément. Finalement, pour s'assurer d'une comparaison équitable entre les deux mécanismes, leur architecture comporte les mêmes rayons de points d'attaches à la plateforme et à la base, les mêmes caractéristiques d'actionneurs et les mêmes débattements maximums pour les articulations passives. Les points d'attache à la base et à la plateforme pour chacune des pattes des mécanismes standard et cinématiquement redondant qui ont été utilisés pour les prochaines simulations sont répertoriés dans les tableaux suivants, et la Figure 3.1 représente ces points dans le plan pour des fins de comparaison.

$\mathbf{a}_{1,1}$	$\mathbf{a}_{1,2}$	$\mathbf{a}_{2,1}$	$\mathbf{a}_{2,2}$	$\mathbf{a}_3$	$\mathbf{a}_4$	$\mathbf{a}_5$	$\mathbf{a}_6$
$\begin{bmatrix} 0.816 \\ 0.758 \\ 0 \end{bmatrix}$	$\begin{bmatrix} 0.816 \\ -0.758 \\ 0 \end{bmatrix}$	$\begin{bmatrix} -0.816 \\ -0.758 \\ 0 \end{bmatrix}$	$\begin{bmatrix} -0.816 \\ 0.758 \\ 0 \end{bmatrix}$	$\begin{bmatrix} 0.756 \\ -0.816 \\ 0 \end{bmatrix}$	$\begin{bmatrix} -0.756 \\ -0.816 \\ 0 \end{bmatrix}$	$\begin{bmatrix} -0.756 \\ 0.816 \\ 0 \end{bmatrix}$	$\begin{bmatrix} 0.756 \\ 0.816 \\ 0 \end{bmatrix}$

TABLE 3.1 – Vecteurs de points d'attache à la base dans le repère fixe pour le mécanisme cinématiquement redondant.

$\mathbf{b}'_1$	$\mathbf{b}'_2$	$\mathbf{b}'_3$	$\mathbf{b}'_4$	$\mathbf{b}'_5$	$\mathbf{b}'_6$
$\begin{bmatrix} 0.350 \\ 0 \\ 0 \end{bmatrix}$	$\begin{bmatrix} -0.350 \\ 0 \\ 0 \end{bmatrix}$	$\begin{bmatrix} 0.046 \\ -0.347 \\ 0 \end{bmatrix}$	$\begin{bmatrix} -0.046 \\ -0.347 \\ 0 \end{bmatrix}$	$\begin{bmatrix} -0.046 \\ 0.347 \\ 0 \end{bmatrix}$	$\begin{bmatrix} 0.046 \\ 0.347 \\ 0 \end{bmatrix}$

TABLE 3.2 – Vecteurs de points d'attache à la plateforme dans le repère mobile pour le mécanisme cinématiquement redondant.

Le débattement maximal des articulations passives de Cardan à la base est fixé à 45° dans toutes les directions. Le débattement maximal des articulations passives sphériques à la plateforme est de 150° dans toutes les directions par rapport au premier axe de rotation du joint (qui est normal au plan de la plateforme). Les actionneurs choisis, suivant ceux utilisés pour un premier modèle CAO du mécanisme cinématiquement redondant, sont des EMC-80 de la compagnie Rexroth, pouvant supporter une charge de 5200 N, et dont la longueur (centre

$\mathbf{a}_1$	$\mathbf{a}_2$	$\mathbf{a}_3$	$\mathbf{a}_4$	$\mathbf{a}_5$	$\mathbf{a}_6$
$\begin{bmatrix}-0.042\\1.113\\0\end{bmatrix}$	$\begin{bmatrix}0.042\\1.113\\0\end{bmatrix}$	$\begin{bmatrix}0.985\\-0.520\\0\end{bmatrix}$	$\begin{bmatrix}0.943\\-0.593\\0\end{bmatrix}$	$\begin{bmatrix}-0.943\\-0.593\\0\end{bmatrix}$	$\begin{bmatrix}-0.985\\-0.520\\0\end{bmatrix}$

TABLE 3.3 – Vecteurs de points d'attache à la base dans le repère fixe pour le mécanisme standard.

$\mathbf{b'}_1$	$\mathbf{b'}_2$	$\mathbf{b'}_3$	$\mathbf{b'}_4$	$\mathbf{b'}_5$	$\mathbf{b'}_6$
$\begin{bmatrix}-0.278\\0.213\\0\end{bmatrix}$	$\begin{bmatrix}0.278\\0.213\\0\end{bmatrix}$	$\begin{bmatrix}0.323\\0.134\\0\end{bmatrix}$	$\begin{bmatrix}0.046\\-0.347\\0\end{bmatrix}$	$\begin{bmatrix}-0.046\\-0.347\\0\end{bmatrix}$	$\begin{bmatrix}-0.323\\0.134\\0\end{bmatrix}$

TABLE 3.4 – Vecteurs de points d'attache à la plateforme dans le repère mobile pour le mécanisme standard.

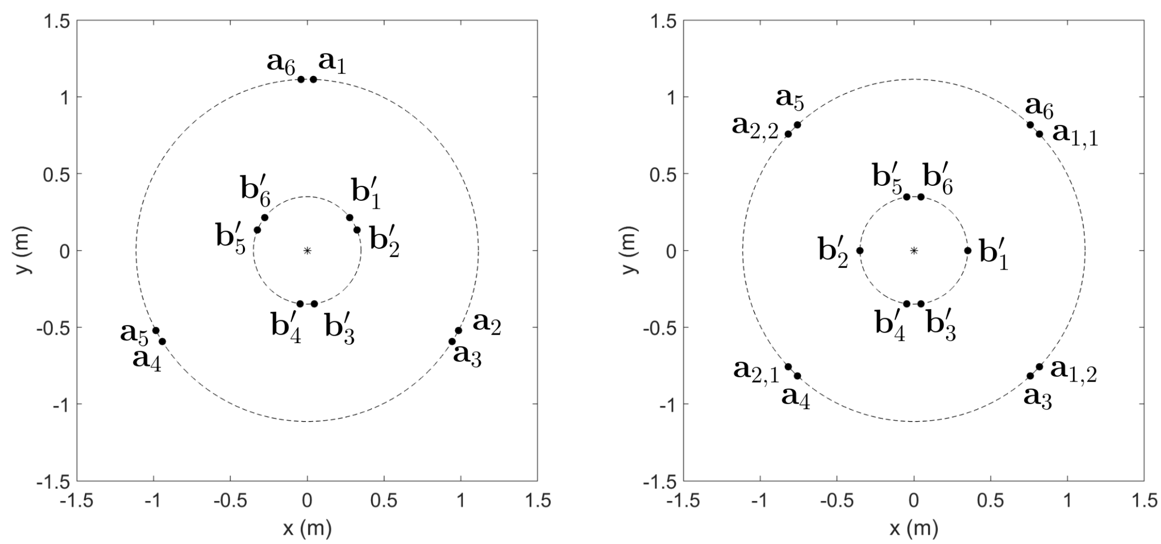

FIGURE 3.1 – Localisation des points d'attache à la base et à la plateforme pour les mécanismes standard (gauche) et cinématiquement redondant (droite).

du joint de cardan au centre du joint sphérique) complètement rétractée est de 1.569 m, et la longueur complètement allongée est de 2.419 m.

3.3 Espace atteignable en orientation pour les mécanismes standard et cinématiquement redondant

Les graphes d'espace en orientation sont construits en coordonnées cylindriques, et suivant la représentation des rotations Inclinaison et Torsion, telle que décrite dans [47]. La coordonnée radiale correspond à l'angle d'inclinaison θ de la plateforme. La coordonnée angulaire correspondant à l'angle ϕ de l'axe dans le plan de la base autour duquel est effectuée l'inclinaison de la plateforme. La coordonnée axiale (verticale) correspond à l'angle de torsion σ de la plateforme. L'espace atteignable en orientation pour le mécanisme standard et pour le mécanisme cinématiquement redondant est présenté aux Figures 3.2 et 3.3. Une vue de dessus de ces mêmes graphiques est représentée aux Figures 3.4 et 3.5. Les frontières de ces espaces atteignables sont définies par les singularités (rouge), les limites d'élongation des actionneurs prismatiques (bleu), les plages de débattement maximal pour les articulations passives (vert) et les interférences physiques entre deux actionneurs (magenta). Les Figures 3.2 et 3.4 montrent clairement que l'espace atteignable en orientation est fortement limité par les poses singulières dans la configuration neutre du mécanisme standard, ce qui n'est pas le cas pour le mécanisme redondant.

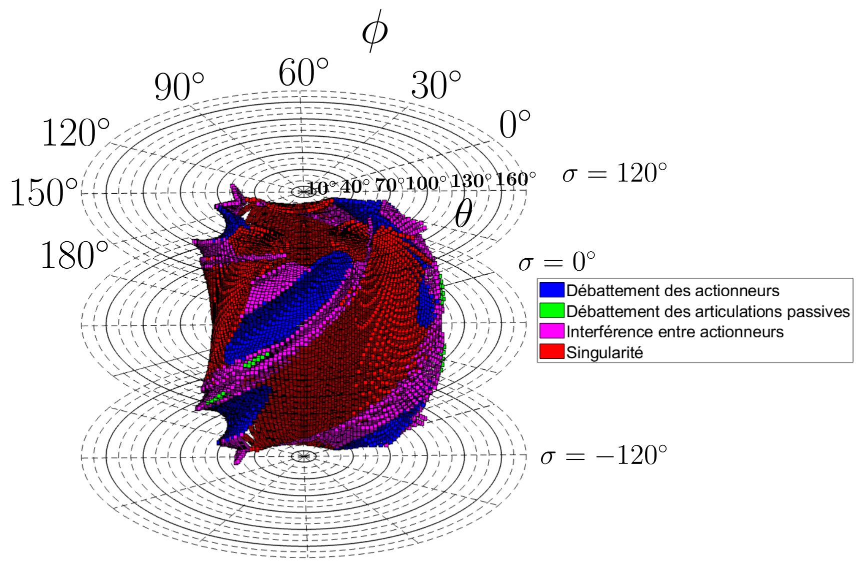

FIGURE 3.2 – Espace atteignable en orientation du mécanisme standard.

D'un autre côté, en comparant les Figures 3.2 et 3.3 ou 3.4 et 3.5, si l'espace atteignable du mécanisme cinématiquement redondant peut ne pas sembler à première vue tant avantageux par rapport au mécanisme standard malgré la quasi absence de singularités, l'ajout de l'étude des forces dans les actionneurs à l'intérieur de cet espace atteignable pour une tâche de déplacement de charge montre mieux l'intérêt du mécanisme redondant. On s'in-

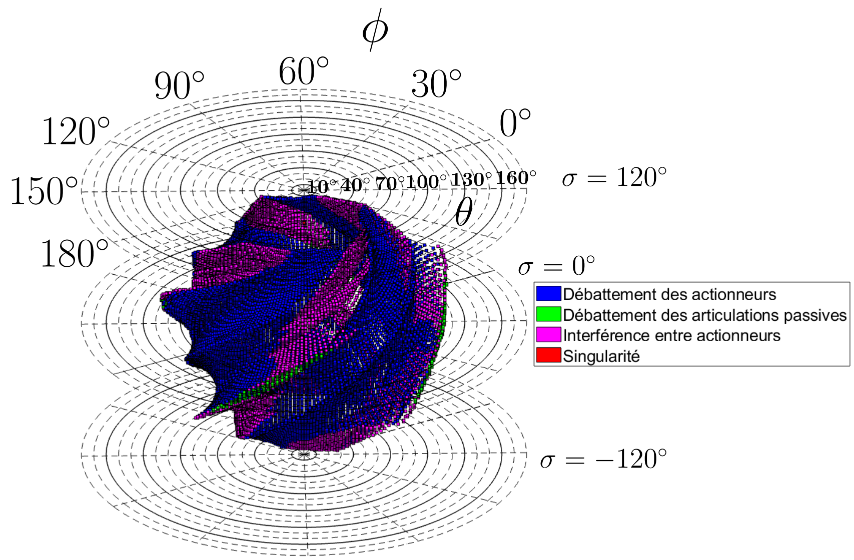

FIGURE 3.3 – Espace atteignable en orientation du mécanisme cinématiquement redondant.

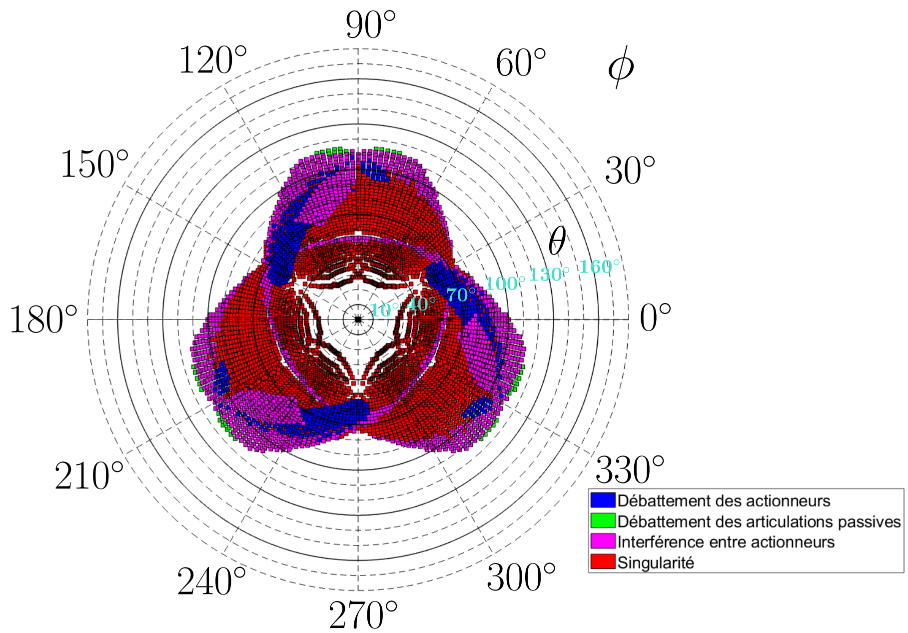

FIGURE 3.4 – Espace atteignable en orientation du mécanisme standard, vue de dessus.

téresse donc à une section de l'espace atteignable pour chacun des mécanismes à $\sigma = 0°$, par exemple, où on peut visualiser l'effort maximal nécessaire parmi tous les actionneurs du mécanisme concerné en chaque point à l'intérieur des frontières de l'espace atteignable, en régime statique. En effet, pour un manipulateur parallèle, nous avons que

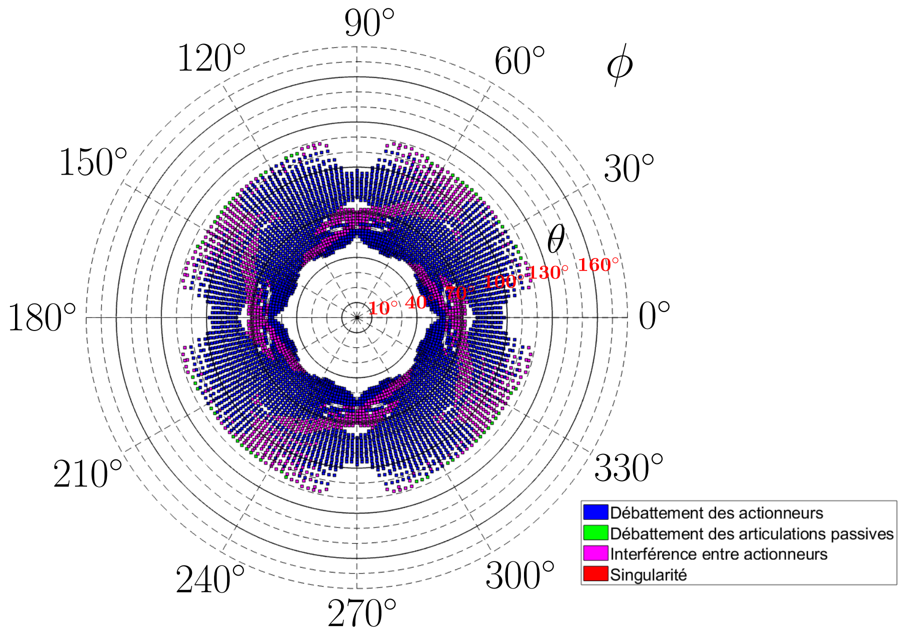

FIGURE 3.5 – Espace atteignable en orientation du mécanisme cinématiquement redondant, vue de dessus.

$$\boldsymbol{\tau} = \mathbf{K}^T \mathbf{J}^{-T} \mathbf{w}, \tag{3.1}$$

où $\boldsymbol{\tau}$ est le vecteur des efforts articulaires, $\mathbf{K}$ et $\mathbf{J}$ sont les matrices jacobiennes du manipulateur, et $\mathbf{w}$ est le vecteur des efforts appliqués à l'effecteur (force et moment). Ainsi, pour un vecteur d'efforts $\mathbf{w}$ et une configuration donnée de la plateforme, il est possible de déterminer quel est la force maximale présente dans tous les actionneurs du mécanisme, et s'en servir comme limitation mécanique supplémentaire à l'espace atteignable en orientation. En ce qui concerne spécifiquement le mécanisme cinématiquement redondant, on peut utiliser la redondance afin de minimiser les efforts requis dans les actionneurs. En effet, pour une configuration donnée de la plateforme, on peut balayer toutes les combinaisons d'orientations des membrures redondantes qui respectent leurs propres interférences mécaniques. Pour chacune de ces combinaisons, on calcule l'effort maximal retrouvé parmi les huit actionneurs. Lorsque toutes les combinaisons d'orientation de membrures redondantes ont été testées, on choisit l'effort minimal parmi tous les efforts maximums enregistrés plus tôt. Cet effort minimal correspondra donc à la configuration des membrures redondantes qui minimise l'effort maximal retrouvé parmi les huit actionneurs pour une pose donnée de l'effecteur.

Afin de mesurer les forces dans les actionneurs, chaque mécanisme est soumis à une même tâche qui consiste à orienter une charge de 80 kg, dont le centre de masse se situe à une distance de deux rayons de plateforme et par rapport au plan de celle-ci, dans toutes les configurations à l'intérieur de leur espace atteignable respectif pour un angle de torsion nul. Les résultats sont montrés aux Figures 3.6 et 3.7.

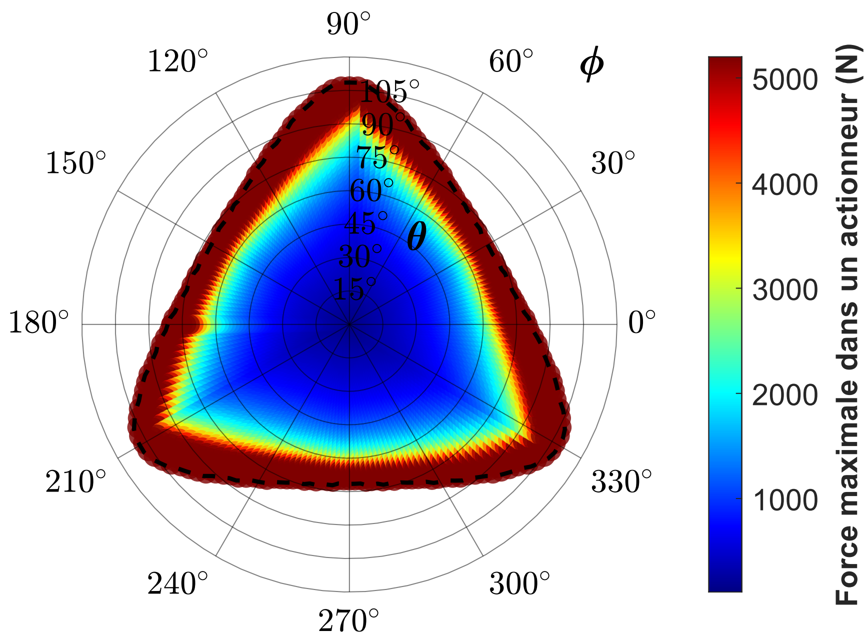

FIGURE 3.6 – Espace atteignable en orientation à torsion nulle en prenant en compte les limites en efforts des actionneurs pour le mécanisme standard.

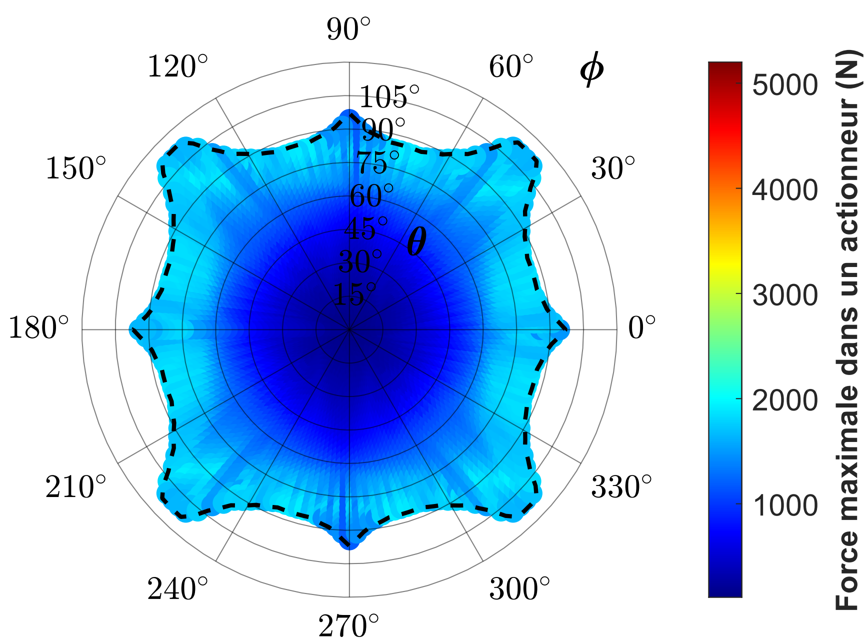

FIGURE 3.7 – Espace atteignable en orientation à torsion nulle en prenant en compte les limites en efforts des actionneurs pour le mécanisme cinématiquement redondant.

Dans ces graphes, les courbes en pointillés représentent les limites mécaniques uniquement dues aux débattements maximums des actionneurs et des articulations passives, ainsi que des collisions entre actionneurs. En observant la Figure 3.6, on peut remarquer qu'après une certaine inclinaison θ de la plateforme, dans certaines directions ϕ, l'effort maximal retrouvé parmi les six actionneurs augmente rapidement jusqu'à dépasser la valeur limite tolérée par les spécifications. En effet, la plus grande partie de la frontière associée à la limite atteignable à torsion nulle pour le mécanisme non redondant avant l'analyse des forces était constituée de configurations singulières. On vérifie donc qu'à l'approche de telles configurations, les efforts requis dans les actionneurs augmentent vivement, ce qui réduit considérablement l'espace atteignable réel. L'angle d'inclinaison θ de la plateforme que l'on peut effectuer dans toutes les directions ϕ sans dépasser les limites en force est d'environ $60°$.

D'un autre côté, on remarque que les limites en force des actionneurs pour le mécanisme cinématiquement redondant, à la Figure 3.7, sont bien moins contraignantes à son espace atteignable. En effet, puisque la frontière de l'espace atteignable ne contient pas de singularités inévitables, on peut s'en approcher sans remarquer d'augmentation critique des efforts requis aux actionneurs. De plus, on peut se servir de la redondance afin de minimiser ces efforts. L'angle d'inclinaison θ maximal de la plateforme que l'on peut effectuer dans toutes les directions ϕ est alors de $86°$.

Ainsi, suite à cette comparaison d'espaces atteignables, lorsque l'on inclut les efforts maximums pouvant être supportés par les actionneurs comme limite mécanique additionnelle, on se rend compte que l'espace en orientation du mécanisme standard est plutôt amputé suite à une telle contrainte autour des configurations singulières. De l'autre côté, par ses capacités d'évitement des singularités, le mécanisme cinématiquement redondant voit son espace atteignable beaucoup moins affecté par cette contrainte mécanique supplémentaire, ce qui contribue grandement à favoriser cet espace en orientation par rapport à celui du mécanisme standard non redondant. De plus, puisque les frontières de l'espace atteignable du mécanisme cinématiquement redondant ne sont pas contraintes par des singularités à la position à laquelle celui-ci a été déterminé, mais bien uniquement par des limitations mécaniques, si l'on décide plutôt d'utiliser, par exemple, des actionneurs à plus grand débattement, on se retrouvera à augmenter de manière appréciable son espace en orientation. De son côté, l'espace atteignable en orientation pour le mécanisme standard non redondant, affecté des mêmes changements, sera toujours contraint par des surfaces de singularités. Ces diminutions de limitations mécaniques n'auront donc aucun impact ou presque sur son espace atteignable en orientation.

3.4 Conclusion

Ce chapitre a présenté une comparaison graphique entre les espaces de travail atteignables en orientation pour les mécanismes parallèles standard et cinématiquement redondant. Afin de rendre cette comparaison aussi significative que possible, les mêmes limites mécaniques ont été imposées aux deux mécanismes. De plus, pour que les mécanismes soient à la même échelle, les points d'attache des actionneurs à la base et à la plateforme de chacun ont été disposés sur des cercles de mêmes rayons. L'analyse des espaces de travail atteignables sans considérer les forces dans les actionneurs a montré que, bien que celui du mécanisme cinématiquement redondant soit sensiblement plus étendu, la différence n'est à première vue pas si significative. En effet, les deux mécanismes sont contraints en angle de torsion σ de $\pm 90°$. En ce qui concerne les angles d'inclinaison θ et ϕ, le mécanisme cinématiquement redondant est plus performant pour son espace atteignable. Lorsqu'une contrainte liée aux efforts dans les actionneurs a été ajoutée afin de vérifier l'impact d'être à proximité d'une configuration singulière, on a observé que l'espace atteignable en orientation du mécanisme standard en est fortement affecté par rapport à celui du mécanisme cinématiquement redondant. Suite à cette seconde analyse, on a pu montrer visuellement dans ce troisième chapitre l'impact de la redondance cinématique dans un mécanisme parallèle pour l'augmentation de son espace de travail en rotation.

Conclusion

Ce mémoire avait pour objectif principal l'analyse des lieux de singularité pour un manipulateur parallèle cinématiquement redondant à (6+2) degrés de liberté. Le travail a été présenté sous la forme de deux articles, le premier évaluant les configurations singulières pour le cas spécifique où l'angle de torsion est nul à la plateforme, et le second évaluant les configurations singulières pour le cas général, c'est-à-dire lorsque l'angle de torsion n'est pas nécessairement nul à l'effecteur. Un troisième chapitre a permis de comparer graphiquement l'espace de travail en orientation du mécanisme cinématiquement redondant avec celui d'un mécanisme standard non redondant.

Dans le premier chapitre, le modèle cinématique du robot a été décrit. La définition d'une singularité inévitable fut donnée. À partir de cette définition, un outil mathématique, l'expansion linéaire du déterminant, a été employé afin d'élaborer plus facilement les conditions conduisant à un lieu de singularités inévitables. La résolution du système d'équations hautement non-linéaires a montré que, pour le cas où la torsion est nulle à l'effecteur du manipulateur, les singularités inévitables se situent en-dehors des limites de l'espace atteignable en orientation du mécanisme. Autrement dit, le manipulateur rencontre une limitation mécanique avant d'atteindre la configuration singulière. Une démonstration de trajectoire à grand débattement en inclinaison de la plateforme montre que celle-ci ne rencontre aucune singularité, ce qui n'aurait pas été possible avec un mécanisme standard non-redondant. La découverte de l'absence de singularités inévitables à l'intérieur de l'espace atteignable en orientation du mécanisme pour une torsion nulle à l'effecteur montre que, pour des applications d'usinage ou de soudage où l'outil est axisymétrique, deux degrés de liberté cinématiquement redondants sont suffisants pour assurer un espace de travail exempt de singularités inévitables.

Dans le second chapitre, le modèle cinématique du robot a été rappelé ainsi que la méthode de construction du système d'équations à résoudre. Les différentes possibilités pour résoudre le système d'équations sont présentées, et substituées tour à tour afin de vérifier quelles conditions mènent réellement à des lieux de singularités d'intérêt. Il est montré tout d'abord que, lorsque la torsion est non nulle à l'effecteur, donc pour le cas général des orientations de la plateforme, certaines singularités inévitables demeurent à l'intérieur de l'espace atteignable du mécanisme. Or, malgré cette limitation de l'espace utile en orientation du mécanisme, le lieu des singularités inévitables est tout-de-même décrit par des équations mathématiques simples sous forme analytique, un élément pouvant faciliter grandement la planification de trajectoire.

Dans le troisième chapitre, les limites mécaniques principales restreignant l'espace atteignable en orientation d'un mécanisme parallèle dont l'architecture est similaire à celle de la plateforme de Gough-Stewart ont été décrites. Une analyse de l'espace en orientation pour un mécanisme standard et un mécanisme cinématiquement redondant a été menée, avec et sans contraintes des efforts maximums dans les actionneurs. Il a par la suite été observé que la contrainte des efforts maximums dans les actionneurs pour une tâche de déplacement de charge affecte beaucoup l'espace atteignable pour le mécanisme non redondant par rapport au mécanisme cinématiquement redondant, ce dernier pouvant profiter de sa redondance pour minimiser les efforts transmis aux actionneurs.

Dans son ensemble, ce travail a présenté une méthode de résolution pour déterminer le lieu des singularités inévitables pour un mécanisme parallèle cinématiquement redondant à (6+2) degrés de liberté. Bien que pour l'architecture donnée, la méthode utilisée ait fourni des équations analytiques plutôt simples, il est à noter que l'obtention de telles expressions et la résolution du système d'équations sous forme analytique dépend fortement de la symétrie de l'architecture du mécanisme, et des paires de déterminants utilisées pour l'application du résultant des polynômes en cascade. Néanmoins, cette méthode s'est avérée efficace pour déterminer le lieu des singularités inévitables pour un mécanisme parallèle avec un haut degré de redondance. Suite à cette analyse, il a été montré que le mécanisme cinématiquement redondant à (6+2) degrés de liberté semble être un bon candidat pour nombre d'applications robotiques malgré les quelques configurations singulières résiduelles dans son espace de travail. Tout d'abord, parce que toutes les tâches ne requérant pas de rotation en torsion à l'effecteur peuvent être menées sans craindre de rencontrer une configuration singulière, et ensuite, pour les tâches nécessitant toutes les orientations, des équations analytiques simples décrivent les configurations du mécanisme à éviter. Le fait de bénéficier de deux degrés de liberté redondants au lieu de trois dans l'architecture cinématique affecte bien l'espace de travail en orientation du mécanisme cinématiquement redondant, mais cet espace atteignable demeure somme toute beaucoup plus intéressant que celui du mécanisme standard équivalent à six degrés de liberté.

Bibliographie

[1] J. Liu, Y. Li, Y. Zhang, Q. Gao, and B. Zuo, “Dynamics and control of a parallel mechanism for active vibration isolation in space station,” Nonlinear Dynamics, vol. 76, no. 3, pp. 1737–1751, 2014.

[2] I. Bonev, “Delta parallel robot-the story of success,” Newsletter, available at http ://www. parallelmic. org, 2001.

[3] J. Iqbal, Z. H. Khan, and A. Khalid, “Prospects of robotics in food industry,” Food Science and Technology, vol. 37, pp. 159–165, 2017.

[4] T. Essomba, Y. Hsu, J. S. Sandoval Arevalo, M. A. Laribi, and S. Zeghloul, “Kinematic optimization of a reconfigurable spherical parallel mechanism for robotic-assisted craniotomy,” Journal of Mechanisms and Robotics, vol. 11, no. 6, p. 060905, 2019.

[5] T. Essomba, M. A. Laribi, S. Zeghloul, and G. Poisson, “Optimal synthesis of a spherical parallel mechanism for medical application,” Robotica, vol. 34, no. 3, pp. 671–686, 2016.

[6] A. Yaşır, G. Kiper, and M. C. Dede, “Kinematic design of a non-parasitic 2R1T parallel mechanism with remote center of motion to be used in minimally invasive surgery applications,” Mechanism and Machine Theory, vol. 153, p. 104013, 2020.

[7] N. Badeau, C. Gosselin, S. Foucault, T. Laliberté, and M. E. Abdallah, “Intuitive physical human-robot interaction : Using a passive parallel mechanism,” IEEE Robotics & Automation Magazine, vol. 25, no. 2, pp. 28–38, 2018.

[8] G. Boucher, T. Laliberté, and C. Gosselin, “A parallel low-impedance sensing approach for highly responsive physical human-robot interaction,” in 2019 International Conference on Robotics and Automation (ICRA), pp. 3754–3760, IEEE, 2019.

[9] J. Lee, B.-W. Song, and W. Yang, “Design of exoskeleton-type wrist human–machine interface based on over-actuated coaxial spherical parallel mechanism,” Advances in Mechanical Engineering, vol. 10, no. 2, p. 1687814017753896, 2018.

[10] R. Meziane, P. Cardou, and M. J.-D. Otis, "Cable interference control in physical interaction for cable-driven parallel mechanisms," Mechanism and Machine Theory, vol. 132, pp. 30–47, 2019.

[11] S. Briot and I. A. Bonev, "Pantopteron : a new fully decoupled 3DOF translational parallel robot for pick-and-place applications," 2009.

[12] Q. Meng, F. Xie, and X.-J. Liu, "Conceptual design and kinematic analysis of a novel parallel robot for high-speed pick-and-place operations," Frontiers of Mechanical Engineering, vol. 13, no. 2, pp. 211–224, 2018.

[13] D. Chablat and P. Wenger, "Architecture optimization of a 3-DOF translational parallel mechanism for machining applications, the orthoglide," IEEE Transactions on Robotics and Automation, vol. 19, no. 3, pp. 403–410, 2003.

[14] J. Kim, F. C. Park, S. J. Ryu, J. Kim, J. C. Hwang, C. Park, and C. C. Iurascu, "Design and analysis of a redundantly actuated parallel mechanism for rapid machining," IEEE Transactions on robotics and automation, vol. 17, no. 4, pp. 423–434, 2001.

[15] C. Gosselin, J. Angeles, et al., "Singularity analysis of closed-loop kinematic chains.," IEEE transactions on robotics and automation, vol. 6, no. 3, pp. 281–290, 1990.

[16] B. N. R. Abadi, M. Farid, and M. Mahzoon, "Redundancy resolution and control of a novel spatial parallel mechanism with kinematic redundancy," Mechanism and Machine Theory, vol. 133, pp. 112–126, 2019.

[17] R. Boudreau and S. Nokleby, "Force optimization of kinematically-redundant planar parallel manipulators following a desired trajectory," Mechanism and Machine Theory, vol. 56, pp. 138–155, 2012.

[18] J. V. de Carvalho Fontes, F. T. Colombo, N. B. F. da Silva, and M. M. da Silva, "Model-based joint and task space control strategies for a kinematically redundant parallel manipulator," Robotica, vol. 40, no. 5, pp. 1570–1586, 2022.

[19] J. Cavacanti Santos and M. Martins da Silva, "Redundancy resolution of kinematically redundant parallel manipulators via differential dynamic programing," Journal of Mechanisms and Robotics, vol. 9, no. 4, p. 041016, 2017.

[20] L.-T. Schreiber and C. Gosselin, "Schönflies motion parallel robot (SPARA) : a kinematically redundant parallel robot with unlimited rotation capabilities," IEEE/ASME Transactions on Mechatronics, vol. 24, no. 5, pp. 2273–2281, 2019.

[21] H. Qu and S. Guo, "Kinematics analysis of a novel planar parallel manipulator with kinematic redundancy," Journal of Mechanical Science and Technology, vol. 31, no. 4, pp. 1927–1935, 2017.

[22] H. Qu, L. Hu, and S. Guo, "Singularity analysis and avoidance of a planar parallel mechanism with kinematic redundancy under a fixed orientation," Proceedings of the Institution of Mechanical Engineers, Part C : Journal of Mechanical Engineering Science, vol. 235, no. 18, pp. 3534–3553, 2021.

[23] J. Landuré and C. Gosselin, "Kinematic analysis of a novel kinematically redundant spherical parallel manipulator," Journal of Mechanisms and Robotics, vol. 10, no. 2, p. 021007, 2018.

[24] K. Wen, T. S. Nguyen, D. Harton, T. Laliberté, and C. Gosselin, "A backdrivable kinematically redundant (6+3)-degree-of-freedom hybrid parallel robot for intuitive sensorless physical human–robot interaction," IEEE Transactions on Robotics, vol. 37, no. 4, pp. 1222–1238, 2020.

[25] C. Gosselin and L.-T. Schreiber, "Kinematically redundant spatial parallel mechanisms for singularity avoidance and large orientational workspace," IEEE Transactions on Robotics, vol. 32, no. 2, pp. 286–300, 2016.

[26] I. Ebrahimi, J. A. Carretero, and R. Boudreau, "3-PRRR redundant planar parallel manipulator : Inverse displacement, workspace and singularity analyses," Mechanism and Machine Theory, vol. 42, no. 8, pp. 1007–1016, 2007.

[27] C. Gosselin, T. Laliberté, and A. Veillette, "Singularity-free kinematically redundant planar parallel mechanisms with unlimited rotational capability," IEEE Transactions on Robotics, vol. 31, no. 2, pp. 457–467, 2015.

[28] C. Gosselin and L.-T. Schreiber, "Redundancy in parallel mechanisms : A review," Applied Mechanics Reviews, vol. 70, no. 1, 2018.

[29] A. Müller, "Stiffness control of redundantly actuated parallel manipulators," in Proceedings 2006 IEEE International Conference on Robotics and Automation, 2006. ICRA 2006., pp. 1153–1158, IEEE, 2006.

[30] T. Harada and M. Nagase, "Impedance control of a redundantly actuated 3-DOF planar parallel link mechanism using direct drive linear motors," in 2010 IEEE International Conference on Robotics and Biomimetics, pp. 501–506, IEEE, 2010.

[31] A. Müller and T. Hufnagel, "Model-based control of redundantly actuated parallel manipulators in redundant coordinates," Robotics and Autonomous systems, vol. 60, no. 4, pp. 563–571, 2012.

[32] A. Müller, "Internal preload control of redundantly actuated parallel manipulators—its application to backlash avoiding control," IEEE Transactions on Robotics, vol. 21, no. 4, pp. 668–677, 2005.

[33] A. Müller and P. Maisser, "Generation and application of prestress in redundantly full-actuated parallel manipulators," Multibody System Dynamics, vol. 18, no. 2, pp. 259–275, 2007.

[34] T. Harada and P. Liu, "Internal and external forces measurement of planar 3-DOF redundantly actuated parallel mechanism by axial force sensors," International Scholarly Research Notices, vol. 2013, 2013.

[35] F. Firmani and R. P. Podhorodeski, "Force-unconstrained poses for a redundantly-actuated planar parallel manipulator," Mechanism and Machine Theory, vol. 39, no. 5, pp. 459–476, 2004.

[36] I. Bouchard, "Lieux de singularité des manipulateurs parallèles à actionnement redondant," Master's thesis, Université Laval, 2002.

[37] T. Harada, "Mode changes of redundantly actuated asymmetric parallel mechanism," Proceedings of the Institution of Mechanical Engineers, Part C : Journal of Mechanical Engineering Science, vol. 230, no. 3, pp. 454–462, 2016.

[38] Y. H. Cheung, N. Baron, and N. Rojas, "Full-rotation singularity-safe workspace for kinematically redundant parallel robots," in Annual Conference Towards Autonomous Robotic Systems, pp. 436–447, Springer, 2019.

[39] N. Baron, A. Philippides, and N. Rojas, "A novel kinematically redundant planar parallel robot manipulator with full rotatability," Journal of Mechanisms and Robotics, vol. 11, no. 1, p. 011008, 2019.

[40] M. Isaksson, C. Gosselin, and K. Marlow, "An introduction to utilising the redundancy of a kinematically redundant parallel manipulator to operate a gripper," Mechanism and Machine Theory, vol. 101, pp. 50–59, 2016.

[41] K. Wen, D. Harton, T. Laliberté, and C. Gosselin, "Kinematically redundant (6+3)-DOF hybrid parallel robot with large orientational workspace and remotely operated gripper," in 2019 International Conference on Robotics and Automation (ICRA), pp. 1672–1678, IEEE, 2019.

[42] L.-T. Schreiber and C. Gosselin, "Exploiting the kinematic redundancy of a (6+3) degrees-of-freedom parallel mechanism," Journal of Mechanisms and Robotics, vol. 11, no. 2, 2019.

[43] N. Baron, A. Philippides, and N. Rojas, "On the false positives and false negatives of the jacobian matrix in kinematically redundant parallel mechanisms," IEEE Transactions on Robotics, vol. 36, no. 3, pp. 951–958, 2020.

[44] N. Baron, A. Philippides, and N. Rojas, "A geometric method of singularity avoidance for kinematically redundant planar parallel robots," in International Symposium on Advances in Robot Kinematics, pp. 187–194, Springer, 2018.

[45] N. Baron, A. Philippides, and N. Rojas, "A robust geometric method of singularity avoidance for kinematically redundant planar parallel robot manipulators," Mechanism and Machine Theory, vol. 151, p. 103863, 2020.

[46] B. M. St-Onge and C. M. Gosselin, "Singularity analysis and representation of the general Gough-Stewart platform," The International Journal of Robotics Research, vol. 19, no. 3, pp. 271–288, 2000.

[47] I. Bonev, D. Zlatanov, and C. Gosselin, "Advantages of the modified Euler angles in the design and control of PKMs," in 2002 Parallel Kinematic Machines International Conference, pp. 171–188, Citeseer, 2002.

[48] G. Strang, "Linear algebra and its applications, (1988)," Hartcourt Brace Jovanovich College Publishers, 1988.

[49] E. F. Fichter, "A stewart platform-based manipulator : general theory and practical construction," The International Journal of Robotics Research, vol. 5, no. 2, pp. 157–182, 1986.

[50] J.-P. Merlet, Parallel robots, vol. 128. Springer Science & Business Media, 2005.

[51] B. Liao and W. Liu, "Pseudoinverse-type bi-criteria minimization scheme for redundancy resolution of robot manipulators," Robotica, vol. 33, no. 10, pp. 2100–2113, 2015.

[52] J. A. Saglia and J. S. Dai, "Geometry and kinematic analysis of a redundantly actuated parallel mechanism for rehabilitation," in International Design Engineering Technical Conferences and Computers and Information in Engineering Conference, vol. 48094, pp. 1081–1090, 2007.

[53] L.-T. Schreiber and C. Gosselin, "Kinematically redundant planar parallel mechanisms : Kinematics, workspace and trajectory planning," Mechanism and Machine Theory, vol. 119, pp. 91–105, 2018.

[54] J. Wang and C. M. Gosselin, "Kinematic analysis and design of kinematically redundant parallel mechanisms," J. Mech. Des., vol. 126, no. 1, pp. 109–118, 2004.

[55] I. Ebrahimi, J. A. Carretero, and R. Boudreau, "A family of kinematically redundant planar parallel manipulators," Journal of Mechanical Design, vol. 130, no. 6, 2008.

[56] H. Liao, T. Li, and X. Tang, "Singularity analysis of redundant parallel manipulators," in 2004 IEEE International Conference on Systems, Man and Cybernetics (IEEE Cat. No. 04CH37583), vol. 5, pp. 4214–4220, IEEE, 2004.

[57] X.-J. Liu, C. Wu, and J. Wang, "A new approach for singularity analysis and closeness measurement to singularities of parallel manipulators," Journal of Mechanisms and Robotics, vol. 4, no. 4, 2012.

[58] R. Boudreau and R. Podhorodeski, "Singularity analysis of a kinematically simple class of 7-jointed revolute manipulators," Transactions of the Canadian Society for Mechanical Engineering, vol. 34, no. 1, pp. 105–117, 2010.

[59] T. Stigger, M. Pfurner, and M. Husty, "Workspace and singularity analysis of a 3-RUU parallel manipulator," in European Conference on Mechanism Science, pp. 325–332, Springer, 2018.

[60] F. Zhao, S. Guo, C. Zhang, H. Qu, and D. Li, "Singularity analysis and dexterity performance on a novel parallel mechanism with kinematic redundancy," International Journal of Advanced Robotic Systems, vol. 16, no. 5, p. 1729881419872641, 2019.

[61] B. Li, Y. Cao, Q. Zhang, and Z. Huang, "Position-singularity analysis of a special class of the Stewart parallel mechanisms with two dissimilar semi-symmetrical hexagons," Robotica, vol. 31, no. 1, pp. 123–136, 2013.

[62] J. Lacombe and C. Gosselin, "Singularity analysis of a kinematically redundant (6+2)-DOF parallel mechanism for zero-torsion configurations," Mechanism and Machine Theory, vol. 170, p. 104682, 2022.

Annexe A

Expression des résultants f, g, h du système d'équations de la Figure 1.6

A.1 Expression de $f(y, z, t_1, t_2)$

$$f(y,z,t_1,t_2) = f_1(t_1,t_2) f_2(y,z,t_1,t_2) f_3(y,z,t_1,t_2) \tag{A.1}$$

avec

$$f_1(t_1,t_2) = \frac{2^{15}\beta^7 t_1^3 (t_2^2-1)^2}{(t_1^2+1)^6 (t_2^2+1)^7} \tag{A.2}$$

$$\begin{aligned} f_2(y,z,t_1,t_2) = \big(&yzt_1\big({t_1}^2+1\big){t_2}^6 + \big(-4\,z^2{t_1}^4 + \big(-6\,z^2 - 4\,\beta + 4\big){t_1}^2 - 2\,z^2\big){t_2}^5 \\ &- 5\,yzt_1\big({t_1}^2+1\big){t_2}^4 + \big(8\,z^2{t_1}^4 + \big(4\,z^2 + 24\,\beta + 8\big){t_1}^2 - 4\,z^2\big){t_2}^3 \\ &- 5\,yzt_1\big({t_1}^2+1\big){t_2}^2 + \big(-4\,z^2{t_1}^4 + \big(-6\,z^2 - 4\,\beta + 4\big){t_1}^2 - 2\,z^2\big)t_2 + yzt_1\big({t_1}^2+1\big)\big) \end{aligned} \tag{A.3}$$

$$\begin{aligned} f_3(y,z,t_1,t_2) = \big(&-z\big({t_1}^2+1\big)\big(\beta-1\big){t_2}^4 + 4\,yt_1{t_2}^3 - 2\,\big(\big(\beta+3\big){t_1}^2 + \beta - 1\big)z{t_2}^2 + 4\,yt_1t_2 \\ &- z\big({t_1}^2+1\big)\big(\beta-1\big)\big) \end{aligned} \tag{A.4}$$

A.2 Expression de $g(y, z, t_1, t_2)$

$$g(y,z,t_1,t_2) = g_1(t_1,t_2) g_2(z,t_1,t_2) g_3(y,z,t_1,t_2) \tag{A.5}$$

avec

$$g_1(t_1,t_2) = \frac{2^{14}\beta^7 t_1^2(t_2^2-1)}{(t_1^2+1)^6(t_2^2+1)^6} \tag{A.6}$$

$$g_2(z,t_1,t_2) = \left(z\left({t_1}^2+1\right){t_2}^2-4\,t_1t_2+z\left({t_1}^2+1\right)\right)\left(z\left({t_1}^2+1\right){t_2}^2+4\,t_1t_2+z\left({t_1}^2+1\right)\right) \tag{A.7}$$

$$\begin{aligned} g_3(y,z,t_1,t_2) = \Big(yzt_1\left({t_1}^2+1\right){t_2}^6 + \left(-z^2{t_1}^4+\left(-4\,\beta^2+4\,y^2+4\,\beta\right){t_1}^2+z^2\right){t_2}^5 \\ -9\,z\left({t_1}^2-\frac{7}{9}\right)t_1y{t_2}^4+\left(6\,z^2{t_1}^4+\left(-8\,\beta^2+8\,y^2-8\,z^2-8\,\beta\right){t_1}^2+2\,z^2\right){t_2}^3 \\ -9\,z\left({t_1}^2-\frac{7}{9}\right)t_1y{t_2}^2+\left(-z^2{t_1}^4+\left(-4\,\beta^2+4\,y^2+4\,\beta\right){t_1}^2+z^2\right)t_2+yzt_1\left({t_1}^2+1\right)\Big) \end{aligned} \tag{A.8}$$

A.3 Expression de $h(z,t_1,t_2)$

$$h(z,t_1,t_2) = h_1(t_1,t_2)h_2(z,t_1,t_2)h_3(z,t_1,t_2) \tag{A.9}$$

avec

$$h_1(t_1,t_2) = \frac{2^{60}\beta^{29}t_1^{14}t_2^2(t_2^2-1)^6((\beta-1)t_2^4+2(\beta+1)t_2^2+\beta-1)}{(t_1^2+1)^{24}(t_2^2+1)^{22}} \tag{A.10}$$

$$h_2(z,t_1,t_2) = \left(z\left({t_1}^2+1\right){t_2}^2-4\,t_1t_2+z\left({t_1}^2+1\right)\right)^4\left(z\left({t_1}^2+1\right){t_2}^2+4\,t_1t_2+z\left({t_1}^2+1\right)\right)^4 \tag{A.11}$$

$$\begin{aligned} h_3(z,t_1,t_2) = \left(3{t_2}^4-2\,{t_2}^2+3\right)\left({t_2}^2+1\right)^2z^2{t_1}^4+\Big(\big(6\,z^2-4\left(\beta-1\right)^2\big){t_2}^8+ \\ \big(48\,\beta^2+8\,z^2-32\,\beta-16\big){t_2}^6+\big(-152\,\beta^2+4\,z^2-80\,\beta-24\big){t_2}^4+ \\ \big(48\,\beta^2+8\,z^2-32\,\beta-16\big){t_2}^2+6\,z^2-4\left(\beta-1\right)^2\Big){t_1}^2+\left(3{t_2}^4-2\,{t_2}^2+3\right)\left({t_2}^2+1\right)^2z^2 \end{aligned} \tag{A.12}$$